Search for decays of the Higgs boson into scalar particles decaying into four or six b quarks using pp collisions at $\sqrt{s} = 13$ TeV with the ATLAS detector

G. Aad *et al.*[*]
(ATLAS Collaboration)

(Received 7 July 2025; accepted 21 August 2025; published 17 October 2025)

A search for exotic decays of the Higgs boson H into new scalar or pseudoscalar particles that subsequently decay into b-quarks is presented. The search considers ZH production with several decay scenarios for the Higgs boson; first to a pair of identical scalars, $H \to 2a \to 4b$, second to a pair of scalars with different masses ($m_{a1} < m_{a2}$), either directly, $H \to a_1 a_2 \to 4b$, or via a longer decay chain, $H \to a_1 a_2 \to 3a_1 \to 6b$. The analysis uses proton-proton collision data at $\sqrt{s} = 13$ TeV collected with the ATLAS detector at the Large Hadron Collider, corresponding to an integrated luminosity of 140 fb^{-1}. No significant excess above the Standard Model prediction is observed. The search sets upper limits at 95% confidence level on the ratio of the Higgs boson production cross section to the SM prediction times the branching ratio of Higgs bosons decaying into $4b$ or $6b$, between 4% and 25% for $\sigma(ZH)/\sigma_{\mathrm{SM}}(ZH) \times \mathcal{B}(H \to 2a \to 4b)$, between 24% and 38% for $\sigma(ZH)/\sigma_{\mathrm{SM}}(ZH) \times \mathcal{B}(H \to a_1 a_2 \to 4b)$, and between 10% and 20% for $\sigma(ZH)/\sigma_{\mathrm{SM}}(ZH) \times \mathcal{B}(H \to a_1 a_2 \to 3a_1 \to 6b)$, depending on the masses of the scalar particles.

DOI: 10.1103/mzld-ldlt

I. INTRODUCTION

Since the observation of the Higgs boson with mass m_H near 125 GeV by the ATLAS and CMS Collaborations [1,2], a comprehensive program of measurements is being pursued to characterize the properties of this particle. The branching fraction of the Higgs boson into undetected beyond the Standard Model (BSM) particles are constrained by analyses of Higgs boson properties to approximately $\mathcal{B}_{\mathrm{u}} \lesssim 12\%$ [3,4]. Higgs boson decays are particularly sensitive to new physics due to the small total width ($\Gamma_H \approx 4$ MeV). Even very small couplings to new particles can give sizable branching fractions [5] and can be compatible with available measurements of the Higgs boson couplings [3].

Extensions of the Standard Model (SM) that include new light scalars, called a-bosons, can result in exotic Higgs boson decays $H \to 2a$. Such new light particles appear in theories with an extended Higgs sector [6–10], dark matter models [11–15], models with a first-order electroweak phase transition [16,17], and theories of neutral naturalness [18,19]. Signatures of $H \to 2a$ can also arise in models with hidden-sector particles that are singlets under the SM gauge transformations [5,20–23]. In scenarios where the a-boson mixes with the Higgs boson and inherits its Yukawa couplings to fermions, decays of the a-boson into heavy fermions such as b-quarks are favored, and the process $H \to 2a \to (b\bar{b})(b\bar{b})$, shown in Fig. 1(a), is expected to have a sizable branching fraction in the mass range $2m_b < m_a < m_H/2$ [5,24]. Because of the scalar nature of the a-boson and the hadronization of the b-quarks, the results presented here do not depend on the parity assumed for the a-boson and can be interpreted in terms of Higgs boson decays into scalars or pseudoscalars.

Scenarios with multiple new hidden-sector particles, such as two real scalar singlets, referred to as a_1 and a_2 ($m_{a_1} < m_{a_2}$) have also been considered in the literature [22]. In these scenarios, the Higgs boson can then decay into two different scalars, $H \to a_1 a_2 \to 4b$, shown in Fig. 1(b). Another possibility is the successive decay into the lightest scalar state, $H \to a_1 a_2 \to 3a_1 \to 6b$, which gives rise to a high multiplicity final state, shown in Fig. 1(c). In models with two additional light scalars, the partial width of $a_2 \to a_1 a_1$ has to be much larger than any decay into SM fermions $a_2 \to f_{\mathrm{SM}} \bar{f}_{\mathrm{SM}}$ for the model to be consistent with measurements of Higgs boson couplings [22]. As such, when $m_{a_1} < m_{a_2}/2$, only the decay $H \to a_1 a_2 \to 3a_1$ is relevant. The search for models with multiple a-bosons can thus be effectively split into two independent channels; one with four b-quarks in the final state and one with six b-quarks in the final state, which are analyzed separately.

[*]Full author list given at the end of the article.

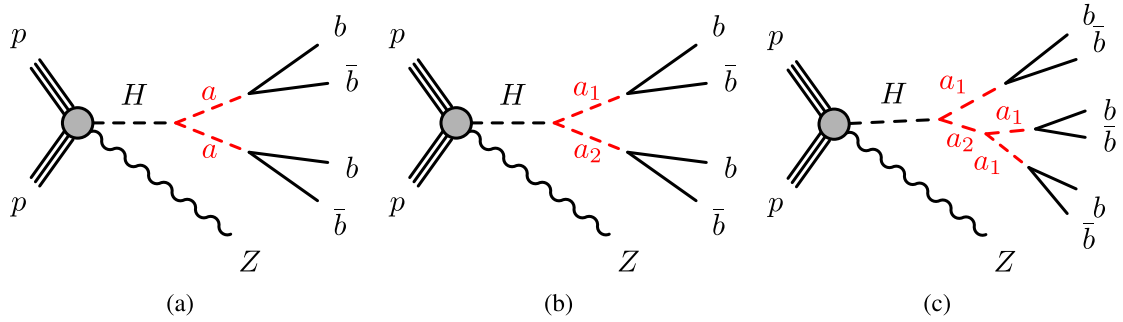

FIG. 1. Representative Feynman diagrams for ZH production with the (a) $H \to 2a \to 4b$, (b) $H \to a_1 a_2 \to 4b$, and (c) $H \to a_1 a_2 \to 3a_1 \to 6b$ processes considered in this search.

This paper presents a search for the exotic Higgs boson decay $H \to 2a/a_1 a_2 \to 4b/6b$ over the mass range $12 < m_a < 60$ GeV using the full Run 2 proton–proton (pp) collision data at $\sqrt{s} = 13$ TeV collected with the ATLAS detector at the Large Hadron Collider (LHC) [25], corresponding to an integrated luminosity of 140 fb^{-1}. The analysis targets the Higgs boson produced in association with a Z boson (ZH), where the Z boson decay provides a trigger and suppresses the $t\bar{t}$ backgrounds. The WH associated production is not used since early results [26] show that this channel is less sensitive due to larger backgrounds. Different analysis categories are defined depending on the decay mode of the Z boson, which can be either into charged leptons (electrons e or muons μ), referred to as 2ℓ, or into neutrinos that leave a signature of transverse momentum imbalance ($E_{\mathrm{T}}^{\mathrm{miss}}$), referred to as 0ℓ. Due to the relatively low mass of the Higgs boson and the four- or six-body final state, the b-quarks tend to have low transverse momentum, typically below $p_{\mathrm{T}} \lesssim 50$ GeV and are challenging to trigger on. Therefore, the analysis uses the electron or muon triggers for the 2ℓ category and uses $E_{\mathrm{T}}^{\mathrm{miss}}$ triggers for the 0ℓ category. The analysis defines different event selections depending on the Z boson decay mode; 2ℓ or 0ℓ, and on the b-quark multiplicity; $4b$ or $6b$. The main backgrounds to the signal process are Drell-Yan production of charged leptons or neutrinos in association with heavy-flavor jets and $t\bar{t}$, which may also be produced in association with heavy-flavor jets.

Several novel reconstruction techniques are used to identify the b-hadron decay products. For $m_a \lesssim 20$ GeV, the a-boson has a relatively large Lorentz boost and its decay products are collimated. Consequently, the $a \to b\bar{b}$ final state is reconstructed as a single jet that contains the hadronization products of the two b-quarks. While several techniques exist to resolve merged jets [27], most of them are only efficient in the case of high-mass and high-p_{T} jets. The merged $a \to b\bar{b}$ jet from the decay products of a Higgs boson have low p_{T}. A dedicated algorithm is used to identify low-mass, merged, "double b-quark" jets (B-jets) [28]. For $m_a \gtrsim 25$ GeV, the b-quark decays are typically well separated, so each reconstructed jet captures the hadronization of a single b-quark and standard algorithms are used to identify such jets (b-jets) [29,30]. The sensitivity to high-multiplicity final states is also enhanced by the use of soft secondary vertices reconstructed outside of jets [31]. The search considers events with one or two B-jets, three or four b-jets, and up to one soft secondary vertex reconstructed outside of a jet, which are used to define several analysis categories.

Similar searches in the $4b$ decay channel were performed by the ATLAS Collaboration [26,32,33] and the CMS Collaboration [34]. The latest search has placed 95% confidence level (CL) upper limits on the branching fractions in the range of 1.1 for $m_a = 20$ GeV to 0.36 for $m_a = 60$ GeV using 138 fb^{-1} of Run 2 data at $\sqrt{s} = 13$ TeV [34]. This result improves the sensitivity of previous analyses by using dedicated heavy-flavor reconstruction algorithms, particularly in the low mass regime ($m_a < 20$ GeV). It is also complementary to other searches for $H \to 2a$ decays performed by the ATLAS and CMS Collaborations using both $\sqrt{s} = 8$ TeV and $\sqrt{s} = 13$ TeV data in several final states including $\mu^+\mu^-\mu^+\mu^-$ [35–37], $\mu^+\mu^-\tau^+\tau^-$ [38–41], $\tau^+\tau^-\tau^+\tau^-$ [40,42,43], $b\bar{b}\mu^+\mu^-$ [44–47], $b\bar{b}\tau^+\tau^-$ [48–50], $\gamma\gamma\gamma\gamma$ [51–53], and $\gamma\gamma gg$ [54].

II. ATLAS DETECTOR

The ATLAS detector [55] at the LHC covers nearly the entire solid angle around the collision point.[1] It consists of an inner tracking detector surrounded by a thin superconducting solenoid, electromagnetic and hadronic

[1]ATLAS uses a right-handed coordinate system with its origin at the nominal interaction point (IP) in the center of the detector and the z-axis along the beam pipe. The x-axis points from the IP to the center of the LHC ring, and the y-axis points upwards. Polar coordinates (r, ϕ) are used in the transverse plane, ϕ being the azimuthal angle around the z-axis. The pseudorapidity is defined in terms of the polar angle θ as $\eta = -\ln\tan(\theta/2)$ and is equal to the rapidity $y = \frac{1}{2}\ln(\frac{E+p_z}{E-p_z})$ in the relativistic limit. Angular distance is measured in units of $\Delta R \equiv \sqrt{(\Delta y)^2 + (\Delta\phi)^2}$.

calorimeters, and a muon spectrometer incorporating three large superconducting air-core toroidal magnets.

The inner-detector system (ID) is immersed in a 2T axial magnetic field and provides charged-particle tracking in the range of $|\eta| < 2.5$. The high-granularity silicon pixel detector covers the vertex region and typically provides four measurements per track, the first hit generally being in the insertable B-layer (IBL) installed before Run 2 [56,57]. It is followed by the SemiConductor Tracker (SCT), which provides on average eight measurements per track. These silicon detectors are complemented by the transition radiation tracker (TRT), which enables radially extended track reconstruction up to $|\eta| = 2.0$. The TRT also provides electron identification information based on the fraction of hits (typically 30 in total) above a higher energy-deposit threshold corresponding to transition radiation.

The calorimeter system covers the pseudorapidity range $|\eta| < 4.9$. Within the region $|\eta| < 3.2$, electromagnetic calorimetry is provided by barrel and end cap high-granularity lead/liquid-argon (LAr) calorimeters, with an additional thin LAr presampler covering $|\eta| < 1.8$ to correct for energy loss in material upstream of the calorimeters. Hadronic calorimetry is provided by the steel/scintillator-tile calorimeter, segmented into three barrel structures within $|\eta| < 1.7$, and two copper/LAr hadronic endcap calorimeters. The solid angle coverage is completed with forward copper/LAr and tungsten/LAr calorimeter modules optimized for electromagnetic and hadronic energy measurements, respectively.

The muon spectrometer (MS) comprises separate trigger and high-precision tracking chambers measuring the deflection of muons in a magnetic field generated by the superconducting air-core toroidal magnets. The field integral of the toroids ranges between 2.0 Tm and 6.0 Tm across most of the detector. Three layers of precision chambers, each consisting of layers of monitored drift tubes, cover the region $|\eta| < 2.7$, complemented by cathode-strip chambers in the forward region, where the background is highest. The muon trigger system covers the range $|\eta| < 2.4$ with resistive-plate chambers in the barrel, and thin-gap chambers in the end cap regions.

The luminosity is measured mainly by the LUCID–2 [58] detector that records Cherenkov light produced in the quartz windows of photomultipliers located close to the beam pipe. Events are selected by the first-level trigger system implemented in custom hardware, followed by selections made by algorithms implemented in software in the high-level trigger [59]. The first-level trigger accepts events from the 40 MHz bunch crossings at a rate below 100 kHz, which the high-level trigger further reduces to record complete events to disk at about 1 kHz. A software suite [60] is used in data simulation, in the reconstruction and analysis of real and simulated data, in detector operations, and in the trigger and data acquisition systems of the experiment.

III. DATA AND SIMULATION SAMPLES

The analysis uses pp collision data at a center-of-mass energy of $\sqrt{s} = 13$ TeV collected with the ATLAS detector in Run 2 of the LHC from 2015 to 2018, corresponding to a total integrated luminosity of 140 fb^{-1} [61]. Only events for which the LHC beams were in stable-collision mode and all relevant subsystems were operational are used [62]. Events with charged leptons are selected using single-lepton triggers with either a low p_{T} threshold and an isolation requirement, or a higher threshold but a looser identification criterion without any isolation requirement. For data collected in 2015 (2016–2018), the lowest p_{T} threshold in the single-muon trigger was 20 (26) GeV [63] and in the single-electron trigger was 24 (26) GeV [64]. Events without charged leptons are selected using $E_{\mathrm{T}}^{\mathrm{miss}}$ triggers whose threshold varied over time from 70 GeV to 110 GeV due to the increasing average effect of multiple inelastic interactions in the same and neighboring bunch crossings (pile-up).

Simulated signal and background samples are used to describe background sources, estimate signal efficiency and acceptance, design and optimize the analysis event selection, and model systematic uncertainties. Monte Carlo (MC) samples were produced using either the full ATLAS detector simulation [65] based on Geant4 [66] or a faster simulation where the full Geant4 simulation of the calorimeter response is replaced by a parametrization [65]. The pile-up effects were modeled by overlaying each simulated hard-scattering event with inelastic pp events generated with Pythia8.186 [67] using the NNPDF2.3lo set of parton distribution functions (PDFs) [68] and the A3 set of tuned parameters (tune) [69]. Simulated events are reweighted to match the pile-up conditions observed in the Run 2 data sample. All simulated events are processed through the same reconstruction algorithms and analysis chain as the data. Table I summarizes all the generated samples.

The signal event samples focus on Higgs bosons produced in association with a Z boson (ZH). Two processes are included, $qq \to ZH$ and $gg \to ZH$, where the latter contributes about 10% of the total production cross section. The sample of Higgs bosons is generated at next-to-leading-order (NLO) accuracy in QCD using Powheg Box v2 [82–86] with the NNPDF3.0nlo PDF set [68,87] with mass $m_H = 125$ GeV. The simulated Higgs boson production samples are normalized using dedicated higher-order cross sections calculated at next-to-next-to-leading-order (NNLO) in QCD with NLO electroweak (EW) corrections [70]. The Higgs boson is decayed into a pair of scalars that then each decay either into a pair of scalars or into a pair of b-quarks, where the decays are performed in the narrow-width approximation. Events are showered and hadronized with Pythia 8.244 or Pythia 8.245 for the 2ℓ or 0ℓ channels, respectively, [67] using the AZNLO tune to model the underlying event [88].

TABLE I. Sample generator setups. The precision of the ME generator is NLO in QCD if no additional information is provided in parentheses, such as the number of partons at ME accuracy and [EW] for electroweak production. To treat the overlap between $t\bar{t}$ and tW diagrams, the sample using the diagram removal scheme is listed as [DR]. The higher-order cross section used to normalize these samples is listed in the last column if different from the one of the generator. If no information is in this column, no higher-order k-factor is applied to this process. If multiple samples are listed for the same process, the first one corresponds to the one used for the predictions, while the subsequent ones are used to derive systematic uncertainties.

Process	ME generator	ME PDF	PS	Normalization
Signal				
$H \to 4b/6b$	Powheg Box v2	NNPDF3.0nlo	Pythia8.244/5	NNLO + NLO (EW) [70]
	Powheg Box v2	NNPDF3.0nlo	Herwig 7.04	NNLO + NLO (EW) [70]
Top				
$t\bar{t}$	Powheg Box v2	NNPDF3.0nlo	Pythia 8.230	NNLO + NNLL [71–77]
	Powheg Box v2	NNPDF3.0nlo	Herwig 7.13	NNLO + NNLL [71–77]
	MadGraph5_aMC@NLO2.6.0	NNPDF3.0nlo	Pythia 8.230	NNLO + NNLL [71–77]
$t\bar{t} + b\bar{b}$	Powheg Box Res	NNPDF3.1nnlo nf4	Pythia 8.230	···
tW	Powheg Box v2[DR]	NNPDF3.0nlo	Pythia 8.230	NLO + NNLL [78]
t-channel	Powheg Box v2	NNPDF3.0nlo nf4	Pythia 8.230	NLO [79,80]
s-channel	Powheg Box v2	NNPDF3.0nlo	Pythia 8.230	NLO [79,80]
Z/W + jets				
Z + jets	Sherpa 2.2.11 (NLO [2j], LO [5j])	NNPDF3.1nnlo	Sherpa	NNLO [81]
	MadGraph5_aMC@NLO2.6.5 (NLO [3j])	NNPDF3.0nlo	Pythia 8.240	NNLO [81]
W + jets	Sherpa 2.2.11 (NLO [2j], LO [4j])	NNPDF3.1nnlo	Sherpa	NNLO [81]
	MadGraph5_aMC@NLO2.6.5 (NLO [3j])	NNPDF3.0nlo	Pythia 8.240	NNLO [81]
Other				
VV (had.)	Sherpa 2.2.1	NNPDF3.0nnlo	Sherpa	···
VV (lep.)	Sherpa 2.2.2	NNPDF3.0nnlo	Sherpa	···
VV (lep) + jj	Sherpa 2.2.2 (LO [EW])	NNPDF3.0nnlo	Sherpa	···
$t\bar{t}W$	MadGraph5_aMC@NLO2.3.3	NNPDF3.0nlo	Pythia 8.210	NLO + NLO (EW) [70]
	Sherpa2.0.0 (LO [2j])	NNPDF3.0nnlo	Sherpa	NLO + NLO (EW) [70]
$t\bar{t}\ell\ell$	MadGraph5_aMC@NLO2.3.3	NNPDF3.0nlo	Pythia 8.210	NLO + NLO (EW) [70]
	Sherpa 2.0.0 (LO [1j])	NNPDF3.0nnlo	Sherpa	NLO + NLO (EW) [70]
$t\bar{t}Z$ $(qq, \nu\nu)$	MadGraph5_aMC@NLO2.3.3	NNPDF3.0nlo	Pythia 8.210	NLO + NLO (EW) [70]
	Sherpa 2.0.0 (LO [2j])	NNPDF3.0nnlo	Sherpa	NLO + NLO (EW) [70]

For the 0ℓ channel, five signal samples are simulated for $H \to 2a \to 4b$ ($m_a = 12$, 16, 20, 25, and 30 GeV). For the 2ℓ channel, signal simulation samples are produced for the same mass hypotheses and three more at higher masses ($m_a = 40$, 50, and 60 GeV). In addition, for the 2ℓ case, three signal samples are produced for $H \to a_1 a_2 \to 4b$, with mass hypotheses $(m_{a_1}, m_{a_2}) = (20, 30), (40, 60)$, and (50, 70) GeV, and four for $H \to a_1 a_2 \to 3a_1 \to 6b$, with mass hypotheses $(m_{a_1}, m_{a_2}) = (15, 50), (15, 90), (20, 70)$, and (30, 80) GeV. The values of the mass hypotheses for the signal samples are chosen to cover the available parameter space given the mass resolution, which varies in the range 15–20 GeV depending on the properties of the final-state particles.

The main SM backgrounds are, in order of importance, Drell-Yan production with decays into charged leptons or neutrinos $Z/\gamma^* \to \ell\ell/\nu\nu$ produced in association with jets (Z + jets), and top-quark production ($t\bar{t}$ or single top quarks) where at least one of the W bosons decays leptonically. Other backgrounds from diboson production and vector bosons produced in association with $t\bar{t}$ are also included. Processes such as triboson and four-top production are considered but found to be very small, and contributions from SM Higgs boson decays such as $H \to ZZ^* \to 4b$ are found to be negligible. For the 0ℓ case, there is an additional background from events with multiple jets, referred to as QCD multijet background, which is estimated using a data-driven method.

The precision of the matrix element (ME) generators is NLO in QCD for most samples. All samples using Pythia8 for the parton shower (PS), hadronization, and multiparton interactions (MPI) simulate the decays of b- and c-hadrons with EvtGen 1.6.0 and use the A14 tune [89] and the NNPDF2.3lo PDF set. Several simulation samples were produced with the Sherpa 2.2 generator [90]. In this setup, NLO-accurate MEs for up to two partons and MEs with

leading-order (LO) accuracy for up to four partons were calculated with the Comix [91] and OpenLoops libraries [92]. They were matched with the Sherpa parton shower [93] by using the MEPS@NLO prescription [94–97] with the set of tuned parameters developed by the Sherpa authors and based on the NNPDF3.0nnlo set of PDFs [87]. The top-quark mass was set to $m_t = 172.5$ GeV. Additional samples with alternative generators, parton shower models, and other model parameters, such as matching and resummation scales, were used to derive modeling uncertainties, as described in Sec. VIII.

Generator-level categorization of simulated events

Using a procedure similar to that described in Ref. [98], $t\bar{t}+$ jets and $Z+$ jets events are categorized depending on the flavor of associated jets. Generator-level particle jets are reconstructed from stable particles (mean lifetime $\tau > 3 \times 10^{-11}$ s) with the anti-k_t algorithm [99] with a radius parameter $R = 0.4$ and are required to satisfy $p_{\mathrm{T}} > 15$ GeV and $|\eta| < 2.5$. The flavor of a jet is determined by counting weakly decaying b- or c-hadrons with $p_{\mathrm{T}} > 5$ GeV within $\Delta R < 0.3$ of the jet axis. Events are labeled as $t\bar{t}+ \geq 1B$ or $Z+ \geq 1B$ if at least one additional jet, not originating from the decay of the $t\bar{t}$ or Z system, is matched to at least two b-hadrons and $t\bar{t}+ \geq 1b$ or $Z+ \geq 1b$ if at least one additional jet is matched to one b-hadron and no additional jets are matched to at least two b-hadrons. Similarly, events are labeled as $t\bar{t}+ \geq 1c$ or $Z+ \geq 1c$ if at least one additional jet is matched to at least one c-hadron and no jet is matched to a b-hadron. The remaining events, including those with no additional jets matched to a b-hadron or c-hadron, are labeled $t\bar{t}+$ light or $Z+$ light. Unless explicitly indicated, the category $\geq 1c$ is combined with the light category.

IV. OBJECT SELECTION

A. Tracks and primary vertex

Tracks are reconstructed in the ATLAS ID [100] and are used to reconstruct primary vertex candidates based on a pattern recognition algorithm and an adaptive vertex fitter with annealing [101]. Only events with at least one vertex are used in this search. If more than one vertex is reconstructed, the one with the highest sum of squared transverse momenta of associated tracks is chosen as the primary vertex (PV). Tracks are used to reconstruct leptons and jets. In addition, track-jets, track-subjets, and isolated secondary vertices use tracks that satisfy a *loose* selection criteria: transverse momentum $p_{\mathrm{T}} > 0.5$ GeV, longitudinal impact parameter relative to the PV multiplied by the sine of the polar angle $|z_0 \sin\theta| < 5$ mm, and transverse impact parameter relative to the beam line $|d_0| < 3.5$ mm [28].

B. Leptons

Electron candidates are reconstructed from clusters of energy deposits in the electromagnetic calorimeter associated with reconstructed tracks in the ID [102–104]. Candidates are selected with $p_{\mathrm{T}} > 10$ GeV and $|\eta| < 2.47$, excluding the calorimeter transition region $1.37 < |\eta| < 1.52$. Electrons must satisfy the *tight* likelihood-based identification criterion defined in Ref. [103] that is based on shower shape, track-quality, and track-to-cluster matching observables. Electrons are also required to satisfy a multivariate isolation criteria based on the transverse momentum of calorimeter topological clusters and tracks around the electron, and the properties of highly displaced tracks in the same region to distinguish real prompt electrons from electron candidates from hadronic jets, photon conversions, and heavy-flavor hadron decays (nonprompt electrons) [105]. Finally, the electron track is required to originate from the primary vertex by requiring $|z_0 \sin\theta| < 0.5$ mm and $|d_0/\sigma(d_0)| < 5$, where $\sigma(d_0)$ is the transverse impact parameter uncertainty computed relative to the PV.

Muon candidates are reconstructed from track segments in the various layers of the muon spectrometer and matched with tracks from the ID [106]. The final muon candidates are refitted using the complete track information from both detector systems, and are required to satisfy $p_{\mathrm{T}} > 10$ GeV and $|\eta| < 2.5$. Muons are required to satisfy the *medium* identification requirements defined in Ref. [106], an analogous multivariate isolation criteria to that used for electrons, and $|z_0 \sin\theta| < 0.5$ mm and $|d_0/\sigma(d_0)| < 3$. In the 0ℓ channel, the transverse momentum requirement for electrons and muons is lowered to $p_{\mathrm{T}} > 7$ GeV to remove backgrounds containing leptons. Muon candidates satisfying $p_{\mathrm{T}} > 4$ GeV, $|\eta| < 2.5$, and the *medium* identification requirements, are used to identify semileptonic b-hadron decays and apply a *muon-in-jet* correction [107].

C. Jets

Jets are reconstructed using the anti-k_t algorithm [99] implemented in the FastJet package [108,109] with a radius parameter $R = 0.4$. Jets are required to satisfy $p_{\mathrm{T}} > 15$ GeV and $|\eta| < 2.5$. The inputs to the clustering algorithm are determined with a particle flow algorithm that matches tracks to calorimeter topological clusters [30]. A multivariate jet vertex tagger (JVT) identifies jets with $p_{\mathrm{T}} < 60$ GeV and $|\eta| < 2.4$ as originating from the PV, suppressing jets from pile-up interactions [110]. A dedicated measurement of the JVT efficiency is carried out using $Z \to \mu\mu$ events, which is used to improve the simulation and study the performance down to $p_{\mathrm{T}} > 15$ GeV.

The uncalibrated jet four-momentum is estimated as the sum of the four-momenta of the constituent particle-flow inputs. The energy is corrected for pile-up effects, and simulations are used to calibrate the average jet energy response to the particle-jet level. A dedicated calibration is used for jets with $p_{\mathrm{T}} > 15$ GeV based on the global neural network calibration method to improve the energy resolution by correcting the jet energy scale as a function of the tracks and topological cluster shapes without

changing the average scale [111]. These sets of corrections account for variations coming from the flavor of the jet and the specific hadron composition arising from jet fragmentation. A residual *in situ* calibration is applied to data to correct the residual difference between data and MC simulations [112].

An isolation criteria for jets is defined by reclustering calibrated jets [113] with an anti-k_t algorithm and radius parameter $R = 0.8$. Jets that are the sole constituent of a reclustered jet are defined as *isolated*. The jet is not considered isolated if electrons or muons are found in the ring region $0.4 < \Delta R < 0.8$ around a jet, and if such a lepton has a relative isolation, calculated based on the sum of energies of the calorimeter topological clusters within a radius of $\Delta R < 0.3$ of the lepton, less than 0.1.

D. Large-*R* track-jet and subjet

The decay $a \to b\bar{b}$ with high p_{T}^{a}/m_a can yield a single jet originating from the hadronization of the two b-quarks. In this merged regime, the standard jet reconstruction [30] does not capture all the tracks from the hadronization of the two b-quarks, preventing efficient flavor tagging with the standard track collection associated with a jet. To capture a more representative collection of particles from a merged $a \to b\bar{b}$ decay, a track-jet with an extended track collection is associated with each isolated jet with $p_{\mathrm{T}} > 20$ GeV and $|\eta| < 2.0$. The jet is required to be isolated so that there is no ambiguity on the origin of the additional tracks. Track-jets are reconstructed by reclustering jets and tracks using an anti-k_t algorithm with radius parameter $R = 0.8$. The tracks are ghost-associated with the jets during the jet reconstruction [114]. This process creates large-R track-jets around each isolated jet. The same radius parameter was successfully used in a previous version of this search [33]. The four-momentum of the track-jet is estimated as the sum of the four-momenta of the constituent tracks.

An exclusive-k_t (EX$k_t^{(2)}$) clustering [115] of the track-jet tracks is used to reconstruct the flight axes of the two b-quark decays within a large-R track-jet. The exclusive-k_t algorithm is a sequential clustering algorithm that compares the relative k_t-distance $\min(p_{\mathrm{T},i}, p_{\mathrm{T},j}) \times \Delta R_{ij}$ between pairs of components (i, j) and the beam distance $p_{\mathrm{T},i}$. If the smallest value in the set is the beam distance, the component is removed. On the other hand, if the smallest value is the k_t-distance, then components i and j are clustered together into a pseudojet. The algorithm then iterates over the merged pseudojets and stops when two pseudojets remain, which are the track-subjets used to estimate the flight direction of the two particle-jets merged together. Studies based on boosted Higgs boson decays into a pair of b-quarks show that the exclusive-k_t clustering identifies two subjets with the correct generator-level flavor in approximately 90% of the jets [116].

E. Heavy-flavor tagging

The signal is characterized by the presence of multiple b-quarks in the final state, $4b$ or $6b$, which often can be challenging to identify using traditional methods since the decay products can be soft or overlapping in the detector. Heavy-flavor identification is extremely important in this search and several algorithms are used to identify b-hadron decays.

Two algorithms are used to classify the flavor of jets. DeXTer is an algorithm used to identify jets coming from the overlapping hadronization of two b-quarks [28]. The DeXTer algorithm uses the tracks from the associated large-R track-jet to reconstruct secondary vertices, which provide a distinctive signature of merged b-decays when more than one is reconstructed inside the same jet or when they merge in a single secondary vertex with very high mass. Displaced tracks, secondary vertices, and the properties of the two EX$k_t^{(2)}$ jets are used in a deep-set neural network (NN) to classify the flavor of the jet. The NN exploits the presence of highly displaced tracks along the two flight axes and the reconstruction of multiple secondary vertices with sufficiently large mass to identify the merged hadronization of two b-quarks. Jets that satisfy the DeXTer 60% efficiency working point (WP) are classified as B-jets. The classification is further refined by defining a tighter 40% WP. When the distinction between the two WPs is needed, jets satisfying the looser 60% WP but not the 40% WP are referred to as B_l, while jets satisfying the tighter 40% WP are referred to as B_t. The misidentification efficiency for jets with a single b-hadron is up to 2.5% and 7%, for the 40% and 60% working points, respectively, as measured using $t\bar{t}$ events [28]. Contributions from other jet flavors are found to be negligible in this search. In the 2ℓ channel, since the signal contains only low p_{T} jets, the DeXTer algorithm is not used for jets with $p_{\mathrm{T}} > 200$ GeV.

The three-momentum of a B-jet is defined by summing the three-momentum of the isolated jet with up to one muon candidate per EX$k_t^{(2)}$ -associated track-subjet if $\Delta R(\mu, \text{track-subjets}) < 0.3$. The main goal of this *muon-in-jet* correction is to include muons arising from semileptonic b-decays, which are expected to be close to the flight axes of the two b-decays represented by the EX$k_t^{(2)}$ axes. If multiple muon candidates satisfy this ΔR requirement, the highest p_{T} one is used. The mass of a B-jet is derived using a NN-based regression with a similar structure to the one used for the DeXTer algorithm, but with an additional deep-set encoder for muons inside the track-jet. The NN regression is trained using a Huber loss [117] with parameter $\delta = 1$ using signal MC samples that contain merged $a \to b\bar{b}$ decays. The target of the regression is defined as the ratio of the generator-level mass, defined by clustering all stable generator-level particles with an anti-k_t algorithm with radius parameter $R = 0.8$, and the track-jet mass.

Jets that are not classified as B-jets, either because they fail to satisfy the isolation criteria or fail to meet the 60% DeXTer WP, are classified as either b-jets or light-flavored jets (called light jets), using the DL1r algorithm [29]. The DL1r algorithm uses a deep NN combining information from several specialized low-level taggers using information from the interaction point, the impact parameter of tracks, and secondary vertices to determine the probability for a jet to be b-, c-, or light-flavored. The DL1r discriminant combines the probabilities to define WPs based on the efficiency to identify b-jets. Jets satisfying the 85% WP are classified as b-jets, and otherwise as light jets. Four WPs are defined, corresponding to efficiencies of 85%, 77%, 70%, and 60%. The five intervals define a *pseudo-continuous* (PC) b-tagging score for b-jets. The four-momentum of a b-jet is defined by summing the four-momentum of the jet with that of up to one muon candidate if $\Delta R(\mu, \text{jet}) < 0.3$.

Finally, soft secondary vertices (soft-v, or simply v) are used to identify heavy-flavor hadron production that is not energetic enough to form a jet. Soft vertices are reconstructed by clustering tracks using the TC-LVT algorithm [31]. The clustering is based on the ΔR between the tracks and the closest high-p_{T}, displaced seed tracks, defined as $p_{\mathrm{T}} > 1.5$ GeV and $|d_0/\sigma(d_0)| > 0.5$. A secondary-vertex finding algorithm is run on all tracks inside a cluster, which rejects tracks until a single vertex can be fitted [118]. The four-momentum of the soft-v is estimated as the vector sum of the tracks that fit the single vertex. Soft vertices are required to satisfy a mass requirement $0.6 < m < 6$ GeV and have $p_{\mathrm{T}} > 3$ GeV.

The generator-level flavor of nonisolated reconstructed jets and of soft vertices is defined by ΔR-matching of weakly-decaying b- and c-hadrons [29]. The generator-level flavor of isolated reconstructed jets is defined by ghost-association of b- and c-hadrons using an anti-k_t clustering algorithm with radius parameter $R = 0.8$. Only b- and c-hadrons within $\Delta R < 0.3$ of one of the two EX$k_t^{(2)}$ axes are counted.

The B-jet identification efficiency of the DeXTer algorithm is measured in collider data by using $t\bar{t}$ and $Z + g(\to b\bar{b})$ events [28]. This measurement is used to correct the identification efficiency of heavy-flavor jets in simulation as a function of the jet p_{T} and η to match the one observed in data. The efficiency scale factors are in the range of 1.0–1.9 with uncertainties in the range of 0.1–0.5 [28]. The b-jet identification efficiency of the DL1r algorithm is also measured using $t\bar{t}$, $Z+$jets, $W+$jets, and multijet events [119–121]. In addition, $t\bar{t}$ and $Z+$jets events are used to measure the identification efficiency for the DL1r algorithm for jets with $15 < p_{\mathrm{T}} < 20$ GeV [50] and the soft-v identification efficiency of the TC-LVT algorithm [31]. Discrepancies between the identification efficiency in simulation and in data stem from both mismodeling of the detector response and of the underlying physics processes.

F. Overlap removal

An overlap removal algorithm is applied to prevent double-counting of objects. Electrons are removed if they share their track with a muon. If an electron is within $\Delta R < 0.2$ of a jet, the jet is removed. However, if the closest jet surviving is in the range of $0.2 < \Delta R < 0.4$ of a selected electron, then the electron is removed. Muons are usually rejected if they are separated from the nearest jet by $\Delta R < 0.4$, though the muon is still used in the definition of the four-momentum of b-jets (see Sec. IV E). However, if this jet has fewer than three associated tracks, the jet is removed instead to avoid an inefficiency for high-energy muons undergoing significant energy loss in the calorimeter. Soft vertices within $\Delta R < 0.4$ of a jet or within $\Delta R < 0.8$ of a B-jet are removed.

G. Construction of b-objects

Figure 2 shows a summary of the different heavy-flavor algorithms used. The concept of a b-object is introduced to provide a unified approach to heavy-flavor identification. In the case of a b-jet or a soft-v, the four momentum of the b-object is defined as the four-momentum of the b-jet or of the soft-v, respectively. Two b-objects are defined per B-jet by projecting the four-momentum of the B-jet onto the four-momenta of the two EX$k_t^{(2)}$ jets.

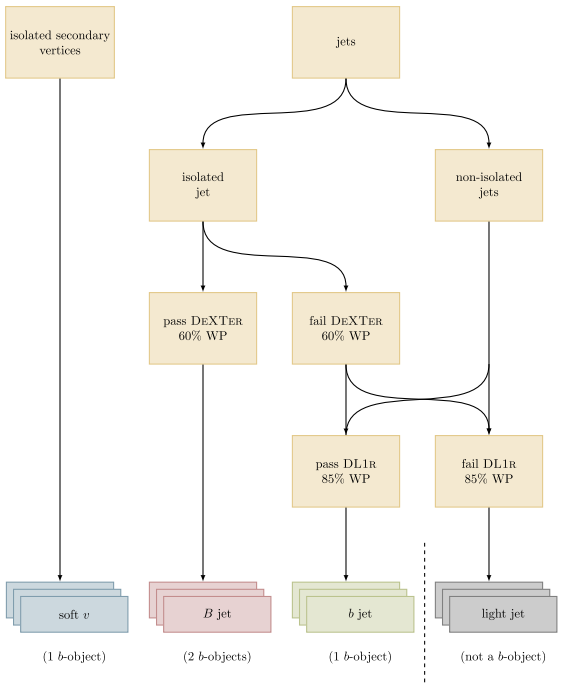

FIG. 2. Schematic overview summarizing the heavy-flavor algorithms used and the criteria used to define the b-objects.

H. Missing transverse momentum

The missing transverse momentum $\vec{p}_{\mathrm{T}}^{\,\mathrm{miss}}$, with magnitude $E_{\mathrm{T}}^{\mathrm{miss}}$, is calculated as the negative vector sum of the $\vec{p}_{\mathrm{T}}$ of all reconstructed objects and any additional tracks not associated with any reconstructed objects in the event, called the soft term [122]. It measures the imbalance of the transverse momentum in the detector, for example from $Z \to \nu\nu$.

The *effective missing transverse momentum*, $E_{\mathrm{T}}^{\mathrm{miss,eff}}$, is defined as the magnitude of the vector:

$$\vec{p}_{\mathrm{T}}^{\,\mathrm{miss,eff}} = \vec{p}_{\mathrm{T}}^{\,\mathrm{miss}} + \sum_{\mathrm{leptons}} \vec{p}_T(\ell).$$

The $E_{\mathrm{T}}^{\mathrm{miss,eff}}$ variable considers the leptons as part of the $E_{\mathrm{T}}^{\mathrm{miss}}$, facilitating comparisons of the $E_{\mathrm{T}}^{\mathrm{miss}}$ variables in samples with different lepton multiplicities.

V. EVENT SELECTION

The analysis requires at least three b-objects, $n_b + 2n_B + n_v \geq 3$, as defined in Sec. IV G. Events with exactly three b-objects are used to derive corrections to the background modeling in simulation, as described in Sec. VII. Events with at least four b-objects are used to define the signal regions (SR) and control regions (CR).

The analysis uses events with zero, one, or two charged leptons. The highest-p_{T} lepton in events with at least one lepton is required to have $p_{\mathrm{T}} > 27$ GeV and to be matched to an object reconstructed at trigger level with $\Delta R < 0.15$ to ensure good modeling of the trigger in simulation. Events with two same-flavor (SF) opposite-charge leptons are required to satisfy a requirement on the invariant mass of the two leptons $m_{\ell\ell} > 50$ GeV. Events without charged leptons are required to satisfy the $E_{\mathrm{T}}^{\mathrm{miss}}$ trigger requirement and have $E_{\mathrm{T}}^{\mathrm{miss}} > 150$ GeV to ensure trigger efficiency in the plateau, where the trigger is fully efficient [123]. After applying these requirements, the event sample is predominantly comprised of $Z+$ jets and $t\bar{t}$ events.

For the 2-lepton channel, regions are defined depending on the flavor of the leptons. SRs are required to have two SF opposite-charge leptons satisfying $|m_{\ell\ell} - m_Z| < 20$ GeV. The same condition is applied to CRs enriched in the $Z+$ jets events. CRs enhanced in $t\bar{t}$ use events with different-flavor (DF) leptons. In the $H \to 2a/a_1a_2 \to (b\bar{b})(b\bar{b})$ analyses, events are placed in SRs and CRs depending on how compatible a quadruplet of b-objects in the event is with the signal Higgs boson decay. The compatibility of each quadruplet in the event is assessed by a NN, called the *quadruplet selection NN*. This NN is invariant under permutations of b-objects and permutations of a-bosons, and is parametrized as a function of the two a-boson-mass hypotheses: m_{a_1} and m_{a_2}. Events in which no quadruplets compatible with the $H \to 2a/a_1a_2 \to (b\bar{b})(b\bar{b})$ decay are found are placed in CRs that are categorized based on the number of b-jets, B-jets, and soft-v in the event. Events with at least one compatible quadruplet are placed in SRs categorized based on the number of b-jets, B-jets, and soft-v used to form the most compatible quadruplet in the event. For the $H \to a_1a_2 \to 3a_1 \to 3(b\bar{b})$ analysis, where full reconstruction of all the objects in the final state is very rare, events are categorized according to the number of reconstructed b-jets, B-jets, and soft-v.

For the 0-lepton channel, only events with exactly two B-jets or with exactly one B-jet and two b-jets are used. Events with exactly one lepton are used to define a CR enriched in $t\bar{t}$ events. Events with zero leptons are used in SRs and CRs depending on how compatible the only quadruplet of b-objects in the event is with a signal Higgs boson decay, based on the invariant mass of the quadruplet as described in Sec. V C. Events are placed in SRs categorized based on the number of jets (n_j), b-jets, and B-jets. A summary of the event selection requirements, and the signal and control region definitions are shown in Table II.

A. 2ℓ channel: $H \to 2a \to 4b$ and $H \to a_1a_2 \to 4b$

In the $4b$ case, a quadruplet selection NN is used to identify the b-objects in the final state. The signal $H \to 2a/a_1a_2 \to 4b$ can result in different combinations of reconstructed b-objects: b-jets, B-jets, or soft vertices. The NN is trained to identify the best combination of objects under the signal hypothesis of a Higgs boson decay through two intermediate a-bosons, according to the NN structure shown in Fig. 3. The diagram corresponds to an example input combination that highlights that different b-object inputs (B-jet, b-jet, and soft-v) have different encoder NNs in the leftmost column. The second column shows different encoder NNs for the two different a-bosons, such that each possible quadruplet and each possible pairing of a quadruplet goes through different NNs in different orders, yielding different compatibility scores that are used to select the best pairing.

The NN contains fully connected encoders for b-jets, B-jets, and soft vertices. The encoded information is then used in a pair of deep-set NNs, which ensure that the overall NN score is invariant under permutations of $(b\bar{b}) \leftrightarrow (b\bar{b})$ (Higgs boson deep sets) and $b \leftrightarrow \bar{b}$ (a-boson deep sets). The a-boson deep-sets training depends on the true m_a value, since the reconstruction modes depend on the boost of the a-bosons. When considering models with additional a-bosons, $H \to a_1a_2$ permutation invariance is broken by assigning the different true mass values to each of the two a-boson encoders.

The NN is built from up to five b-objects, as shown in Fig. 4 for an example combination of objects. In cases where more than five objects are reconstructed, the

TABLE II. Summary of the event selection, and signal and control region definitions, for the 0ℓ and 2ℓ channels. The different variables are defined in Secs. IV and V.

	0ℓ	2ℓ	
Analysis channels	$H \to 2a \to 4b$	$H \to 2a/a_1a_2 \to 4b$	$H \to a_1a_2 \to 6b$
	Common selection		
Triggers	$E_{\mathrm{T}}^{\mathrm{miss}}$	Single lepton	
Leptons	$p_{\mathrm{T}} > 7$ GeV	Lead $p_{\mathrm{T}} > 27$ GeV, sublead $p_{\mathrm{T}} > 10$ GeV	
b-object multiplicity	$n_b = 2$, $n_B = 1$ or $n_B = 2$	$n_b + 2n_B + n_{\mathrm{v}} \geq 4$	
	Signal regions		
Leptons	0 leptons	2 SFOS leptons	2 SFOS leptons
$E_{\mathrm{T}}^{\mathrm{miss}}$	$E_{\mathrm{T}}^{\mathrm{miss}} > 150$ GeV	…	…
Z boson selection	…	$\lvert m_{\ell\ell} - m_Z \rvert < 20$ GeV	$\lvert m_{\ell\ell} - m_Z \rvert < 20$ GeV
Higgs boson selection	$\lvert m_{aa} - m_H \rvert < 50$ GeV	High quadruplet NN score	…
Multijet rejection	$\min \Delta\phi(E_{\mathrm{T}}^{\mathrm{miss}}, a\,\mathrm{cand}) > 60°$	…	…
Categorization	$n_j, n_b, n_{B_t}, n_{B_l}$	Quadruplet NN prediction	$n_{\mathrm{v}}, n_b, n_{B_t}, n_{B_l}$
Binning	…	Loose, Medium, Tight BDT bins	Medium, Tight BDT bins
	Control regions		
Multijet	*ABCD method*	…	…
	$150 < m_{aa} - m_H < 250$ GeV		
	$\min \Delta\phi(E_{\mathrm{T}}^{\mathrm{miss}}, a\,\mathrm{cand}) < 30°$		
Lost lepton		…	…
Signal veto	$\lvert m_{aa} - m_H \rvert > 50$ GeV		
Leptons	1 lepton, $p_{\mathrm{T}} > 27$ GeV, $\Delta R(\ell, B) > 0.8$		
$E_{\mathrm{T}}^{\mathrm{miss}}$	$E_{\mathrm{T}}^{\mathrm{miss,eff}} > 150$ GeV		
Categorization	n_b, n_{B_t}, n_{B_l}		
Z + jets *enriched*			
Signal veto	$\lvert m_{aa} - m_H \rvert > 50$ GeV	Low quadruplet NN score	Loose BDT bins
Leptons	2 SFOS leptons, lead $p_{\mathrm{T}} > 27$ GeV	2 SFOS leptons	2 SFOS leptons
$E_{\mathrm{T}}^{\mathrm{miss}}$	$E_{\mathrm{T}}^{\mathrm{miss}} < 50$ GeV, $E_{\mathrm{T}}^{\mathrm{miss,eff}} > 30$ GeV	$E_{\mathrm{T}}^{\mathrm{miss}} < 60$ GeV	$E_{\mathrm{T}}^{\mathrm{miss}} < 60$ GeV
Z boson selection	$\lvert m_{\ell\ell} - m_Z \rvert < 10$ GeV	$\lvert m_{\ell\ell} - m_Z \rvert < 10$ GeV	$\lvert m_{\ell\ell} - m_Z \rvert < 10$ GeV
Categorization	n_b, n_{B_t}, n_{B_l}	$n_{\mathrm{v}}, n_b, n_{B_t}, n_{B_l}$	$n_{\mathrm{v}}, n_b, n_{B_t}, n_{B_l}$
$t\bar{t}$ *enriched*	…		
Leptons		2 DFOS leptons	
Categorization		$n_{\mathrm{v}}, n_b, n_{B_t}, n_{B_l}$	

b-objects with highest p_{T} are used. Input combinations with more than one soft-v are not considered, since they do not contribute significantly to the acceptance. Kinematic variables characterizing the Z boson are also used in the NN. Table III summarizes the input features used for the quadruplet selection NN. The input features include the four-momenta of each input object and the likelihood for their flavor to be properly reconstructed.

The NN is trained with all $H \to 2a \to 4b$ signal simulation samples. In addition, it also uses background events, Z + jets and $t\bar{t}$ to provide training samples with broader quadruplet p_{T} and m distributions. The samples are split into training and validation samples, and the validation sample is used to measure the performance and check for overtraining. All permutations satisfying the selection criteria described above are included in the training and the correct permutation is identified based on the generator-level event history information. The NN is trained by minimizing a binary cross-entropy loss in which the correct permutation has label one and all wrong permutations have label zero. In the case of background events, all permutations have label zero.

The reconstructed event hypothesis with the largest score and the value of the NN score, $\hat{y}_{\mathrm{pred}}^{m_a}$, are used for event classification. The accuracy of associating b-partons to b-objects ranges from 60% to 98% depending on the type and properties of the reconstructed object and the signal.

Signal regions: Five SRs are defined based on the objects of the selected quadruplet and the value of the score $\hat{y}_{\mathrm{pred}}^{m_a}$. For events with quadruplets formed with two B-jets ($2B$), the score is required to be larger than $\hat{y}_{\mathrm{pred}}^{m_a} > 0.5$. For the

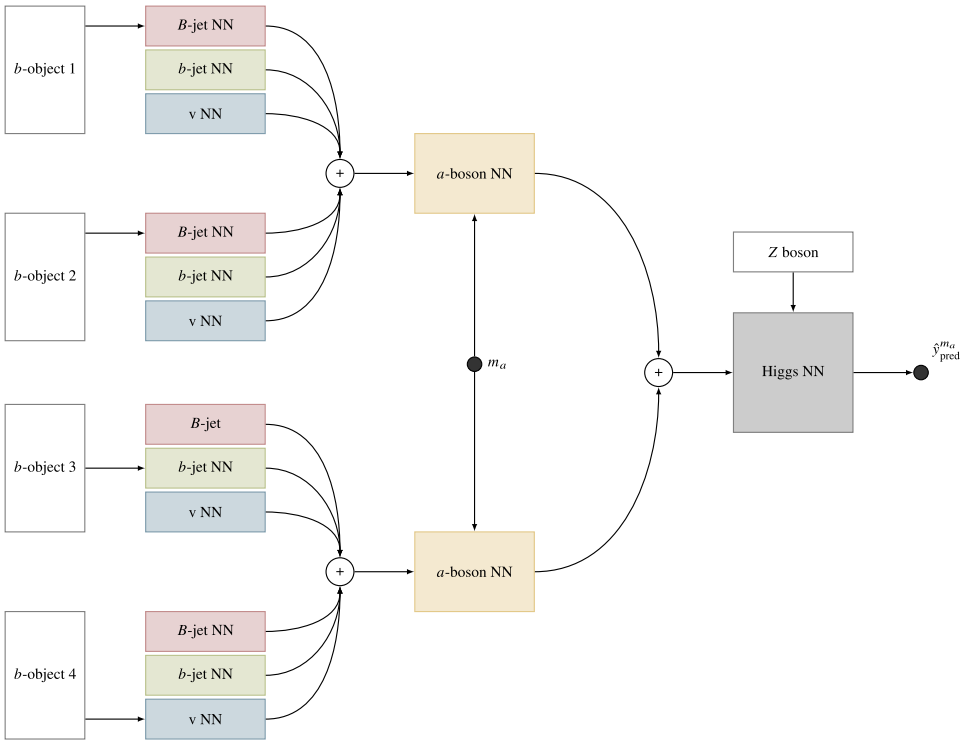

FIG. 3. Diagram of the NN used for an example of a quadruplet selection showing the case of a hypothesis with B-jets, b-jets, and soft-ν. All filled blocks are dense multilayer perceptrons (MLP) that share common weights between MLPs of the same color. The a-boson MLPs are parametrized as a function of the mass hypothesis m_a. Unfilled rectangles are inputs from the four b-objects and the Z boson. The value of the quadruplet selection score, $\hat{y}^{m_a}_{\text{pred}}$, is used to classify the b-object quadruplet. In events with more than 4b-objects, different quadruplets are tested to identify the one with highest likelihood to come from a Higgs boson decay.

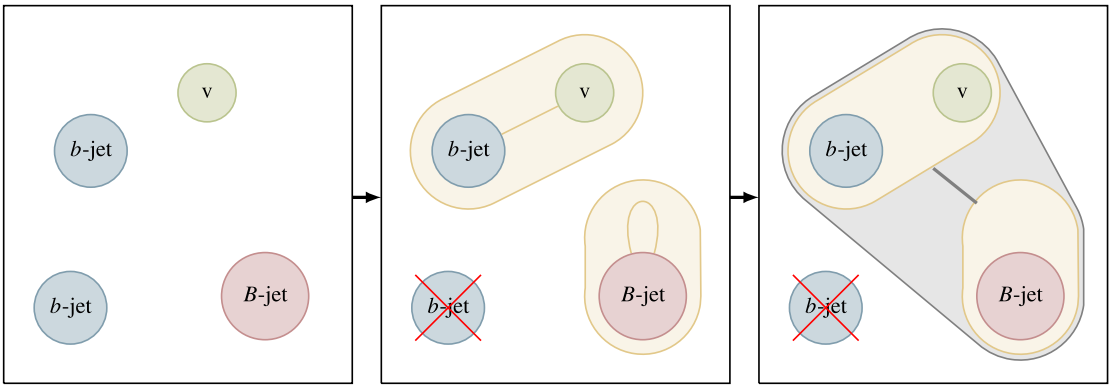

FIG. 4. Diagram depicting an example of how the NN selects a quadruplet. Each b-object is represented as an MLP (b-object MLP). The a-boson is represented as a pairing between b-objects, which also corresponds to an MLP (a-boson MLP). All physically motivated pairings are considered, including loop pairings representing merged reconstructed objects. The a-bosons themselves form new pairings representing the fully reconstructed Higgs boson, which also corresponds to an MLP (Higgs MLP). The value of this last pairing is used to select the quadruplet. The middle diagram shows the two reconstructed a-boson candidates and the rightmost diagram shows the final Higgs boson candidate.

cases where the quadruplet is formed with one B-jet and two b-jets (1B2b); with one B-jet, one b-jet and one ν (1B1b1ν); with three b-jets and one ν (3b1ν); and with four b-jets (4b); the score is required to be larger than $\hat{y}^{m_a}_{\text{pred}} > 0.05$. The choice of this $\hat{y}^{m_a}_{\text{pred}}$ requirement is intended to maintain high acceptance while ensuring accurate reconstruction of the Higgs boson decay for signal samples across the mass range probed. The $\hat{y}^{m_a}_{\text{pred}}$

TABLE III. List of features used as input for the quadruplet selection NN. The input objects are described in Sec. IV. The Z boson candidate is reconstructed as the sum of the four-momenta of the two leptons.

Feature	Description
	DeXTer-tagged B-jet
$p_{\mathrm{T}}(B)$	Jet transverse momentum
m_B	Track jet mass
$\eta(B)$	Jet pseudorapidity
$\phi(B)$	Jet azimuthal angle
B_l or B_t	Satisfies loose or tight DeXTer requirement
	DL1r -tagged b-jet
$p_{\mathrm{T}}(b)$	Jet transverse momentum
m_b	Jet mass
$\eta(b)$	Jet pseudorapidity
$\phi(b)$	Jet azimuthal angle
PC score	The pseudocontinuous DL1r score
	Soft secondary vertex v
m_{v}	Track mass of the secondary vertex
$p_{\mathrm{T}}(\mathrm{v})$	Secondary vertex transverse momentum
$\eta(\mathrm{v})$	Secondary vertex pseudorapidity
$\phi(\mathrm{v})$	Secondary vertex azimuthal angle
L_{3D}	Decay length relative to the PV
$S_{L_{3D}}$	Decay length significance
	Z boson candidate
$p_{\mathrm{T}}(Z)$	Z boson candidate transverse momentum
$\eta(Z)$	Z boson candidate pseudorapidity
$\phi(Z)$	Z boson candidate azimuthal angle
$m_{\ell\ell}$	Z boson candidate mass

requirements are not optimized to reject background since a dedicated discriminator is used based on the properties of the selected quadruplet. Figure 5 shows example distributions of the $\hat{y}^{m_a}_{\mathrm{pred}}$ observable for the $2B$ and $1B2b$ cases.

Control regions: Six CRs for each of the main backgrounds $Z+$jets and $t\bar{t}$ are used based on the b-object multiplicity, as summarized in Table IV. The regions distinguish between events containing jets satisfying the loose and tight DeXTer tagging requirements to enhance the sensitivity to different heavy-flavor background components. The control regions including the combination of b-objects corresponding to $1B2b$ and $1B1b1\mathrm{v}$ are combined due to the low expected number of events. The $Z+$jets control regions are defined by inverting the requirements on the quadruplet selection NN score $\hat{y}^{m_a}_{\mathrm{pred}}$. Additional requirements are applied to the $Z+$jets control region to increase the purity: $|m_{\ell\ell}-m_Z|<10$ GeV and $E_{\mathrm{T}}^{\mathrm{miss}}<60$ GeV. The same categorization is used to build the control regions enriched in $t\bar{t}$ events using events with two charged leptons of DF. In this case, no quadruplet selection is applied, since the signal has SF leptons, and no additional mass cut is imposed, since the region is already very pure in $t\bar{t}$ events.

B. 2ℓ channel: $H\to a_1a_2\to 3a_1\to 6b$

The $6b$ search targets signals where the Higgs boson decays into two a-bosons with different mass $H\to a_1a_2$ and the heavier one can then decay into the lighter one, $a_2\to 2a_1$, resulting in six b-quarks in the final state $H\to a_1a_2\to 3a_1\to 6b$. In only approximately 1% of the signal decays, the six b-objects would be reconstructed and if the full reconstruction of the Higgs boson cascade

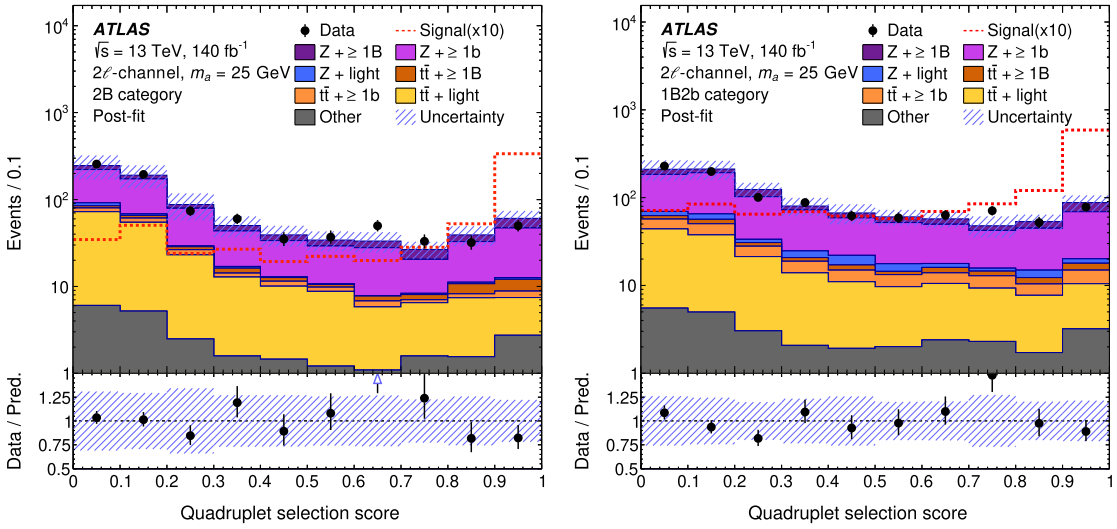

FIG. 5. The quadruplet selection score $\hat{y}^{m_a}_{\mathrm{pred}}$ distribution assuming the signal hypothesis $m_a=25$ GeV for the b-object categories (a) $2B$ and (b) $1B2b$. Signal events for the $m_a=25$ GeV mass hypothesis are also shown, assuming $\mathcal{B}=1$ and scaling this signal by a factor of ten. The category labeled "Other" includes processes with small contributions to the total yield (diboson, $t\bar{t}Z$, and $t\bar{t}W$). The lower panels show the ratio of the observed to the estimated SM background. The hashed area represents the total uncertainty in the background.

TABLE IV. Overview of the b-object multiplicity regions used for the control regions in the search targeting the $4b$ final state. The subscripts in B_l and B_t refer to the DeXTer B-jet loose and tight working points, respectively.

$2\ell 4b$ control regions	B-jets	b-jets	Soft v
B_tB_l	$\geq 2B_t$ or $1B_t + 1B_l$	⋯	⋯
$2B_l$	$\geq 2B_l$	⋯	⋯
$1B_t2b$ (includes $1B_t1b1\text{v}$)	$1B_t$	≥ 2 (or ≥ 1	and ≥ 1)
$1B_l2b$ (includes $1B_l1b1\text{v}$)	$1B_l$	≥ 2 (or ≥ 1	and ≥ 1)
$4b$	0	≥ 4	⋯
$3b1\text{v}$	0	≥ 3	≥ 1

TABLE V. Overview of the multiplicity regions designed to target the $6b$ final state for both signal and control regions. No requirement on the number of soft vertices is applied for the $2B0b$, $2B1b$, and $1B2b$ regions.

$2\ell 6b$ regions	B-jets	b-jets	Soft vertices
2B0b	≥ 2	0	⋯
2B1b	≥ 2	≥ 1	⋯
1B2b	1	≥ 2	⋯
4b0v	0	≥ 4	0
4b1v	0	≥ 4	≥ 1
3b1v	0	3	≥ 1

decay were required, the signal efficiency would be low. Instead, the analysis is performed with partially reconstructed events that are classified solely based on the number and type of reconstructed b-objects, and no attempt to identify all the b-objects in the event is made. Moreover, the regions are not defined exclusively to account for the rare cases where more than four b-objects are reconstructed. Table V summarizes the b-object multiplicity used to form the event regions when searching for signals with six b-quarks in the final state.

The SRs and the Z + jets CRs are defined by the boosted decision tree (BDT) discriminators described in Sec. VI B. To increase the purity of Z + jets events and suppress $t\bar{t}$ contributions in the CRs, stricter requirements are applied on the dilepton invariant mass $|m_{\ell\ell} - m_Z| < 10$ GeV and the missing transverse momentum $E_{\text{T}}^{\text{miss}} < 60$ GeV. The $t\bar{t}$ control regions are defined using the same b-object multiplicity categories shown in Table V. As in the case of $4b$, events with different-flavor leptons are selected, and no additional selection is applied on the invariant mass of the leptons $m_{\ell\ell}$.

C. 0ℓ channel: $H \to 2a \to 4b$

Since it uses a relatively simpler signal region selection and background discrimination strategy, the 0ℓ channel is used only to search for $H \to 2a \to 4b$ decays. Events in the 0ℓ channel are sorted into eight regions depending on the total number of jets (j), the B-jet multiplicity and whether they are tight or loose (B_t or B_l), and the b-jet multiplicity, as shown in Table VI. The regions with two b-jets are also required to have $\Delta\phi(b_1, b_2) < 100°$ to suppress contributions from QCD multijet production.

In each category, the heavy-flavor jets are used to reconstruct the Higgs boson. This parton-jet matching is nearly fully accurate due to the large Higgs boson boost imposed by the $E_{\text{T}}^{\text{miss}}$ trigger requirement. The $2B$ channels target a-boson masses in the range of $m_a \simeq$ 10–20 GeV, while the $1B2b$ channel is more sensitive to $m_a \simeq 20$–30 GeV. The Higgs boson mass $m_H \approx m_{aa}$ is defined as the invariant mass of the a-candidate jets, depending on the final state. For the final state channel with two B-jets, each B-jet is an a-candidate, and thus m_{aa} is defined as m_{2B}. For the final state channels with one B-jet and two b-jets, the B-jet is an a-candidate and the two b-jets combined are an a-candidate, and thus m_{aa} is defined

TABLE VI. Overview of the signal regions for the $0\ell 4\text{b}$ final state. The requirements on the number of jets are exclusive.

$0\ell 4b$ Regions	B-jets	b-jets	light-jets	Additional selections
$2B_t(2j)$	$2B_t$	0	0	⋯
$B_tB_l(2j)$	$1B_t + 1B_l$	0	0	⋯
$2B_l(2j)$	$2B_l$	0	0	⋯
$2B_t(3j)$	$2B_t$	0	1	⋯
$B_tB_l(3j)$	$1B_t + 1B_l$	0	1	⋯
$2B_l(3j)$	$2B_l$	0	1	⋯
$1B_t2b$	$1B_t$	2	0	$\Delta\phi(b_1, b_2) < 100°$
$1B_l2b$	$1B_l$	2	0	$\Delta\phi(b_1, b_2) < 100°$

as m_{1B2b}. Events are categorized into regions based on the number of leptons and $E_{\mathrm{T}}^{\mathrm{miss,eff}}$.

Signal regions: Events are required to be selected with the $E_{\mathrm{T}}^{\mathrm{miss}}$ trigger and satisfy $E_{\mathrm{T}}^{\mathrm{miss}} > 150$ GeV to ensure high trigger efficiency. Events are also required to have no charged leptons with $p_{\mathrm{T}} > 7$ GeV and satisfy $|m_{aa} - 125| < 50$ GeV. An additional selection requirement on the minimum azimuthal distance between the $E_{\mathrm{T}}^{\mathrm{miss}}$ vector and the two reconstructed a-bosons, $\min \Delta\phi(E_{\mathrm{T}}^{\mathrm{miss}}, a\,\mathrm{cand}) > 60°$, is imposed to suppress multijet backgrounds.

Control regions: Events in the 1ℓ CR are selected with single-lepton triggers and requiring exactly one charged lepton with $p_{\mathrm{T}} > 27$ GeV matched to the object reconstructed at trigger level. The lepton is also required to have $\Delta R(\ell, B) > 0.8$, since most sources of backgrounds do not have leptons produced close to the jets. In order for the CR to be as similar to the SR as possible, events are required to satisfy $E_{\mathrm{T}}^{\mathrm{miss,eff}} > 150$ GeV. Finally, events must have $|m_{aa} - 125| > 50$ GeV to remove contributions from the signal $W(\to \ell\nu)H$ production mode. The processes in the 1ℓ CR are also background processes in the SR when the lepton is outside of acceptance region or when it is not successfully reconstructed and identified (lost-lepton background).

A CR with 2ℓ is used for results using the 0ℓ channel only, mainly to study the sensitivity of this channel alone. This region contains events selected with the single-lepton trigger with exactly two charged leptons with $p_{\mathrm{T}} > 15$ GeV. The leading lepton is additionally required to satisfy $p_{\mathrm{T}} > 27$ GeV and to match to an object reconstructed at trigger level. Leptons are required to have $\Delta R(\ell, B) > 0.8$ and events are required to satisfy $E_{\mathrm{T}}^{\mathrm{miss,eff}} > 30$ GeV. Events are also required to have $|m_{aa} - 125| > 50$ GeV to remove contributions from the $Z(\to \ell\ell)H$ production mode and are required to have $|m_{\ell\ell} - m_Z| < 10$ GeV and $E_{\mathrm{T}}^{\mathrm{miss}} < 50$ GeV to improve the purity of $Z \to \ell\ell$ events.

VI. SIGNAL AND BACKGROUND DISCRIMINATION

A. 2ℓ channel: $H \to 2a \to 4b$ and $H \to a_1a_2 \to 4b$

As described in Sec. V A, the 2ℓ quadruplet selection NN selects the best combination of four b-objects to reconstruct the decay chain $H \to 2a/a_1a_2 \to 4b$. The score of the best hypothesis provides strong discrimination between signal and background since the main sources of background do not have a similar cascade decay. The Higgs boson is constructed from the two a-bosons and the Z boson is constructed from the two leptons. Additional kinematic properties further discriminate signal from background, and these variables are used as inputs to a BDT.

The BDT is trained using the input features summarized in Table VII separately for each mass hypothesis and for each region. Signal events are characterized by the presence of a resonance resulting from the Higgs boson decay $H \to 2a/a_1a_2 \to 4b$, where these four b-objects are determined by the quadruplet selection NN. Several variables are used to reconstruct the particles from the signal decay chain and probe their kinematic properties. These include the kinematics of the a-bosons, particularly the transverse momentum $p_{\mathrm{T}}(a)$ and the reduced mass, defined as:

$$m_a^{\mathrm{red}} = m_a - m_a^{\mathrm{gen}}$$

where m_a^{gen} corresponds to the mass hypothesis under consideration. Other variables include the transverse momentum of the Higgs boson $p_{\mathrm{T}}(H)$ and the reduced Higgs boson mass m_H^{red} reconstructed from the two a-bosons, defined as:

$$m_H^{\mathrm{red}} = \left(m_H - m_H^{\mathrm{gen}}\right) - \left(m_{a_1} - m_{a_1}^{\mathrm{gen}}\right) - \left(m_{a_2} - m_{a_2}^{\mathrm{gen}}\right),$$

where $m_H^{\mathrm{gen}} = 125$ GeV corresponds to the Higgs boson mass, and $m_{a_1}^{\mathrm{gen}}$ and $m_{a_2}^{\mathrm{gen}}$ to the a-boson mass hypotheses being considered, where these can be equal to each other or correspond to two different a-bosons. The ordering $a_{1,2}$ of the two reconstructed a-bosons is determined by the quadruplet selection NN, which ensures consistent ordering in the case of models with different a-bosons, and consistent ordering based on reconstruction channel in models with a single a-boson. The reduced mass m_H^{red} has better resolution than m_H due to correlations in the energy response of the jets.

Additional kinematic variables show differences between signal and background and are used as input variables for the BDT. The cosine of the polar angle of the a-boson in the rest frame of the Higgs boson, $\cos\theta^*$, is sensitive to the spin-0 nature of the Higgs boson. The spin-1 nature of the Z boson is probed by the cosine of the angle between the two leptons (ℓ_1 and ℓ_2) in the Collins-Soper (SC) frame [124] $\cos\theta_{\mathrm{CS}}$, defined as

$$\cos\theta_{\mathrm{CS}} = 2\frac{\ell_1^+\ell_2^- - \ell_1^-\ell_2^+}{m_{\ell\ell}\sqrt{m_{\ell\ell}^2 + p_{\mathrm{T}}^2(Z)}},$$

where $\ell_i^{\pm} = (E_i \pm p_{z,i})/\sqrt{2}$ with E_i and $p_{z,i}$ corresponding to the energy and momentum along the z-direction of the lepton $i = 1, 2$, and where $p_{\mathrm{T}}(Z)$ is the Z boson transverse momentum. The variables capturing the kinematics of the Z boson are $p_{\mathrm{T}}(Z)$ and the Z boson mass $m_{\ell\ell}$. In addition, the kinematics of the ZH events, where the Z boson is recoiling against the Higgs boson in the case of the signal, is probed by the separation in ϕ and η between the Z boson and the Higgs boson, $\Delta\phi(H, Z)$ and $\Delta\eta(H, Z)$, respectively. Finally, the $E_{\mathrm{T}}^{\mathrm{miss}}$ variable is used to distinguish the $t\bar{t}$ background, which contains neutrinos in the final state, from the signal.

TABLE VII. List of input variables for the multivariate BDT discriminant used to distinguish signal and background in the 2ℓ channel.

Feature	Description
	$2\ell 4b$ Variables
$p_{\mathrm{T}}(a_1)$, $p_{\mathrm{T}}(a_2)$	a-boson transverse momenta
$m_{a_1}^{\mathrm{red}}$, $m_{a_2}^{\mathrm{red}}$	a-boson reduced masses
$m_{\mathrm{H}}^{\mathrm{red}}$	Higgs boson reduced mass
$p_{\mathrm{T}}(H)$	Higgs boson transverse momentum
$\cos\theta^*$	Cosine of the a-boson polar angle in the Higgs boson rest frame
$\cos\theta_{\mathrm{CS}}$	Cosine of the angle between leptons in the Collins-Soper frame [124]
$p_{\mathrm{T}}(Z)$	Z boson transverse momentum
$m_{\ell\ell}$	Z boson invariant mass
$\lvert\Delta\phi(Z,H)\rvert$	Azimuthal angle between the Higgs boson and the Z boson
$\lvert\Delta\eta(Z,H)\rvert$	Pseudorapidity separation between the Higgs boson and the Z boson
$\hat{y}_{\mathrm{pred}}^{m_a}$	Quadruplet selection NN score
$E_{\mathrm{T}}^{\mathrm{miss}}$	Missing transverse energy
	$2\ell 6b$ Variables
m_{incl}	Invariant mass of all b-objects
$\Delta R(B,B)$	ΔR between the two leading B-jets
$\Delta R(B,bb)$	ΔR between the leading B-jet and the 4-momentum sum of the two leading b-jets
$\Delta R^{\mathrm{average}}(b,b)$	ΔR between two b-jets, averaged over all possible pairs of b-jets
$\Delta R(\mathrm{EX}k_t^{(2)},\mathrm{EX}k_t^{(2)})$	ΔR between the two $\mathrm{EX}k_t^{(2)}$ associated track-subjets for the leading B-jet
$\cos\theta^*(2B)$	Cosine of the sum of the two leading B-jets in the ZH rest frame
$\cos\theta^*(1B2b)$	Cosine of the sum of the leading B-jet and the two leading b-jets in the ZH rest frame
$\cos(\theta^*)(\mathrm{incl})$	Cosine of the sum of all b-objects (B-jets, b-jets and soft vertices) in the ZH rest frame
$E_{\mathrm{T}}^{\mathrm{miss}}$	Missing transverse energy
$H_{\mathrm{T}}^{\mathrm{had}}$	Scalar sum of the p_{T} of all jets
$\Delta R(\ell,\ell)$	ΔR between the two leptons

Figure 6 shows several key kinematic distributions used as inputs for the BDT. The BDT training is performed using the XGBOOST framework [125]. The output score is used to define three bins (loose, medium, and tight), which are optimized for each signal mass hypothesis and each region based on the expected signal significance. The loose and medium regions are enriched in backgrounds and are used to validate the agreement between the data and the background predictions for the BDT input variables in several regions that probe different background composition. Good agreement between data and the background prediction is observed.

B. 2ℓ channel: $H \to a_1a_2 \to 3a_1 \to 6b$

As described in Sec. V B, six regions are used to search for $H \to a_1a_2 \to 3a_1 \to 6b$ decays based on the number of b-objects in the final state. Even though there is no attempt to identify all the objects in the final state, a similar strategy is employed to discriminate signal and background by combining kinematic variables into a multivariate BDT discriminant in each region. The Higgs boson is constructed from the sum of the b-objects, while the Z boson is determined from the two leptons. The input variables are summarized in Tables VII and VIII shows the combination of variables used in each region.

The kinematic variables include the invariant mass of all reconstructed b-objects, m_{incl}, which peaks around the Higgs boson mass for the signal. Additional variables probe differences between the angular separation between b-objects in signal and background, which are typically more separated for backgrounds such as $t\bar{t}$ since the b-objects originate from the decays of different particles. The separation variables depend on the b-objects available in the final state and if multiple b-objects are available, the ones with the highest transverse momentum are used. If B-jets are available, the angular separation between two B-jets $\Delta R(B,B)$, between a B-jet and the sum of two b-jets $\Delta R(B,bb)$, or between the two $\mathrm{EX}k_t^{(2)}$ track-subjets in the B-jet $\Delta R(\mathrm{EX}k_t^{(2)},\mathrm{EX}k_t^{(2)})$ are used. In the case of multiple b-jets, the angular separation between the b-jets, averaged over all combinations of b-jets, $\Delta R^{\mathrm{average}}(b,b)$, is also used as an input variable.

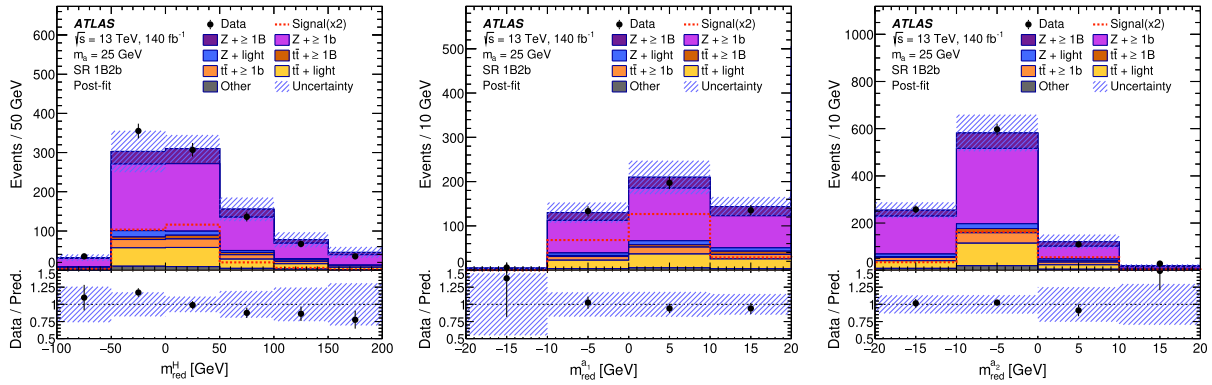

(a) (b) (c)

FIG. 6. The kinematic distributions for events in the $1B2b$ signal region assuming the a-boson signal mass hypothesis $m_a = 25$ GeV; (a) the reduced mass of the reconstructed Higgs boson, (b) the reduced mass of the reconstructed a_1-boson, and (c) the reduced mass of the reconstructed a_2-boson. The SM background is compared with the expected signal events assuming $\mathcal{B}(H \to 2a \to 4b) = 1$ and scaling such an expected signal by a factor of two. These are the highest-ranked variables in the BDT used to discriminate between signal and background. The category labeled "Other" includes processes with small contributions to the total yield (diboson, $t\bar{t}Z$, and $t\bar{t}W$). The lower panels show the ratio of the observed to the estimated SM background. The hashed area represents the total uncertainty in the background.

In addition, the variable $\cos\theta^*$ can also be used to distinguish signal and backgrounds since it probes the spin-0 nature of the Higgs boson. In this case, the polar angle of the Higgs boson is used in the rest frame of the parent ZH system. Three variables are used to discriminate signal from background based on the properties of the backgrounds. These include the $E_{\mathrm{T}}^{\mathrm{miss}}$ variable, which is expected to be larger in the case of the $t\bar{t}$ background, due to the presence of neutrinos, and the $H_{\mathrm{T}}^{\mathrm{had}}$ variable, defined as the scalar sum of the p_{T} of all jets, which is also expected to be larger in $t\bar{t}$ events due to the larger mass and hadronic activity. Finally, the separation between the leptons $\Delta R(\ell,\ell)$ tends to be smaller for signal than for the $Z+$ jets background since the Z boson tends to have lower transverse momentum in the latter case. The BDT is trained similarly to the $4b$ regions (see Sec. VI A).

TABLE VIII. List of variables used for the multivariate BDT discriminant in the $6b$ regions.

Variable	2B0b	2B1b	1B2b	4b	4b1v	3b1v
m_{incl}	✓	✓	✓	✓	✓	✓
$\Delta R(B,B)$	✓	✓	…	…	…	…
$\Delta R(B,bb)$	…	…	✓	…	…	…
$\Delta R^{\mathrm{average}}(b,b)$	…	…	…	✓	✓	✓
$\Delta R(\mathrm{EX}k_t^{(2)},\mathrm{EX}k_t^{(2)})$	✓	…	✓	…	…	…
$\cos(\theta^*)(2B)$	✓	…	…	…	…	…
$\cos(\theta^*)(1B2b)$	…	…	✓	…	…	…
$\cos(\theta^*)(\mathrm{incl})$	…	…	…	✓	…	✓
$E_{\mathrm{T}}^{\mathrm{miss}}$	✓	✓	✓	✓	✓	✓
$H_{\mathrm{T}}^{\mathrm{had}}$	✓	…	✓	✓	…	✓
$\Delta R(\ell,\ell)$	✓	✓	✓	✓	✓	✓

VII. BACKGROUND ESTIMATE

A. Background estimate for the 2ℓ channel

The backgrounds in the 2ℓ channel are described using MC simulations that are corrected to data for the two main sources of background events: $Z+$ jets and $t\bar{t}$. The correction factors are derived using data samples enhanced in these two types of background processes following a similar procedure to several other ATLAS analyses [126,127].

Corrections to $t\bar{t}$ are derived using events that have two DF opposite-charge leptons and at least two b-jets. The corrections are also applied to the single top tW process, since it cannot be distinguished from $t\bar{t}$ when additional jets are produced. For $Z+$ jets, corrections are derived using events with two leptons with the same flavor and opposite-sign charge (SFOS) and at least two jets. Events are also required to satisfy $n_b + 2n_B + n_v = 3$, $|m_{\ell\ell} - m_Z| < 20$ GeV, and $E_{\mathrm{T}}^{\mathrm{miss}} < 60$ GeV to reduce $t\bar{t}$ contributions.

A first step, only applied to the $t\bar{t}$ and tW processes, corrects the rate of production of additional heavy flavor (HF) jets, which is known to be mismodeled at high multiplicities of heavy-flavor jets [128]. This correction is derived from the distribution of the sum of the PC b-tagging scores for all jets in the event. The ratio of the observed data and predictions are used to reweight the $t\bar{t}$ and tW events as a function of this distribution, and Fig. 7 shows the variable after the correction is applied.

The second step improves the modeling of kinematic properties, particularly at high jet multiplicities and high jet p_{T}, to match observed distributions in data. For both $t\bar{t}$ and $Z+$ jets events, the jet multiplicity distribution is corrected in simulation to match the data. An additional correction

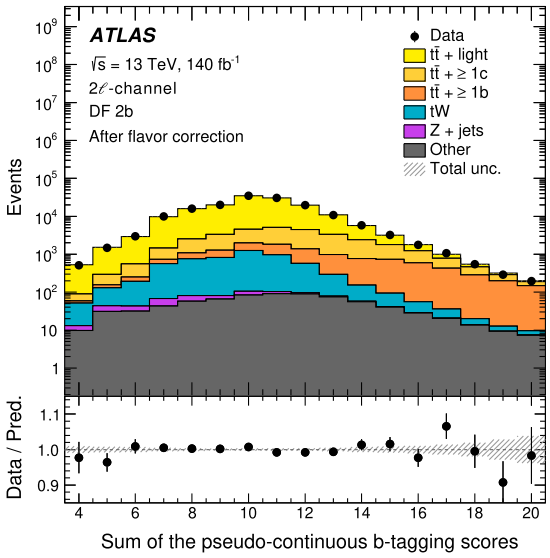

FIG. 7. Comparison of data and simulation for the sum of the PC b-tagging score of all jets per event, after applying a correction to account for the different fractions of $t\bar{t}$ components with additional heavy-flavor jets. The lower panel shows the ratio of the observed to the estimated SM background. The shaded area represents the combination of statistical and flavor-tagging uncertainties. The category labeled "Other" includes processes with small contributions to the total yield (diboson, $t\bar{t}Z$, and $t\bar{t}W$). The correction is less than 5% in the bulk of the distribution, increasing to 20–30% in the tail.

to improve the modeling of the p_{T} of objects in the event is applied using different kinematic variables for $t\bar{t}$ and $Z+$ jets events. For the $t\bar{t}$ background, the variable used for the correction is a modified version of H_{T}, the scalar sum of the p_{T} of all jets and leptons. The reduced H_{T} or $H_{\mathrm{T}}^{\mathrm{red}}$ variable is then defined as the H_{T} corrected by the average p_{T} contributed by each additional jet, where the correction is applied to reduce the dependence on the jet multiplicity. The variable $H_{\mathrm{T}}^{\mathrm{red}}$ is defined as:

$$H_{\mathrm{T}}^{\mathrm{red}} = H_{\mathrm{T}} - (n_{\mathrm{j}} - 2)\Delta H_{\mathrm{T}},$$

where n_{j} is the number of jets in the event, and ΔH_{T} is the approximate contribution of each additional jet to the H_{T}, defined as:

$$\Delta H_{\mathrm{T}} = \left\langle \frac{\langle H_{\mathrm{T}}^{n_{\mathrm{j}}} \rangle - \langle H_{\mathrm{T}}^{n_{\mathrm{j}}=2} \rangle}{n_{\mathrm{j}} - 2} \right\rangle_{n_{\mathrm{j}}=3,4,\ldots,\geq 8},$$

where $H_{\mathrm{T}}{}^{n_{\mathrm{j}}}$ is the H_{T} value for an event with jet multiplicity n_{j}. For the case of $Z+$ jets, the variable used for the correction is the transverse momentum of the Z boson p_{T}^{Z}. The resulting distributions comparing data and simulation after applying the kinematic corrections on the jet multiplicity and on $H_{\mathrm{T}}^{\mathrm{red}}$ or p_{T}^{Z} are displayed in Figs. 8(a) and 8(b) for $t\bar{t}$ and $Z+$ jets, respectively.

B. Background estimate for the 0ℓ channel

For the 0ℓ channel, the backgrounds can be classified according to the source of $E_{\mathrm{T}}^{\mathrm{miss}}$. The first source is $E_{\mathrm{T}}^{\mathrm{miss}}$ from neutrinos, which do not interact with the detector, mainly from $Z+$ jets with $Z \to \nu\nu$. Another source of $E_{\mathrm{T}}^{\mathrm{miss}}$ arises from leptons failing reconstruction, identification, or isolation requirements, referred to as "lost-leptons," primarily from $t\bar{t}+$ jets, $W+$ jets, and single-top events. Finally, $E_{\mathrm{T}}^{\mathrm{miss}}$ also arises from the mis-measurement of the jet energy, which can occasionally cause high $E_{\mathrm{T}}^{\mathrm{miss}}$ that is typically aligned with the jet. This corresponds to the QCD multijet background.

Several methods are used to estimate the background contributions to the SRs, depending on the source of $E_{\mathrm{T}}^{\mathrm{miss}}$. As described in Sec. V C, CRs enhanced in background processes are used to normalize the dominant background predictions to data. The 2ℓ CR is used to normalize the $Z+$ HF background that has $E_{\mathrm{T}}^{\mathrm{miss}}$ from neutrinos, while the 1ℓ CR is used to normalize the backgrounds with lost-leptons.

The QCD multijet background is estimated from data using an "ABCD" method, where requirements are applied on two variables separating signal and background defining four regions. The background yield in the SR is estimated by using the other three CRs. The two variables used are the minimum difference between the azimuthal angle of the $E_{\mathrm{T}}^{\mathrm{miss}}$ vector and the two a-candidates, $\min \Delta\phi(E_{\mathrm{T}}^{\mathrm{miss}}, a)$, and the invariant mass of the two a-candidates that reconstruct the Higgs boson, m_{aa}, where the a-candidates are formed from a B-jet or two b-jets, depending on the final state. The signal tends to have higher $\min \Delta\phi(E_{\mathrm{T}}^{\mathrm{miss}}, a)$ compared with the background, and a requirement of $\min \Delta\phi(E_{\mathrm{T}}^{\mathrm{miss}}, a) > 60°$ is used to define the SR, while events with $\min \Delta\phi(E_{\mathrm{T}}^{\mathrm{miss}}, a) < 30°$ are used in the CRs. Events in the SR are additionally required to satisfy $75\ \mathrm{GeV} < m_{aa} < 175\ \mathrm{GeV}$, while events with $275\ \mathrm{GeV} < m_{aa} < 375\ \mathrm{GeV}$ are used in the CRs. The mass range for the SR is chosen to have high signal efficiency and the range for the CRs are chosen to be of the same size as the SR. Validation regions next to the SRs are used to validate the background estimate. A schematic of the regions is shown in Fig. 9.

The QCD multijet background in each of the CRs: B, C, and D is estimated as the difference between event yields in data and the background prediction for all other processes. The QCD multijet background estimate in the SR A is determined as $\mathrm{A} = \mathrm{B} \times (\mathrm{C}/\mathrm{D})$. The QCD multijet background estimate is validated in a sample that is similar to the SR but enhanced in background events (validation region A*, using control regions B*, C, and D). The validation region shows good agreement between data and the background prediction, indicating that the degree of correlation between the two variables used in the ABCD estimate does not have a significant effect on the result. The

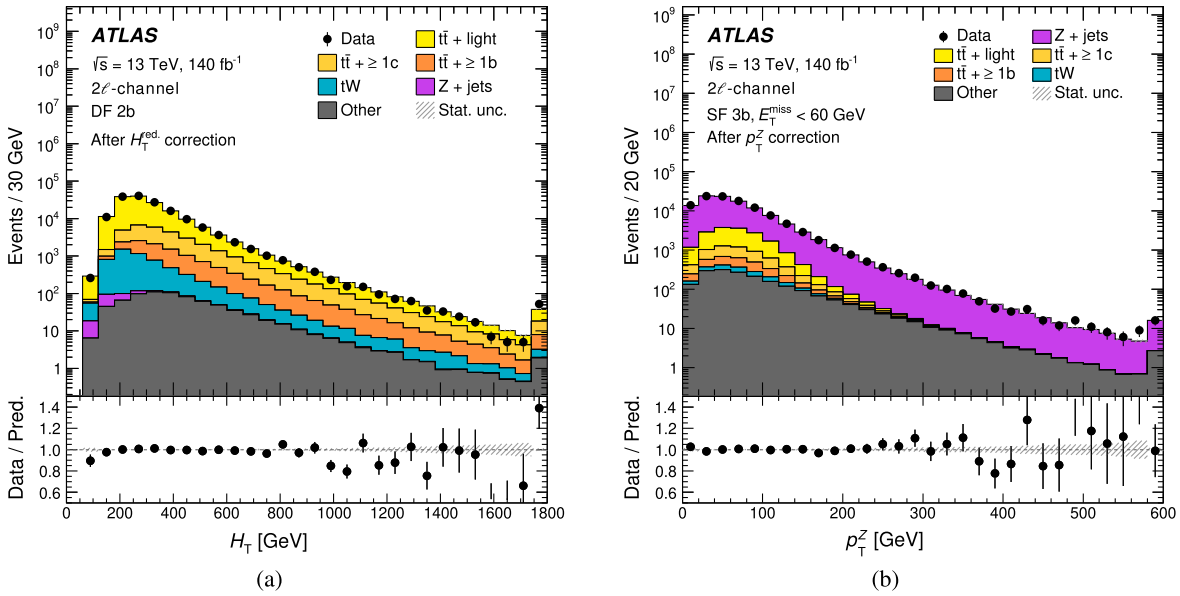

FIG. 8. Comparison of data and simulation for (a) H_{T} distribution used for the modeling of the $t\bar{t}$ background and (b) p_{T}^{Z} distribution used for the modeling of the $Z+$ jets background, after applying corrections. The lower panels show the ratio of the observed to the estimated SM background. The shaded area represents the combination of statistical and flavor-tagging uncertainties. Overflow events are included in the last bin. The category labeled "Other" includes processes with small contributions to the total yield (diboson, $t\bar{t}Z$, and $t\bar{t}W$).

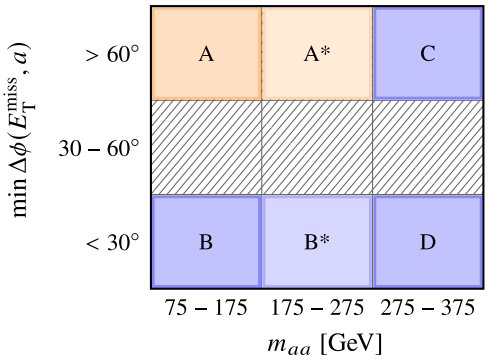

FIG. 9. Diagram of the four regions used in the "ABCD" method to estimate the QCD multijet background for the 0ℓ channel. The regions A* and B* are used to validate the estimate and derive uncertainties.

estimate obtained with the validation region is used to derive an uncertainty in this background contribution, as described in Sec. VIII B.

VIII. SYSTEMATIC UNCERTAINTIES

A. Experimental uncertainties

The uncertainty in the integrated luminosity for the full Run 2 data is 0.83% [61]. An uncertainty associated with the modeling of the pile-up in simulation covers the difference between the predicted and measured fiducial inelastic cross section [129].

Uncertainties associated with charged leptons arise from the trigger, reconstruction, identification, and isolation, and the momentum scale and resolution. Efficiencies, and scale and resolution calibrations are measured using $Z \to \ell^+\ell^-$ and $J/\psi \to \ell^+\ell^-$ events [102,106]. Systematic uncertainties in these measurements are applied to electrons and muons, accounting for 22 independent variations.

Uncertainties associated with the $E_{\mathrm{T}}^{\mathrm{miss}}$ trigger are propagated from a dedicated measurement of data-to-simulation scale factors [123]. The trigger efficiency as a function of the offline $E_{\mathrm{T}}^{\mathrm{miss}}$ for an inclusive sample is compared with events with at least four jets. The differences between the efficiency in these two samples are incorporated as an uncertainty as a function of offline $E_{\mathrm{T}}^{\mathrm{miss}}$ and these differences are below 2%.

The jet energy scale uncertainty is derived by combining information from test-beam data, LHC collision data and simulation [112]. The jet energy resolution uncertainty is derived from simulation and dijet p_{T}-balance measurements as a function of jet p_{T} and rapidity [112]. The uncertainty in the JVT efficiency to identify and remove jets from pile-up is measured in $Z \to \mu^+\mu^-$ events in data [110]. This measurement is extended to cover low-p_{T} jets with 15 GeV $< p_{\mathrm{T}} <$ 20 GeV, with uncertainties in the range of 1–3%. Additional uncertainties are considered related to the jet flavor, pile-up corrections, and high-p_{T} jets. Systematic uncertainties in these measurements account for 32 independent variations.

The uncertainties in the efficiency to tag jets using DL1r are derived using measurements in data as a function of p_{T}

for b-jets, c-jets, and light-jets separately. The efficiency to correctly tag b-jets is measured using dileptonic $t\bar{t}$ events [119]. The mistag rate for c-jets is measured using hadronically decaying W bosons from single-lepton $t\bar{t}$ events [120]. The mistag rate from light jets is measured using a negative-tag method in $Z+$jets events [121]. Several uncertainty components are considered for the calibration of the four working points used, resulting in 45, 20, and 20 uncorrelated variations for b-, c-, and light jets, respectively.

Uncertainties in the efficiency to tag jets using DeXTer are derived using calibration measurements in data as a function of the p_{T} of the jet for B-jets and b-jets [28]. The other flavors have negligible contributions to the analysis. Efficiencies to correctly tag B-jets and mistag b-jets are derived using $t\bar{t}$ and $Z+g(\to b\bar{b})$ events. The efficiency measurement uses gluon splitting $g\to b\bar{b}$, since it is the main SM source of b-quark pairs at low p_{T}. This measurement is extended to cover high-p_{T} jets with 200 GeV $< p_{\mathrm{T}} <$ 500 GeV using the same calibration methods [28], which is particularly important for the 0ℓ channel. The DeXTer efficiencies are measured in several bins of p_{T} and generator-level flavor. All sources of systematic uncertainty are described in Ref. [28]. The covariance matrix from a simultaneous fit to all bins in jet p_{T}, working point range, and generator-level flavor of the jets are diagonalized into 12 uncorrelated eigenvectors that are used as uncertainty variations.

Uncertainties in the reconstruction efficiency for b-decays and the mistag rate for the soft-v identified using the TC-LVT tagger are derived using $t\bar{t}$ events, as described in Ref. [31]. The uncertainties are derived as a function of the actual pile-up and are accounted for as three independent sources. Since the soft-v are reconstructed from tracks, uncertainties in the selection efficiency and the misreconstruction of tracks are propagated to the soft-v four momentum. The tracking uncertainties are derived from studies of the material in the ID and the physics models used in the Geant4 detector simulation [100,130] and are included as 12 independent variations.

A large-R track-jet mass scale correction is determined using $Z+$jets events with one b-jet and one B-jet. These events have large HF jet multiplicity but are not part of any signal or control region. The data-to-simulation mass scale correction is derived from a fit to the observed large-R track-jet mass distribution. The correction required is below 5% and the uncertainty in the fit is propagated to the analysis.

All uncertainties related to the energy scales or resolution of the reconstructed objects are propagated to the $E_{\mathrm{T}}^{\mathrm{miss}}$ calculation. Additional uncertainties are derived using measurements in $Z\to\ell\ell$ events in data [122]. Three additional independent uncertainties associated with the scale and resolution of the soft term are also included.

B. Modeling uncertainties

The systematic uncertainties affecting the modeling of the signal and the main backgrounds, $t\bar{t}$ and $Z+$jets, are due to effects such as missing higher-order terms in the perturbative QCD calculations, and the choice of PDF set, PS and hadronization models. Several uncertainties are derived using alternative simulated MC samples, which are listed in Table I.

For the $t\bar{t}$ background, an uncertainty related to the amount of initial-state radiation (ISR) is estimated by simultaneously varying the renormalization and factorization scales in the ME and in the PS [131], and an uncertainty related to the final-state radiation (FSR) is estimated by varying scales in the PS. For the $Z+$jets background, an uncertainty is derived from the envelope of seven scale variations of the renormalization μ_{R} and factorization μ_{F} scales covering the pairwise combinations of increasing and decreasing the scales by a factor of two. The effect of PDF variations [132] on the shape of distributions and the uncertainty in the value of α_s are also considered.

For the $t\bar{t}$ background, an uncertainty associated with the choice of PS and hadronization model is assessed by comparing the nominal sample generated with Powheg Box v2+PYTHIA 8 to a sample generated with Powheg Box v2+HERWIG 7. A comparison with MADGRAPH5_AMC@NLO+PYTHIA 8 is also used to assess the uncertainty arising from both the ME corrections and the choice of procedure matching ME and PS at NLO.

For the $Z+$jets and $W+$jets backgrounds, the nominal sample generated with Sherpa is compared with an alternative sample with MADGRAPH5_AMC@NLO+PYTHIA 8, which is produced with up to three additional partons at NLO accuracy [133]. The uncertainty in the heavy flavor components is derived by comparing the nominal $Z+$jets sample with alternatives with varied settings for the overlap between matrix element and parton shower emissions and for the resummation scale [134]. An uncertainty in the ME matching (CKKW) is estimated by varying the scale used to distinguish between jets from the ME and the PS [96,97]. An uncertainty in the resummation scale (QSF) is estimated by varying the scale used for the resummation of soft gluon emission by a factor of two [135].

Uncertainties are derived for the modeling corrections applied to the $Z+$jets and $t\bar{t}$ backgrounds, described in Sec. VII A. The uncertainties in the parameters of the functions used to improve the modeling in simulation are propagated to the final result of the analysis.

In the case of the QCD multijet background, described in Sec. VII B, several sources of uncertainties are considered, including the full statistical and systematic uncertainties associated with the contributions from other background sources and the differences between the estimate obtained

with the validation region compared with the SR. Even though the uncertainty in this background component is around 100%, this background is not a significant contributor in the SRs and has a negligible impact on the result.

IX. STATISTICAL TREATMENT

Event yields in each of the control and signal regions are combined to test for the presence of a signal. The statistical analysis is based on a binned likelihood function $\mathcal{L}(\mu,\theta)$ constructed as a product of Poisson probability terms over all BDT bins in the signal region and every control region considered. This function depends on the signal-strength parameter μ, a multiplicative factor to the theoretical signal production cross section for ZH production times the branching fraction of the Higgs boson to the final state considered in each model $\mathcal{B}(H\to 2a\to 4b)$, $\mathcal{B}(H\to a_1a_2\to 4b)$, or $\mathcal{B}(H\to a_1a_2\to 6b)$ and θ, a set of nuisance parameters (NP) that encode the effect of systematic uncertainties in the signal and background expectations and that are implemented in the likelihood function as Gaussian distribution constraint terms. Therefore, the total expected number of events in a given bin depends on μ and θ. The NPs θ allow variations of the expectations for signal and background according to the corresponding systematic uncertainties. Their fitted values correspond to the deviations from the nominal expectations that globally provide the best fit to the data. This procedure reduces the impact of systematic uncertainties in the search sensitivity by taking advantage of the highly populated background-dominated channels included in the likelihood fit. It requires a good understanding of the systematic effects affecting the shapes of the discriminant distributions, for which detailed validation studies of the fitting procedure are performed using the simulation. Statistical uncertainties in each bin of the discriminant distributions are also taken into account by dedicated parameters in the fit.

Systematic uncertainties are pruned away and smoothed to reduce the time for fitting, make the minimization more stable, and deal with unphysical effects due to statistical fluctuations in the uncertainties. The shape and the normalization of systematic uncertainties are pruned separately per region and sample. The pruning algorithm removes systematic uncertainties that have an impact on the normalization below one percent and that cause a negligibly small impact on the shape of the final discriminant (all bins are within one percent of the nominal shape). Smoothing is applied to the systematic variations to mitigate the effects of statistical fluctuations.

The test statistic $\tilde{q}_\mu$ is defined as the profile likelihood ratio, $\tilde{q}_\mu = -2\ln(\mathcal{L}(\mu,\hat{\hat{\theta}}_\mu)/\mathcal{L}(\hat{\mu},\hat{\theta}))$, where $\hat{\mu}$ and $\hat{\theta}$ are the values of the parameters that maximize the likelihood function (with the constraint $0\le\hat{\mu}\le\mu$), and $\hat{\hat{\theta}}_\mu$ are the values of the NP that conditionally maximize the likelihood function for a given value of μ. The test statistic $\tilde{q}_\mu$ is implemented in the RooStats package [136] and is used to measure the compatibility of the observed data with the signal plus background hypothesis (i.e., the exclusion test). The primary statistical analysis package used is TRExFitter [137], which makes use of the RooFit [138] and RooStats [136] packages. The p-value representing the compatibility of the data with the background-only hypothesis is estimated by integrating the distribution of q_0 from signal plus background pseudoexperiments approximated using the definition and asymptotic formulas given in Ref. [139], above the observed value. The observed p-value is checked for each explored signal scenario. In the absence of any significant excess above the background expectation, upper limits on the signal production cross section for each signal scenario are derived using $\tilde{q}_\mu$ in the CLs method [139]. For a given signal hypothesis, values of the branching fractions of exotic Higgs boson decays times the ratio of the production cross section over the SM prediction (parametrized by μ) yielding CLs < 0.05, where CLs is computed using the asymptotic approximation, are excluded at 95% CL. The limits computed with the asymptotic approximation are compared with calculations based on pseudoexperiments for several representative cases and found to have relative differences below 10%.

Statistical uncertainties in each region are taken into account by dedicated NPs with Poisson constraint terms. For the $Z+$jets background, the $Z+\ge 1b$ and $\ge 1B$ components are normalized by one common unconstrained NP that is instead mainly determined using the dedicated $Z+$jets CRs. Extensive studies on the possibility of using separate parameters for additional $Z+$HF categories, e.g., separate parameters for $Z+\ge 1b$ and $Z+\ge 1B$, were carried out. However, due to the lack of CRs with enough purity in additional $Z+$HF categories, the fit does not have the ability to constrain them separately. The uncertainty in the relative fraction of each $Z+$HF background component is accounted for by modeling uncertainties instead. The common $Z+$jets background normalization parameter is fitted in the range of 1.04–1.18 with a typical uncertainty of about 25%. For the $t\bar{t}+$jets background, the overall $t\bar{t}$ normalization, and the fractions of the $t\bar{t}+\ge 1b$ and $t\bar{t}+\ge 1B$ components are normalized by three distinct unconstrained NPs. They are mainly determined in the dedicated $t\bar{t}$ CRs that are split by the reconstructed b-object multiplicity. The overall $t\bar{t}$ normalization parameter is in the range of 0.96–1.03 depending on the mass hypothesis with a typical uncertainty of 20%, while the $t\bar{t}+\ge 1b$ and $t\bar{t}+\ge 1B$ normalization parameters are in the range of 0.87–1.17 and 1.08–1.39, with typical uncertainties of approximately 65% and 80%, respectively. In the 0ℓ channel, since the description of backgrounds coming from lost-leptons is modeled with different methods (see Sec. VII B), an independent normalization parameter is introduced with

TABLE IX. Summary of de-correlated systematic uncertainties used to combine the 0ℓ and 2ℓ channels.

Systematic uncertainties	Channels affected	Motivation for de-correlation
QCD multijet uncertainty $E_{\mathrm{T}}^{\mathrm{miss}}$ trigger scale factor High-p_{T} DeXTer flavor tagging $W+$jets modeling Single top modeling	0ℓ	Only impacts 0ℓ channel
Low-p_{T} DL1r flavor tagging Low-p_{T} JVT TC-LVT flavor tagging	2ℓ	Only impacts 2ℓ channel
$W/Z+$HF modeling $t\bar{t}$ background modeling	Both	Different kinematic phase-space

a fitted value in the range of 1.25–1.28 and a typical uncertainty of 16%.

A. Combination of 0ℓ and 2ℓ channels

The analyses targeting the 0ℓ and $2\ell H \to 2a \to 4b$ channels are combined in the final result. The combination of the two channels is made easier by the fact that both analyses use the same modeling of background samples and the same systematic uncertainty model. The SRs of the 0ℓ and 2ℓ channels are orthogonal thanks to the lepton vetoes of these regions and the strictly looser lepton definition ($p_{\mathrm{T}} > 7$ GeV compared with $p_{\mathrm{T}} > 10$ GeV) of the 0ℓ channel compared with the 2ℓ channel. The 2ℓ CRs of the 0ℓ and 2ℓ channels overlap, so when the combination is performed the $Z+$jets normalization parameter in the 0ℓ channel is constrained by the CRs of the 2ℓ channel. Most common systematic uncertainties are correlated between the two channels. Table IX shows the few de-correlated systematic uncertainties along with the rationale for their treatment.

X. RESULTS

The validation of the background modeling is performed in several different signal-depleted regions. In the 2ℓ channel, the validation is performed after the quadruplet-selection NN using signal-depleted regions corresponding to low BDT discriminator score values. Good agreement is observed as function of several key kinematic variables such as the reconstructed a-boson and Higgs boson masses, as shown in Fig. 6. Further validation is performed using

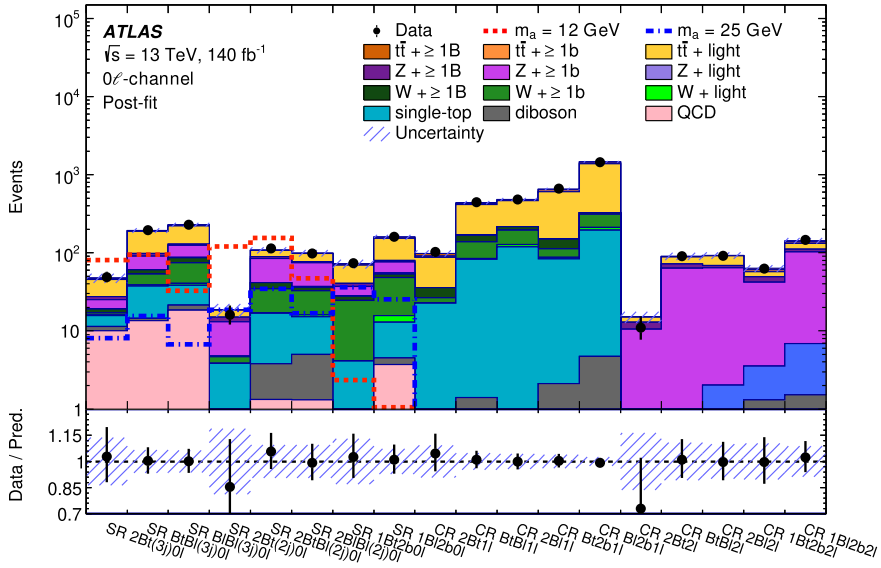

FIG. 10. Observed yields for the signal and control regions in the 0ℓ channel after the background-only fit to data. The signal for the $m_a = 12$ GeV and 25 GeV mass hypotheses are overlaid (dashed line) assuming a branching fraction $\mathcal{B}(H \to 2a \to 4b) = 1$ and the SM rate of production of Higgs bosons. The lower panels show the ratio of the observed to the estimated SM background. The hashed area represents the total uncertainty of the background. The category labeled "Other" includes processes with small contributions to the total yield (diboson, $t\bar{t}Z$, and $t\bar{t}W$).

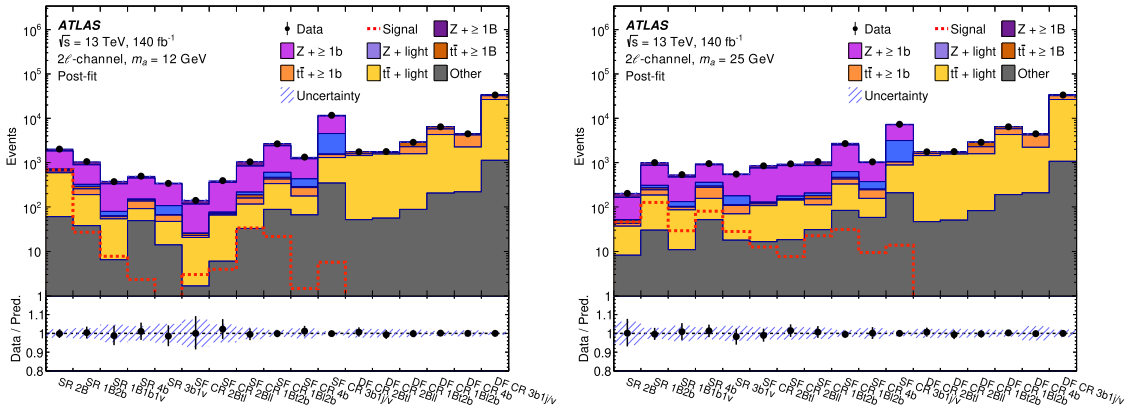

(a) (b)

FIG. 11. Observed yields for the signal and control regions in the 2ℓ channel for the (a) $m_a = 12$ GeV mass hypothesis and the (b) $m_a = 25$ GeV mass hypothesis after the background-only fit to data. The signal is overlaid (dashed line) assuming a branching fraction $\mathcal{B}(H \to 2a \to 4b) = 1$ and the SM rate of production of Higgs bosons. The lower panels show the ratio of the observed to the estimated SM background. The hashed area represents the total uncertainty of the background. The category labeled "Other" includes processes with small contributions to the total yield (diboson, $t\bar{t}Z$, and $t\bar{t}W$).

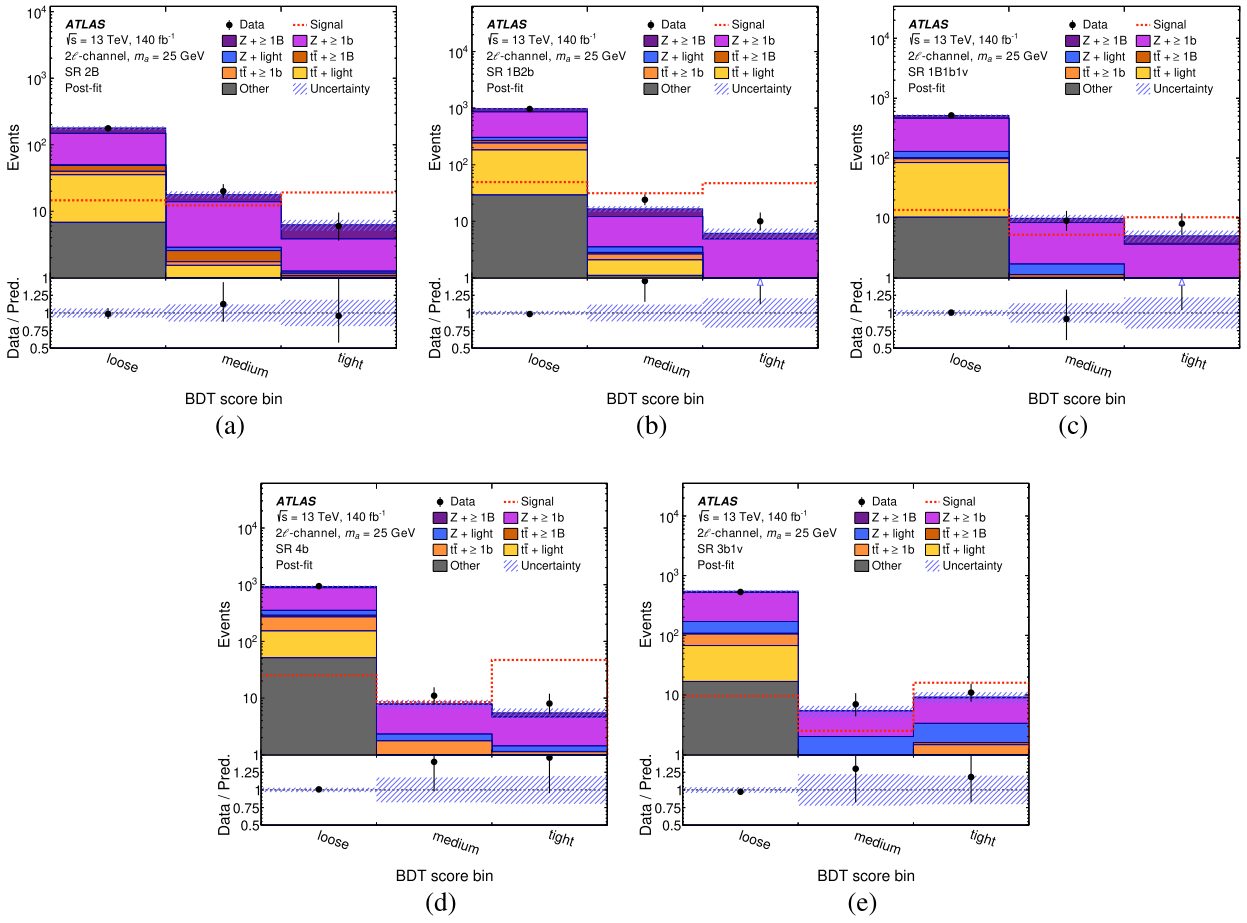

FIG. 12. Observed yields for the signal regions in the 2ℓ channel for the $m_a = 25$ GeV mass hypothesis after the background-only fit to data in the (a) $2B$, (b) $1B2b$, (c) $1B1b1\text{v}$, (d) $4b$, and (e) $3b1\text{v}$ regions. The signal is overlaid (dashed line) assuming a branching fraction $\mathcal{B}(H \to 2a \to 4b) = 1$ and the SM rate of production of Higgs bosons. The lower panels show the ratio of the observed to the estimated SM background. The hashed area represents the total uncertainty of the background. The category labeled "Other" includes processes with small contributions to the total yield (diboson, $t\bar{t}Z$, and $t\bar{t}W$).

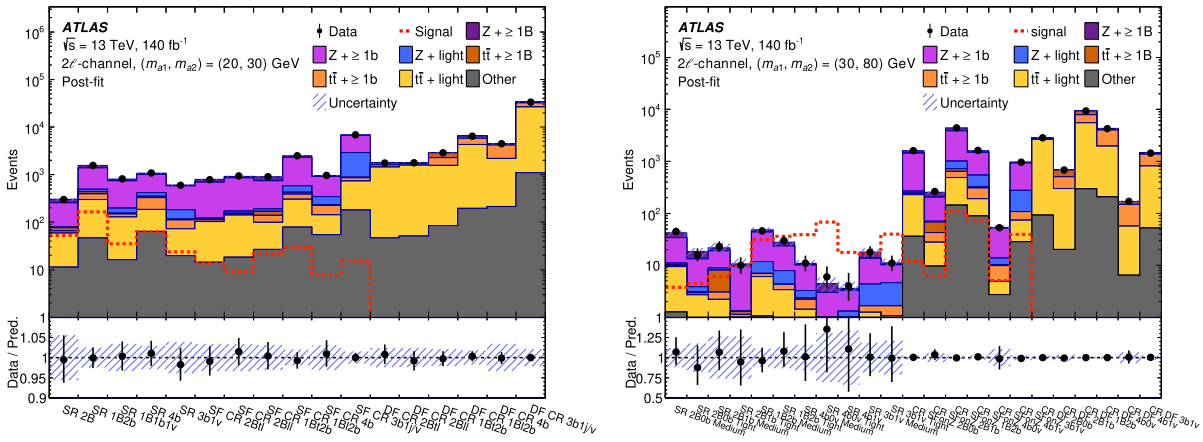

(a) (b)

FIG. 13. Observed yields for the signal and control regions in the 2ℓ channel after the background-only fit to data for signals with two new particles for the case (a) $(m_{a_1}, m_{a_2}) = (20, 30)$ GeV, which gives rise to a signal with $4b$ in the final state, and (b) $(m_{a_1}, m_{a_2}) = (30, 80)$ GeV, which gives rise to a signal with $6b$ in the final state. The signal is overlaid (dashed line) assuming a branching fraction $\mathcal{B}(H \to a_1 a_2 \to 4b/6b) = 1$ and the SM rate of production of Higgs bosons. The lower panels show the ratio of the observed to the estimated SM background. The hashed area represents the total uncertainty of the background. The category labeled "Other" includes processes with small contributions to the total yield (diboson, $t\bar{t}Z$, and $t\bar{t}W$).

events with different-flavor lepton pairs or same-flavor lepton pairs away from the Z boson mass, which are dominated by processes including top quarks. As described in Sec. V (Tables II and IV–VI), these regions are split by the number of B-jets and b-jets to validate the production of heavy-flavor in background processes. Good agreement is observed in all regions, as shown in Figs. 10 and 11.

Figure 12 shows the distributions of the multivariate discriminant for the different object categories for the 2ℓ channel. The signal mass hypothesis $m_a = 25$ GeV has the largest difference between the data and the background prediction in the tightest BDT bins among all masses tested in the $H \to 2a \to 4b$ model. The background-rich bins are consistent between the data and the background prediction. Figure 13 shows the yields for the signal and control regions for the searches for the $H \to a_1 a_2 \to 4b$ and $H \to a_1 a_2 \to 3a_1 \to 6b$ processes. Upper limits on the branching fraction $\mathcal{B}(H \to 2a/a_1 a_2 \to 4b/6b)$ times the ratio of the ZH production cross section to the SM prediction $\sigma(ZH)/\sigma_{\mathrm{SM}}(ZH)$ are determined at 95% CL using the CLs technique [139–141] and the $\tilde{q}_\mu$ test statistic described in Sec. IX. The SM Higgs boson production cross section used is $\sigma_{\mathrm{SM}}(ZH) = 0.88$ pb [142].

Table X shows the impact of dominant sources of systematic uncertainties in the observed upper limit for different signal mass hypotheses. The impact is estimated by the difference between the expected upper limit when only a group of uncertainties is considered and the case where no systematic uncertainty is considered. The B-jet identification efficiency uncertainty is an important source of systematic uncertainty at low value of masses due to the difficulty in measuring the identification efficiency of merged B-jets with low mass and low p_{T}. Modeling uncertainties are also important due to the challenges of modeling associated heavy flavor (defined as b-quarks, unless explicitly mentioned) production of $Z +$ jets and $t\bar{t}$. Figure 14 compares the observed upper limits with the expected limits assuming the median value of $\tilde{q}_\mu$ under the background-only hypothesis for the $H \to 2a \to 4b$ process. The 0ℓ and 2ℓ channels are combined in the mass range of 12 GeV $< m_a <$ 30 GeV. This is the first time the 0ℓ channel is explored and provides an approximately 15% improvement on the limit at the 12 and 16 GeV mass points, which is the region targeted by the channel. Figure 15 shows the corresponding upper limits for the $H \to a_1 a_2 \to 4b$ and $6b$ cases. The values of m_a used for signal simulation and for hypothesis testing were chosen so that the difference between neighboring points is much smaller than the mass resolution of the reconstructed a-boson and Higgs boson, which varies between about 10 GeV and 50 GeV depending on the value of m_a and the type of b-objects used in the selected quadruplet. Interpolation tests are performed by calculating expected limits using Asimov samples [139] with different values of generated m_a than the one being tested. Due to the limited mass resolution, only three points are used when testing models with two different a-bosons for the $H \to a_1 a_2 \to 4b$ case. The phase-space region satisfying $m_{a_1} + m_{a_2} < m_H$, $m_{a_1} > m_{a_2}$, and $m_{a_1}, m_{a_2} \geq 12$ GeV is a narrow wedge that is fully probed by the three mass points used. Four points are similarly chosen to test models with two different a-bosons for the $H \to a_1 a_2 \to 6b$ case.

The limits in the low-mass regime ($m_a < 20$ GeV), where the $b\bar{b}$ system is collimated into a single object,

TABLE X. The upper limit on $\sigma(ZH)/\sigma_{\mathrm{SM}}(ZH) \times \mathcal{B}(H \to 2a \to 4b)$ is determined for the cases without systematic uncertainties (stat-only), when all uncertainties are applied (observed) and when only a group of systematic uncertainties is applied. The larger the difference between the limit obtained for a group of uncertainties and the stat-only limit, the more important the uncertainty group is for the final result. The entries with "-" change by less than 1% relative to the stat-only limit. Impacts are shown for the $m_a = 12$ GeV and 25 GeV mass points for the 0ℓ channel, the 2ℓ channel, and the combination of the 0ℓ and 2ℓ channels. The grouping "Tracks" includes large-R track-jets. The trigger uncertainties are included in the groupings of corresponding objects.

	Upper limit on $\sigma(ZH)/\sigma_{\mathrm{SM}}(ZH) \times \mathcal{B}(H \to 2a \to 4b)$					
	$m_a = 12$ GeV			$m_a = 25$ GeV		
Uncertainty source	0ℓ	2ℓ	0ℓ & 2ℓ	0ℓ	2ℓ	0ℓ & 2ℓ
Stat-only limit	0.060	0.029	0.025	0.35	0.19	0.19
Observed limit	0.12	0.039	0.034	0.89	0.21	0.21
MC statistics	0.065	0.030	0.026	0.37	···	0.19
Systematics	0.12	0.038	0.033	0.88	0.21	0.21
Experimental	0.076	0.032	0.028	0.51	0.20	0.20
Luminosity and pile-up	0.062	···	···	0.36	···	···
DL1r tagging	···	···	···	0.35	0.20	0.20
DeXTer tagging	0.067	0.030	0.026	0.39	···	···
Electrons	···	···	···	···	···	···
Muons	···	···	···	···	···	···
Jets	0.063	0.029	0.025	0.39	···	···
$E_{\mathrm{T}}^{\mathrm{miss}}$	0.063	···	0.025	0.37	···	···
Tracks	0.066	0.029	0.026	0.42	···	0.20
Soft-v		···	···		···	···
Modeling	0.088	0.034	0.030	0.60	0.20	0.20
Top ($t\bar{t}$ and single top)	0.065	···	0.025	0.41	···	0.20
W/Z + jets	0.071	0.033	0.029	0.45	0.19	0.20
Signal	0.066	0.029	0.026	0.37	0.20	0.20
QCD	0.063		···	0.35		···

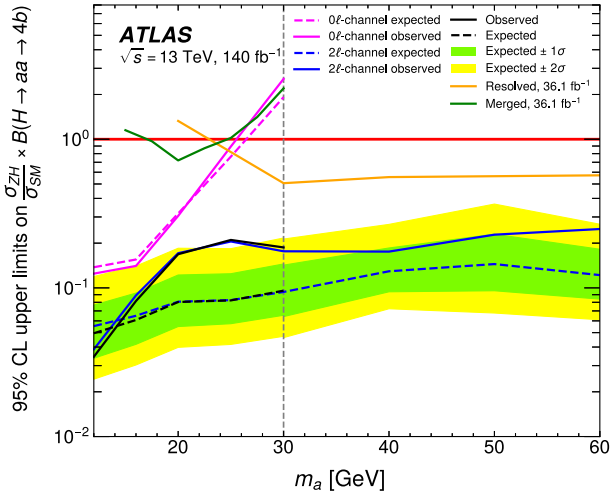

FIG. 14. The observed (solid) 95% CL upper limits on $\sigma(ZH)/\sigma_{\mathrm{SM}}(ZH) \times \mathcal{B}(H \to 2a \to 4b)$ as a function of m_a and the expected (dashed) limits under the background-only hypothesis showing the 0ℓ and 2ℓ separately and their combination. The vertical dashed line at 30 GeV indicates the transition point and for higher masses only the 2ℓ channel is used. For the combined result, the inner and outer shaded bands show the $\pm 1\sigma$ and $\pm 2\sigma$ uncertainties of the expected limits. The mass hypothesis m_a is probed between 12 and 60 GeV. The previous results from the ATLAS Collaboration using a partial Run 2 data sample focusing on the resolved [26] and merged [33] regimes are also shown.

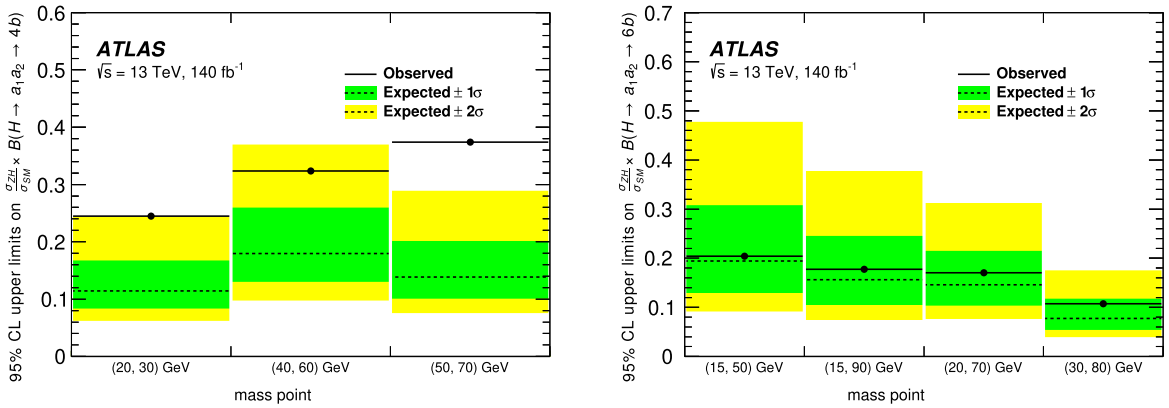

FIG. 15. The observed (solid) 95% CL upper limits on (a) $\sigma(ZH)/\sigma_{\mathrm{SM}}(ZH) \times \mathcal{B}(H \to a_1 a_2 \to 4b)$ and (b) $\sigma(ZH)/\sigma_{\mathrm{SM}}(ZH) \times \mathcal{B}(H \to a_1 a_2 \to 6b)$ for different signal mass hypotheses (m_{a_1}, m_{a_2}). The inner and outer shaded bands show the $\pm 1\sigma$ and $\pm 2\sigma$ uncertainties of the expected limits.

are mostly driven by the 2B category, while limits in the high-mass regime ($m_a > 30$ GeV) are mostly driven by the 4b category. The largest deviations correspond to the $H \to 2a/a_1 a_2 \to 4b$ case in the 2ℓ channel, with a local (global) significance of 2.83 (2.04) for $m_a = 25$ GeV and 3.28 (2.57) for $(m_{a_1}, m_{a_2}) = (50, 70)$ GeV. The global p-value is computed using the formula from Ref. [143], where a reference p-value of 0.5 is used to count the crossings across all tested values of the mass of the new scalar m_a. The value is then extrapolated to the observed local p-value. For models with different m_{a_1} and m_{a_2}, the method is extended using the Euler characteristic instead of up crossings, as described in Ref. [144].

This search increases the sensitivity of previous ATLAS searches for $H \to 2a \to 4b$ [26,32,33] by a factor of about 5–15 depending on the signal mass hypothesis by including a larger data sample, and by using novel identification algorithms for low-mass merged B-jets and including soft secondary vertices reconstructed outside of jets. These techniques enhance the sensitivity at low m_a and to high multiplicity final states. The analysis considers the production mode $pp \to ZH(Z \to \nu\nu)$ for the first time in a search for exotic decays of the Higgs boson. In addition, this is also the first search for exotic decays of the Higgs boson in the final state $H \to a_1 a_2 \to 4b/6b$ over the mass range $12 < m_a < 60$ GeV.

XI. CONCLUSION

This paper presents a search for exotic decays of the Higgs boson into a pair of scalar particles, $H \to 2a$, where each a-boson decays into two b-quarks. It also considers the case of two new a-bosons $H \to a_1 a_2 \to 4b$ and $H \to a_1 a_2 \to 3a_1 \to 6b$. The analysis targets the Higgs boson produced in association with a Z boson (ZH) and is performed using the 140 fb^{-1} of proton–proton collision data at a center-of-mass energy of 13 TeV recorded by the ATLAS detector at the LHC between 2015 and 2018. The search makes use of heavy-flavor-tagging techniques to target collimated $a \to b\bar{b}$ decays and soft secondary vertices reconstructed outside of jets. The analysis categorizes events depending on the number of leptons and the strategy for identifying heavy-flavor jets: one or two B-jets, three or four b-jets, and one soft secondary vertex.

The largest deviations correspond to the $H \to 2a/a_1 a_2 \to 4b$ case in the 2ℓ channel, with a local (global) significance of 2.83 (2.04) for $m_a = 25$ GeV and 3.28 (2.57) for $(m_{a_1}, m_{a_2}) = (50, 70)$ GeV. The global significance is estimated independently for each model. As no significant excess above the SM background expectation is observed, upper limits at 95% CL are set of 4%–25% on $\sigma(ZH)/\sigma_{\mathrm{SM}}(ZH) \times \mathcal{B}(H \to 2a \to 4b)$ for scalar mass values in the range of 12 GeV $\leq m_a \leq 60$ GeV, of 24%–38% on $\sigma(ZH)/\sigma_{\mathrm{SM}}(ZH) \times \mathcal{B}(H \to a_1 a_2 \to 4b)$, and of 10%–20% on $\sigma(ZH)/\sigma_{\mathrm{SM}}(ZH) \times \mathcal{B}(H \to a_1 a_2 \to 3a_1 \to 6b)$ for masses in the ranges of $15 \leq m_{a_1} \leq 50$ GeV and $30 \leq m_{a_2} \leq 80$ GeV. These results contribute to the broad program of searches for $H \to 2a/a_1 a_2$ decays.

ACKNOWLEDGMENTS

We thank CERN for the very successful operation of the LHC and its injectors, as well as the support staff at CERN and at our institutions worldwide without whom ATLAS could not be operated efficiently. The crucial computing support from all WLCG partners is acknowledged gratefully, in particular from CERN, the ATLAS Tier-1 facilities at TRIUMF/SFU (Canada), NDGF (Denmark, Norway, Sweden), CC-IN2P3 (France), KIT/GridKA (Germany), INFN-CNAF (Italy), NL-T1 (Netherlands), PIC (Spain), RAL (UK) and BNL (USA), the Tier-2 facilities worldwide and large non-WLCG resource providers. Major

contributors of computing resources are listed in Ref. [145]. We gratefully acknowledge the support of ANPCyT, Argentina; YerPhI, Armenia; ARC, Australia; BMWFW and FWF, Austria; ANAS, Azerbaijan; CNPq and FAPESP, Brazil; NSERC, NRC and CFI, Canada; CERN; ANID, Chile; CAS, MOST and NSFC, China; Minciencias, Colombia; MEYS CR, Czech Republic; DNRF and DNSRC, Denmark; IN2P3-CNRS and CEA-DRF/IRFU, France; SRNSFG, Georgia; BMFTR, HGF and MPG, Germany; GSRI, Greece; RGC and Hong Kong SAR, China; ICHEP and Academy of Sciences and Humanities, Israel; INFN, Italy; MEXT and JSPS, Japan; CNRST, Morocco; NWO, Netherlands; RCN, Norway; MNiSW, Poland; FCT, Portugal; MNE/IFA, Romania; MSTDI, Serbia; MSSR, Slovakia; ARIS and MVZI, Slovenia; DSI/NRF, South Africa; MICIU/AEI, Spain; SRC and Wallenberg Foundation, Sweden; SERI, SNSF and Cantons of Bern and Geneva, Switzerland; NSTC, Taipei; TENMAK, Türkiye; STFC/UKRI, United Kingdom; DOE and NSF, United States of America. Individual groups and members have received support from BCKDF, CANARIE, CRC and DRAC, Canada; CERN-CZ, FORTE and PRIMUS, Czech Republic; COST, ERC, ERDF, Horizon 2020, ICSC-NextGenerationEU and Marie Skłodowska-Curie Actions, European Union; Investissements d'Avenir Labex, Investissements d'Avenir Idex and ANR, France; DFG and AvH Foundation, Germany; Herakleitos, Thales and Aristeia programmes co-financed by EU-ESF and the Greek NSRF, Greece; BSF-NSF and MINERVA, Israel; NCN and NAWA, Poland; La Caixa Banking Foundation, CERCA Programme Generalitat de Catalunya and PROMETEO and GenT Programmes Generalitat Valenciana, Spain; Göran Gustafssons Stiftelse, Sweden; The Royal Society and Leverhulme Trust, United Kingdom. In addition, individual members wish to acknowledge support from Armenia: Yerevan Physics Institute (FAPERJ); CERN: European Organization for Nuclear Research (CERN DOCT); Chile: Agencia Nacional de Investigación y Desarrollo (FONDECYT 1230812, FONDECYT 1240864, Fondecyt 3240661); China: Chinese Ministry of Science and Technology (MOST-2023YFA1605700, MOST-2023YFA1609300), National Natural Science Foundation of China (NSFC—12175119, NSFC 12275265); Czech Republic: Czech Science Foundation (GACR—24-11373S), Ministry of Education Youth and Sports (ERC-CZ-LL2327, FORTE CZ.02.01.01/00/22_008/0004632), PRIMUS Research Programme (PRIMUS/21/SCI/017); EU: H2020 European Research Council (ERC—101002463); European Union: European Research Council (BARD No. 101116429, No. ERC—948254, and No. ERC 101089007), European Regional Development Fund (SMASH COFUND 101081355, SLO ERDF), Horizon 2020 Framework Programme (MUCCA—CHIST-ERA-19-XAI-00), European Union, Future Artificial Intelligence Research (FAIR-NextGenerationEU PE00000013), Horizon 2020 (EuroHPC—EHPC-DEV-2024D11-051), Italian Center for High Performance Computing, Big Data and Quantum Computing (ICSC, NextGenerationEU); France: Agence Nationale de la Recherche (ANR-21-CE31-0013, ANR-21-CE31-0022, ANR-22-EDIR-0002); Germany: Baden-Württemberg Stiftung (BW Stiftung-Postdoc Eliteprogramme), Deutsche Forschungsgemeinschaft (DFG—469666862, DFG—CR 312/5-2); China: Research Grants Council (GRF); Italy: Istituto Nazionale di Fisica Nucleare (ICSC, NextGenerationEU), Ministero dell'Università e della Ricerca (NextGenEU 153D23001490006 M4C2.1.1, NextGenEU I53D23000820006 M4C2.1.1, NextGenEU I53D23001490006 M4C2.1.1); Japan: Japan Society for the Promotion of Science (JSPS KAKENHI JP22H01227, JSPS KAKENHI JP22H04944, JSPS KAKENHI JP22KK0227, JSPS KAKENHI JP23KK0245, JSPS KAKENHI JP24K23939); Norway: Research Council of Norway (RCN-314472); Poland: Ministry of Science and Higher Education (IDUB AGH, POB8, D4 no 9722), Polish National Science Centre (NCN 2021/42/E/ST2/00350, NCN OPUS 2023/51/B/ST2/02507, NCN OPUS nr 2022/47/B/ST2/03059, NCN UMO-2019/34/E/ST2/00393, UMO-2020/37/B/ST2/01043, UMO-2022/47/O/ST2/00148, UMO-2023/49/B/ST2/04085, UMO-2023/51/B/ST2/00920, UMO-2024/53/N/ST2/00869); Portugal: Foundation for Science and Technology (FCT); Spain: Generalitat Valenciana (Artemisa, FEDER, IDIFEDER/2018/048), Ministry of Science and Innovation (MCIN & NextGenEU PCI2022-135018-2, MICIN & FEDER PID2021-125273NB, RYC2019-028510-I, RYC2020-030254-I, RYC2021-031273-I, RYC2022-038164-I); Sweden: Carl Trygger Foundation (Carl Trygger Foundation CTS 22:2312), Swedish Research Council (Swedish Research Council 2023-04654, VR 2021-03651, VR 2022-03845, VR 2022-04683, VR 2023-03403, VR 2024-05451), Knut and Alice Wallenberg Foundation (KAW 2018.0458, KAW 2022.0358, KAW 2023.0366); Switzerland: Swiss National Science Foundation (SNSF—PCEFP2_194658); United Kingdom: Leverhulme Trust (Leverhulme Trust RPG-2020-004), Royal Society (NIF-R1-231091); United States of America: U.S. Department of Energy (ECA DE-AC02-76SF00515), Neubauer Family Foundation.

DATA AVAILABILITY

The data that support the findings of this article are not publicly available. The data are available from the authors upon reasonable request.

[1] ATLAS Collaboration, Observation of a new particle in the search for the standard model Higgs boson with the ATLAS detector at the LHC, Phys. Lett. B **716**, 1 (2012).

[2] CMS Collaboration, Observation of a new boson at a mass of 125 GeV with the CMS experiment at the LHC, Phys. Lett. B **716**, 30 (2012).

[3] ATLAS Collaboration, A detailed map of Higgs boson interactions by the ATLAS experiment ten years after the discovery, Nature (London) **607**, 52 (2022); **612**, E24 (2022).

[4] CMS Collaboration, A portrait of the Higgs boson by the CMS experiment ten years after the discovery, Nature (London) **607**, 60 (2022); **623**, E4 (2023).

[5] D. Curtin *et al.*, Exotic decays of the 125 GeV Higgs boson, Phys. Rev. D **90**, 075004 (2014).

[6] B. A. Dobrescu and K. T. Matchev, Light axion within the next-to-minimal supersymmetric standard model, J. High Energy Phys. 09 (2000) 031.

[7] U. Ellwanger, J. F. Gunion, C. Hugonie, and S. Moretti, Towards a no-lose theorem for NMSSM Higgs discovery at the LHC, arXiv:hep-ph/0305109.

[8] R. Dermíšek and J. F. Gunion, Escaping the large fine-tuning and little hierarchy problems in the next to minimal supersymmetric model and $h \to aa$ decays, Phys. Rev. Lett. **95**, 041801 (2005).

[9] S. Chang, R. Dermíšek, J. F. Gunion, and N. Weiner, Nonstandard Higgs boson decays, Annu. Rev. Nucl. Part. Sci. **58**, 75 (2008).

[10] D. E. Morrissey and A. Pierce, Modified Higgs boson phenomenology from gauge or gaugino mediation in the next-to-minimal supersymmetric Standard Model, Phys. Rev. D **78**, 075029 (2008).

[11] V. Silveira and A. Zee, Scalar phantoms, Phys. Lett. **161B**, 136 (1985).

[12] M. Pospelov, A. Ritz, and M. Voloshin, Secluded WIMP dark matter, Phys. Lett. B **662**, 53 (2008).

[13] P. Draper, T. Liu, C. E. M. Wagner, L.-T. Wang, and H. Zhang, Dark light-Higgs bosons, Phys. Rev. Lett. **106**, 121805 (2011).

[14] S. Ipek, D. McKeen, and A. E. Nelson, Renormalizable model for the Galactic Center gamma-ray excess from dark matter annihilation, Phys. Rev. D **90**, 055021 (2014).

[15] A. Martin, J. Shelton, and J. Unwin, Fitting the Galactic Center gamma-ray excess with cascade annihilations, Phys. Rev. D **90**, 103513 (2014).

[16] J. Kozaczuk, M. J. Ramsey-Musolf, and J. Shelton, Exotic Higgs boson decays and the electroweak phase transition, Phys. Rev. D **101**, 115035 (2020).

[17] M. Carena, Z. Liu, and Y. Wang, Electroweak phase transition with spontaneous Z_2-breaking, J. High Energy Phys. 08 (2020) 107.

[18] N. Craig, A. Katz, M. Strassler, and R. Sundrum, Naturalness in the dark at the LHC, J. High Energy Phys. 07 (2015) 105.

[19] D. Curtin and C. B. Verhaaren, Discovering uncolored naturalness in exotic Higgs decays, J. High Energy Phys. 12 (2015) 072.

[20] T. Robens and T. Stefaniak, Status of the Higgs singlet extension of the standard model after LHC run 1, Eur. Phys. J. C **75**, 104 (2015).

[21] T. Robens and T. Stefaniak, LHC benchmark scenarios for the real Higgs singlet extension of the standard model, Eur. Phys. J. C **76**, 268 (2016).

[22] T. Robens, T. Stefaniak, and J. Wittbrodt, Two-real-scalar-singlet extension of the SM: LHC phenomenology and benchmark scenarios, Eur. Phys. J. C **80**, 151 (2020).

[23] M. Bauer, M. Neubert, and A. Thamm, Collider probes of axion-like particles, J. High Energy Phys. 12 (2017) 044.

[24] U. Haisch, J. F. Kamenik, A. Malinauskas, and M. Spira, Collider constraints on light pseudoscalars, J. High Energy Phys. 03 (2018) 178.

[25] L. Evans and P. Bryant, LHC machine, J. Instrum. **3**, S08001 (2008).

[26] ATLAS Collaboration, Search for the Higgs boson produced in association with a vector boson and decaying into two spin-zero particles in the $H \to aa \to 4b$ channel in pp collisions at $\sqrt{s} = 13$ TeV with the ATLAS detector, J. High Energy Phys. 10 (2018) 031.

[27] A. J. Larkoski, I. Moult, and B. Nachman, Jet substructure at the large hadron collider: A review of recent advances in theory and machine learning, Phys. Rep. **841**, 1 (2020).

[28] ATLAS Collaboration, DeXTer: Deep sets based neural networks for Low-$p_T X \to b\bar{b}$ identification in ATLAS, Report No. ATL-PHYS-PUB-2022-042, CERN, Geneva, Switzerland, 2022, https://cds.cern.ch/record/2825434.

[29] ATLAS Collaboration, ATLAS flavour-tagging algorithms for the LHC Run 2 pp collision dataset, Eur. Phys. J. C **83**, 681 (2023).

[30] ATLAS Collaboration, Jet reconstruction and performance using particle flow with the ATLAS detector, Eur. Phys. J. C **77**, 466 (2017).

[31] ATLAS Collaboration, Calibration of a soft secondary vertex tagger using proton–proton collisions at $\sqrt{s} =$ 13 TeV with the ATLAS detector, Phys. Rev. D **110**, 032015 (2024).

[32] ATLAS Collaboration, Search for the Higgs boson produced in association with a W boson and decaying to four b-quarks via two spin-zero particles in pp collisions at 13 TeV with the ATLAS detector, Eur. Phys. J. C **76**, 605 (2016).

[33] ATLAS Collaboration, Search for Higgs boson decays into two new low-mass spin-0 particles in the 4b channel with the ATLAS detector using pp collisions at $\sqrt{s} = 13$ TeV, Phys. Rev. D **102**, 112006 (2020).

[34] CMS Collaboration, Search for the decay of the Higgs boson to a pair of light pseudoscalar bosons in the final state with four bottom quarks in proton–proton collisions at $\sqrt{s} = 13$ TeV, J. High Energy Phys. 06 (2024) 097.

[35] ATLAS Collaboration, Search for new light gauge bosons in Higgs boson decays to four-lepton final states in pp collisions at $\sqrt{s} = 8$ TeV with the ATLAS detector at the LHC, Phys. Rev. D **92**, 092001 (2015).

[36] ATLAS Collaboration, Search for Higgs boson decays to beyond-the-Standard-Model light bosons in four-lepton events with the ATLAS detector at $\sqrt{s} = 13$ TeV, J. High Energy Phys. 06 (2018) 166.

[37] ATLAS Collaboration, Search for Higgs bosons decaying into new spin-0 or spin-1 particles in four-lepton final states with the ATLAS detector with 139 fb^{-1} of pp

collision data at $\sqrt{s} = 13$ TeV, J. High Energy Phys. 03 (2022) 041.
[38] ATLAS Collaboration, Search for Higgs bosons decaying to aa in the $\mu\mu\tau\tau$ final state in pp collisions at $\sqrt{s} = 8$ TeV with the ATLAS experiment, Phys. Rev. D **92**, 052002 (2015).
[39] CMS Collaboration, Search for an exotic decay of the Higgs boson to a pair of light pseudoscalars in the final state of two muons and two τ leptons in proton–proton collisions at $\sqrt{s} = 13$ TeV, J. High Energy Phys. 11 (2018) 018.
[40] CMS Collaboration, Search for light pseudoscalar boson pairs produced from decays of the 125 GeV Higgs boson in final states with two muons and two nearby tracks in pp collisions at $\sqrt{s} = 13$ TeV, Phys. Lett. B **800**, 135087 (2020).
[41] CMS Collaboration, Search for a light pseudoscalar Higgs boson in the boosted $\mu\mu\tau\tau$ final state in proton–proton collisions at $\sqrt{s} = 13$ TeV, J. High Energy Phys. 08 (2020) 139.
[42] CMS Collaboration, Search for a very light NMSSM Higgs boson produced in decays of the 125 GeV scalar boson and decaying into τ leptons in pp collisions at $\sqrt{s} = 8$ TeV, J. High Energy Phys. 01 (2016) 079.
[43] ATLAS Collaboration, Search for Higgs boson exotic decays into Lorentz-boosted light bosons in the four-τ final state at $\sqrt{s} = 13$ TeV with the ATLAS detector, arXiv:2503.05463.
[44] ATLAS Collaboration, Search for Higgs boson decays into a pair of light bosons in the $bb\mu\mu$ final state in pp collision at $\sqrt{s} = 13$ TeV with the ATLAS detector, Phys. Lett. B **790**, 1 (2019).
[45] ATLAS Collaboration, Search for Higgs boson decays into a pair of pseudoscalar particles in the $bb\mu\mu$ final state with the ATLAS detector in pp collisions at $\sqrt{s} = 13$ TeV, Phys. Rev. D **105**, 012006 (2022).
[46] CMS Collaboration, Search for light bosons in decays of the 125 GeV Higgs boson in proton–proton collisions at $\sqrt{s} = 8$ TeV, J. High Energy Phys. 10 (2017) 076.
[47] CMS Collaboration, Search for an exotic decay of the Higgs boson to a pair of light pseudoscalars in the final state with two muons and two b quarks in pp collisions at 13 TeV, Phys. Lett. B **795**, 398 (2019).
[48] CMS Collaboration, Search for an exotic decay of the Higgs boson to a pair of light pseudoscalars in the final state with two b quarks and two τ leptons in proton–proton collisions at $\sqrt{s} = 13$ TeV, Phys. Lett. B **785**, 462 (2018).
[49] CMS Collaboration, Search for exotic decays of the Higgs boson to a pair of pseudoscalars in the $\mu\mu$bb and $\tau\tau$bb final states, Eur. Phys. J. C **84**, 493 (2024).
[50] ATLAS Collaboration, Search for decays of the Higgs boson into a pair of pseudoscalar particles decaying into $b\bar{b}\tau^+\tau^-$ using pp collisions at $\sqrt{s} = 13$ TeV with the ATLAS detector, Phys. Rev. D **110**, 052013 (2024).
[51] ATLAS Collaboration, Search for new phenomena in events with at least three photons collected in pp collisions at $\sqrt{s} = 8$ TeV with the ATLAS detector, Eur. Phys. J. C **76**, 210 (2016).
[52] CMS Collaboration, Search for the exotic decay of the Higgs boson into two light pseudoscalars with four photons in the final state in proton–proton collisions at $\sqrt{s} = 13$ TeV, J. High Energy Phys. 07 (2023) 148.
[53] CMS Collaboration, Search for exotic Higgs boson decays $H \to \mathcal{A}\mathcal{A} \to 4\gamma$ with events containing two merged diphotons in proton–proton collisions at $\sqrt{s} = 13$ TeV, Phys. Rev. Lett. **131**, 101801 (2023).
[54] ATLAS Collaboration, Search for Higgs boson decays into pairs of light (pseudo)scalar particles in the $\gamma\gamma jj$ final state in pp collisions at $\sqrt{s} = 13$ TeV with the ATLAS detector, Phys. Lett. B **782**, 750 (2018).
[55] ATLAS Collaboration, The ATLAS experiment at the CERN large hadron collider, J. Instrum. **3**, S08003 (2008).
[56] ATLAS Collaboration, ATLAS insertable B-layer: Technical design report, Reports No. ATLAS-TDR-19, No. CERN-LHCC-2010-013, CERN, Geneva, Switzerland, 2010, https://cds.cern.ch/record/1291633; Addendum: Reports No. ATLAS-TDR-19-ADD-1, No. CERN-LHCC-2012-009, CERN, Geneva, Switzerland, 2012, https://cds.cern.ch/record/1451888.
[57] B. Abbott *et al.*, Production and integration of the ATLAS insertable B-layer, J. Instrum. **13**, T05008 (2018).
[58] G. Avoni *et al.*, The new LUCID-2 detector for luminosity measurement and monitoring in ATLAS, J. Instrum. **13**, P07017 (2018).
[59] ATLAS Collaboration, Performance of the ATLAS trigger system in 2015, Eur. Phys. J. C **77**, 317 (2017).
[60] ATLAS Collaboration, Software and computing for Run 3 of the ATLAS experiment at the LHC, Eur. Phys. J. C **85**, 234 (2025).
[61] ATLAS Collaboration, Luminosity determination in pp collisions at $\sqrt{s} = 13$ TeV using the ATLAS detector at the LHC, Eur. Phys. J. C **83**, 982 (2023).
[62] ATLAS Collaboration, ATLAS data quality operations and performance for 2015–2018 data-taking, J. Instrum. **15**, P04003 (2020).
[63] ATLAS Collaboration, Performance of the ATLAS muon triggers in Run 2, J. Instrum. **15**, P09015 (2020).
[64] ATLAS Collaboration, Performance of electron and photon triggers in ATLAS during LHC Run 2, Eur. Phys. J. C **80**, 47 (2020).
[65] ATLAS Collaboration, The ATLAS simulation infrastructure, Eur. Phys. J. C **70**, 823 (2010).
[66] S. Agostinelli *et al.*, Geant4—a simulation toolkit, Nucl. Instrum. Methods Phys. Res., Sect. A **506**, 250 (2003).
[67] T. Sjöstrand, S. Mrenna, and P. Skands, A brief introduction to Pythia 8.1, Comput. Phys. Commun. **178**, 852 (2008).
[68] R. D. Ball *et al.* (NNPDF Collaboration), Parton distributions with LHC data, Nucl. Phys. **B867**, 244 (2013).
[69] ATLAS Collaboration, The Pythia 8 A3 tune description of ATLAS minimum bias and inelastic measurements incorporating the Donnachie–Landshoff diffractive model, Report No. ATL-PHYS-PUB-2016-017, CERN, Geneva, Switzerland, 2016, https://cds.cern.ch/record/2206965.
[70] D. de Florian *et al.*, Handbook of LHC Higgs cross sections: 4. Deciphering the nature of the Higgs sector, CERN Yellow Rep. Monogr. **2**, 1 (2017).

[71] M. Beneke, P. Falgari, S. Klein, and C. Schwinn, Hadronic top-quark pair production with NNLL threshold resummation, Nucl. Phys. **B855**, 695 (2012).

[72] M. Cacciari, M. Czakon, M. Mangano, A. Mitov, and P. Nason, Top-pair production at hadron colliders with next-to-next-to-leading logarithmic soft-gluon resummation, Phys. Lett. B **710**, 612 (2012).

[73] P. Bärnreuther, M. Czakon, and A. Mitov, Percent-level-precision physics at the tevatron: Next-to-next-to-leading order QCD corrections to $q\bar{q} \to t\bar{t} + X$, Phys. Rev. Lett. **109**, 132001 (2012).

[74] M. Czakon and A. Mitov, NNLO corrections to top-pair production at hadron colliders: The all-fermionic scattering channels, J. High Energy Phys. 12 (2012) 054.

[75] M. Czakon and A. Mitov, NNLO corrections to top pair production at hadron colliders: The quark-gluon reaction, J. High Energy Phys. 01 (2013) 080.

[76] M. Czakon, P. Fiedler, and A. Mitov, Total top-quark pair-production cross section at hadron colliders through $\mathcal{O}(\alpha_S^4)$, Phys. Rev. Lett. **110**, 252004 (2013).

[77] M. Czakon and A. Mitov, Top++: A program for the calculation of the top-pair cross-section at hadron colliders, Comput. Phys. Commun. **185**, 2930 (2014).

[78] N. Kidonakis, Two-loop soft anomalous dimensions for single top quark associated production with a W^- or H^-, Phys. Rev. D **82**, 054018 (2010).

[79] M. Aliev, H. Lacker, U. Langenfeld, S. Moch, P. Uwer, and M. Wiedermann, HATHOR—Hadronic top and heavy quarks cross section calculator, Comput. Phys. Commun. **182**, 1034 (2011).

[80] P. Kant, O. M. Kind, T. Kintscher, T. Lohse, T. Martini, S. Mölbitz, P. Rieck, and P. Uwer, HatHor for single top-quark production: Updated predictions and uncertainty estimates for single top-quark production in hadronic collisions, Comput. Phys. Commun. **191**, 74 (2015).

[81] C. Anastasiou, L. Dixon, K. Melnikov, and F. Petriello, High-precision QCD at hadron colliders: Electroweak gauge boson rapidity distributions at next-to-next-to leading order, Phys. Rev. D **69**, 094008 (2004).

[82] K. Hamilton, P. Nason, E. Re, and G. Zanderighi, NNLOPS simulation of Higgs boson production, J. High Energy Phys. 10 (2013) 222.

[83] K. Hamilton, P. Nason, and G. Zanderighi, Finite quark-mass effects in the NNLOPS POWHEG + MiNLO Higgs generator, J. High Energy Phys. 05 (2015) 140.

[84] S. Alioli, P. Nason, C. Oleari, and E. Re, A general framework for implementing NLO calculations in shower Monte Carlo programs: The Powheg Box, J. High Energy Phys. 06 (2010) 043.

[85] P. Nason, A new method for combining NLO QCD with shower Monte Carlo algorithms, J. High Energy Phys. 11 (2004) 040.

[86] S. Frixione, P. Nason, and C. Oleari, Matching NLO QCD computations with parton shower simulations: The POWHEG method, J. High Energy Phys. 11 (2007) 070.

[87] R. D. Ball *et al.* (NNPDF Collaboration), Parton distributions for the LHC run II, J. High Energy Phys. 04 (2015) 040.

[88] ATLAS Collaboration, Measurement of the $Z/\gamma*$ boson transverse momentum distribution in pp collisions at $\sqrt{s} = 7$ TeV with the ATLAS detector, J. High Energy Phys. 09 (2014) 145.

[89] ATLAS Collaboration, ATLAS Pythia 8 tunes to 7 TeV data, Report No. ATL-PHYS-PUB-2014-021, CERN, Geneva, Switzerland, 2014, https://cds.cern.ch/record/1966419.

[90] E. Bothmann *et al.*, Event generation with Sherpa 2.2, SciPost Phys. **7**, 034 (2019).

[91] T. Gleisberg and S. Höche, Comix, a new matrix element generator, J. High Energy Phys. 12 (2008) 039.

[92] F. Cascioli, P. Maierhöfer, and S. Pozzorini, Scattering amplitudes with open loops, Phys. Rev. Lett. **108**, 111601 (2012).

[93] S. Schumann and F. Krauss, A parton shower algorithm based on Catani–Seymour dipole factorisation, J. High Energy Phys. 03 (2008) 038.

[94] S. Höche, F. Krauss, M. Schönherr, and F. Siegert, A critical appraisal of NLO + PS matching methods, J. High Energy Phys. 09 (2012) 049.

[95] S. Höche, F. Krauss, M. Schönherr, and F. Siegert, QCD matrix elements + parton showers. The NLO case, J. High Energy Phys. 04 (2013) 027.

[96] S. Catani, F. Krauss, B. R. Webber, and R. Kuhn, QCD matrix elements + parton showers, J. High Energy Phys. 11 (2001) 063.

[97] S. Höche, F. Krauss, S. Schumann, and F. Siegert, QCD matrix elements and truncated showers, J. High Energy Phys. 05 (2009) 053.

[98] ATLAS Collaboration, Measurement of Higgs boson decay into b-quarks in associated production with a top-quark pair in pp collisions at $\sqrt{s} = 13$ TeV with the ATLAS detector, J. High Energy Phys. 06 (2022) 097.

[99] M. Cacciari, G. P. Salam, and G. Soyez, The anti-k_t jet clustering algorithm, J. High Energy Phys. 04 (2008) 063.

[100] ATLAS Collaboration, Performance of the ATLAS track reconstruction algorithms in dense environments in LHC Run 2, Eur. Phys. J. C **77**, 673 (2017).

[101] ATLAS Collaboration, Vertex reconstruction performance of the ATLAS detector at $\sqrt{s} = 13$ TeV, Report No. ATL-PHYS-PUB-2015-026, CERN, Geneva, Switzerland, 2015, https://cds.cern.ch/record/2037717.

[102] ATLAS Collaboration, Electron and photon performance measurements with the ATLAS detector using the 2015–2017 LHC proton–proton collision data, J. Instrum. **14**, P12006 (2019).

[103] ATLAS Collaboration, Electron and photon efficiencies in LHC Run 2 with the ATLAS experiment, J. High Energy Phys. 05 (2024) 162.

[104] ATLAS Collaboration, Electron and photon energy calibration with the ATLAS detector using LHC Run 2 data, J. Instrum. **19**, P02009 (2024).

[105] ATLAS Collaboration, Evidence for the associated production of the Higgs boson and a top quark pair with the ATLAS detector, Phys. Rev. D **97**, 072003 (2018).

[106] ATLAS Collaboration, Muon reconstruction and identification efficiency in ATLAS using the full Run 2 pp collision data set at $\sqrt{s} = 13$ TeV, Eur. Phys. J. C **81**, 578 (2021).
[107] ATLAS Collaboration, Evidence for the $H \to b\bar{b}$ decay with the ATLAS detector, J. High Energy Phys. 12 (2017) 024.
[108] M. Cacciari and G. P. Salam, Dispelling the N^3 myth for the k_t jet-finder, Phys. Lett. B **641**, 57 (2006).
[109] M. Cacciari, G. P. Salam, and G. Soyez, FastJet user manual, Eur. Phys. J. C **72**, 1896 (2012).
[110] ATLAS Collaboration, Performance of pile-up mitigation techniques for jets in pp collisions at $\sqrt{s} = 8$ TeV using the ATLAS detector, Eur. Phys. J. C **76**, 581 (2016).
[111] ATLAS Collaboration, New techniques for jet calibration with the ATLAS detector, Eur. Phys. J. C **83**, 761 (2023).
[112] ATLAS Collaboration, Jet energy scale and resolution measured in proton–proton collisions at $\sqrt{s} = 13$ TeV with the ATLAS detector, Eur. Phys. J. C **81**, 689 (2021).
[113] B. Nachman, P. Nef, A. Schwartzman, M. Swiatlowski, and C. Wanotayaroj, Jets from Jets: Re-clustering as a tool for large radius jet reconstruction and grooming at the LHC, J. High Energy Phys. 02 (2015) 075.
[114] M. Cacciari and G. P. Salam, Pileup subtraction using jet areas, Phys. Lett. B **659**, 119 (2008).
[115] S. D. Ellis and D. E. Soper, Successive combination jet algorithm for hadron collisions, Phys. Rev. D **48**, 3160 (1993).
[116] ATLAS Collaboration, Variable radius, exclusive-k_T, and center-of-mass subjet reconstruction for Higgs($\to b\bar{b}$) tagging in ATLAS, Report No. ATL-PHYS-PUB-2017-010, CERN, Geneva, Switzerland, 2017, https://cds.cern.ch/record/2268678.
[117] P. J. Huber, Robust estimation of a location parameter, Ann. Math. Stat. **35**, 73 (1964).
[118] ATLAS Collaboration, Secondary vertex finding for jet flavour identification with the ATLAS detector, Report No. ATL-PHYS-PUB-2017-011, CERN, Geneva, Switzerland, 2017, https://cds.cern.ch/record/2270366.
[119] ATLAS Collaboration, ATLAS b-jet identification performance and efficiency measurement with $t\bar{t}$ events in pp collisions at $\sqrt{s} = 13$ TeV, Eur. Phys. J. C **79**, 970 (2019).
[120] ATLAS Collaboration, Measurement of the c-jet mistagging efficiency in $t\bar{t}$ events using pp collision data at $\sqrt{s} = 13$ TeV collected with the ATLAS detector, Eur. Phys. J. C **82**, 95 (2022).
[121] ATLAS Collaboration, Calibration of the light-flavour jet mistagging efficiency of the b-tagging algorithms with Z + jets events using 139 fb^{-1} of ATLAS proton–proton collision data at $\sqrt{s} = 13$ TeV, Eur. Phys. J. C **83**, 728 (2023).
[122] ATLAS Collaboration, The performance of missing transverse momentum reconstruction and its significance with the ATLAS detector using 140 fb^{-1} of $\sqrt{s} = 13$ TeV pp collisions, Eur. Phys. J. C **85**, 606 (2025).
[123] ATLAS Collaboration, Performance of the missing transverse momentum triggers for the ATLAS detector during Run-2 data taking, J. High Energy Phys. 08 (2020) 080.
[124] J. C. Collins and D. E. Soper, Angular distribution of dileptons in high-energy hadron collisions, Phys. Rev. D **16**, 2219 (1977).
[125] T. Chen and C. Guestrin, XGBoost: A scalable tree boosting system, in *Proceedings of the 22nd ACM SIGKDD International Conference on Knowledge Discovery and Data Mining, KDD '16* (Association for Computing Machinery, San Francisco, California, USA, 2016), p. 785, 10.1145/2939672.2939785.
[126] ATLAS Collaboration, Measurement of the $t\bar{t}t\bar{t}$ production cross section in pp collisions at $\sqrt{s} = 13$ TeV with the ATLAS detector, J. High Energy Phys. 11 (2021) 118.
[127] ATLAS Collaboration, Search for charged Higgs bosons decaying into a top quark and a bottom quark at $\sqrt{s} = 13$ TeV with the ATLAS detector, J. High Energy Phys. 06 (2021) 145.
[128] ATLAS Collaboration, Measurements of inclusive and differential fiducial cross-sections of $t\bar{t}$ production with additional heavy-flavour jets in proton–proton collisions at $\sqrt{s} = 13$ TeV with the ATLAS detector, J. High Energy Phys. 04 (2019) 046.
[129] ATLAS Collaboration, Measurement of the inelastic proton–proton cross section at $\sqrt{s} = 13$ TeV with the ATLAS detector at the LHC, Phys. Rev. Lett. **117**, 182002 (2016).
[130] ATLAS Collaboration, Early inner detector tracking performance in the 2015 Data at $\sqrt{s} = 13$ TeV, Report No. ATL-PHYS-PUB-2015-051, CERN, Geneva, Switzerland, 2015, https://cds.cern.ch/record/2110140.
[131] ATLAS Collaboration, Study of top-quark pair modelling and uncertainties using ATLAS measurements at $\sqrt{s} = 13$ TeV, Report No. ATL-PHYS-PUB-2020-023, CERN, Geneva, Switzerland, 2020, https://cds.cern.ch/record/2730443.
[132] J. Butterworth *et al.*, PDF4LHC recommendations for LHC Run II, J. Phys. G **43**, 023001 (2016).
[133] ATLAS Collaboration, Modelling and computational improvements to the simulation of single vector-boson plus jet processes for the ATLAS experiment, J. High Energy Phys. 08 (2022) 089.
[134] F. Cascioli, S. Höche, F. Krauss, P. Maierhöfer, S. Pozzorini, and F. Siegert, Precise Higgs-background predictions: Merging NLO QCD and squared quark-loop corrections to four-lepton + 0, 1 jet production, J. High Energy Phys. 01 (2014) 046.
[135] E. Bothmann, M. Schönherr, and S. Schumann, Reweighting QCD matrix-element and parton-shower calculations, Eur. Phys. J. C **76**, 590 (2016).
[136] L. Moneta *et al.*, The RooStats project, Proc. Sci. ACAT2010 (**2011**) 057 [arXiv:1009.1003].
[137] TRExFitter documentation, https://trexfitter-docs.web.cern.ch/trexfitter-docs/.
[138] W. Verkerke and D. Kirkby, The RooFit toolkit for data modeling, arXiv:physics/0306116.
[139] G. Cowan, K. Cranmer, E. Gross, and O. Vitells, Asymptotic formulae for likelihood-based tests of new physics, Eur. Phys. J. C **71**, 1554 (2011); **73**, 2501(E) (2013).

[140] A. L. Read, Presentation of search results: The CL_s technique, J. Phys. G **28**, 2693 (2002).
[141] T. Junk, Confidence level computation for combining searches with small statistics, Nucl. Instrum. Methods Phys. Res., Sect. A **434**, 435 (1999).
[142] LHC Higgs Cross Section Working Group, Handbook of LHC Higgs cross sections: 3. Higgs properties, arXiv:1307.1347.
[143] E. Gross and O. Vitells, Trial factors for the look elsewhere effect in high energy physics, Eur. Phys. J. C **70**, 525 (2010).
[144] O. Vitells and E. Gross, Estimating the significance of a signal in a multi-dimensional search, Astropart. Phys. **35**, 230 (2011).
[145] ATLAS Collaboration, ATLAS computing acknowledgements, Report No. ATL-SOFT-PUB-2025-001, CERN, Geneva, Switzerland, 2025, https://cds.cern.ch/record/2922210.

G. Aad,[104] E. Aakvaag,[17] B. Abbott,[123] S. Abdelhameed,[119a] K. Abeling,[55] N. J. Abicht,[49] S. H. Abidi,[30] M. Aboelela,[45] A. Aboulhorma,[36e] H. Abramowicz,[157] Y. Abulaiti,[120] B. S. Acharya,[69a,69b,b] A. Ackermann,[63a] C. Adam Bourdarios,[4] L. Adamczyk,[87a] S. V. Addepalli,[149] M. J. Addison,[103] J. Adelman,[118] A. Adiguzel,[22c] T. Adye,[137] A. A. Affolder,[139] Y. Afik,[40] M. N. Agaras,[13] A. Aggarwal,[102] C. Agheorghiesei,[28c] F. Ahmadov,[39,c] S. Ahuja,[97] X. Ai,[143b] G. Aielli,[76a,76b] A. Aikot,[169] M. Ait Tamlihat,[36e] B. Aitbenchikh,[36a] M. Akbiyik,[102] T. P. A. Åkesson,[100] A. V. Akimov,[151] D. Akiyama,[174] N. N. Akolkar,[25] S. Aktas,[22a] G. L. Alberghi,[24b] J. Albert,[171] P. Albicocco,[53] G. L. Albouy,[60] S. Alderweireldt,[52] Z. L. Alegria,[124] M. Aleksa,[37] I. N. Aleksandrov,[39] C. Alexa,[28b] T. Alexopoulos,[10] F. Alfonsi,[24b] M. Algren,[56] M. Alhroob,[173] B. Ali,[135] H. M. J. Ali,[93,d] S. Ali,[32] S. W. Alibocus,[94] M. Aliev,[34c] G. Alimonti,[71a] W. Alkakhi,[55] C. Allaire,[66] B. M. M. Allbrooke,[152] J. S. Allen,[103] J. F. Allen,[52] P. P. Allport,[21] A. Aloisio,[72a,72b] F. Alonso,[92] C. Alpigiani,[142] Z. M. K. Alsolami,[93] A. Alvarez Fernandez,[102] M. Alves Cardoso,[56] M. G. Alviggi,[72a,72b] M. Aly,[103] Y. Amaral Coutinho,[83b] A. Ambler,[106] C. Amelung,[37] M. Amerl,[103] C. G. Ames,[111] T. Amezza,[130] D. Amidei,[108] B. Amini,[54] K. Amirie,[161] A. Amirkhanov,[39] S. P. Amor Dos Santos,[133a] K. R. Amos,[169] D. Amperiadou,[158] S. An,[84] C. Anastopoulos,[145] T. Andeen,[11] J. K. Anders,[94] A. C. Anderson,[59] A. Andreazza,[71a,71b] S. Angelidakis,[9] A. Angerami,[42] A. V. Anisenkov,[39] A. Annovi,[74a] C. Antel,[56] E. Antipov,[151] M. Antonelli,[53] F. Anulli,[75a] M. Aoki,[84] T. Aoki,[159] M. A. Aparo,[152] L. Aperio Bella,[48] M. Apicella,[31] C. Appelt,[157] A. Apyan,[27] S. J. Arbiol Val,[88] C. Arcangeletti,[53] A. T. H. Arce,[51] J-F. Arguin,[110] S. Argyropoulos,[158] J.-H. Arling,[48] O. Arnaez,[4] H. Arnold,[151] G. Artoni,[75a,75b] H. Asada,[113] K. Asai,[121] S. Asai,[159] S. Asatryan,[179] N. A. Asbah,[37] R. A. Ashby Pickering,[173] A. M. Aslam,[97] K. Assamagan,[30] R. Astalos,[29a] K. S. V. Astrand,[100] S. Atashi,[165] R. J. Atkin,[34a] H. Atmani,[36f] P. A. Atmasiddha,[131] K. Augsten,[135] A. D. Auriol,[41] V. A. Austrup,[103] G. Avolio,[37] K. Axiotis,[56] G. Azuelos,[110,e] D. Babal,[29b] H. Bachacou,[138] K. Bachas,[158,f] A. Bachiu,[35] E. Bachmann,[50] M. J. Backes,[63a] A. Badea,[40] T. M. Baer,[108] P. Bagnaia,[75a,75b] M. Bahmani,[19] D. Bahner,[54] K. Bai,[126] J. T. Baines,[137] L. Baines,[96] O. K. Baker,[178] E. Bakos,[16] D. Bakshi Gupta,[8] L. E. Balabram Filho,[83b] V. Balakrishnan,[123] R. Balasubramanian,[4] E. M. Baldin,[38] P. Balek,[87a] E. Ballabene,[24b,24a] F. Balli,[138] L. M. Baltes,[63a] W. K. Balunas,[33] J. Balz,[102] I. Bamwidhi,[119b] E. Banas,[88] M. Bandieramonte,[132] A. Bandyopadhyay,[25] S. Bansal,[25] L. Barak,[157] M. Barakat,[48] E. L. Barberio,[107] D. Barberis,[18b] M. Barbero,[104] M. Z. Barel,[117] T. Barillari,[112] M-S. Barisits,[37] T. Barklow,[149] P. Baron,[125] D. A. Baron Moreno,[103] A. Baroncelli,[62] A. J. Barr,[129] J. D. Barr,[98] F. Barreiro,[101] J. Barreiro Guimarães da Costa,[14] M. G. Barros Teixeira,[133a] S. Barsov,[38] F. Bartels,[63a] R. Bartoldus,[149] A. E. Barton,[93] P. Bartos,[29a] A. Basan,[102] M. Baselga,[49] S. Bashiri,[88] A. Bassalat,[66,g] M. J. Basso,[162a] S. Bataju,[45] R. Bate,[170] R. L. Bates,[59] S. Batlamous,[101] M. Battaglia,[139] D. Battulga,[19] M. Bauce,[75a,75b] M. Bauer,[79] P. Bauer,[25] L. T. Bayer,[48] L. T. Bazzano Hurrell,[31] J. B. Beacham,[112] T. Beau,[130] J. Y. Beaucamp,[92] P. H. Beauchemin,[164] P. Bechtle,[25] H. P. Beck,[20,h] K. Becker,[173] A. J. Beddall,[82] V. A. Bednyakov,[39] C. P. Bee,[151] L. J. Beemster,[16] M. Begalli,[83d] M. Begel,[30] J. K. Behr,[48] J. F. Beirer,[37] F. Beisiegel,[25] M. Belfkir,[119b] G. Bella,[157] L. Bellagamba,[24b] A. Bellerive,[35] C. D. Bellgraph,[68] P. Bellos,[21] K. Beloborodov,[38] D. Benchekroun,[36a] F. Bendebba,[36a] Y. Benhammou,[157] K. C. Benkendorfer,[61] L. Beresford,[48] M. Beretta,[53] E. Bergeaas Kuutmann,[167] N. Berger,[4] B. Bergmann,[135] J. Beringer,[18a] G. Bernardi,[5] C. Bernius,[149] F. U. Bernlochner,[25] F. Bernon,[37] A. Berrocal Guardia,[13] T. Berry,[97] P. Berta,[136] A. Berthold,[50] A. Berti,[133a] R. Bertrand,[104] S. Bethke,[112] A. Betti,[75a,75b] A. J. Bevan,[96] L. Bezio,[56] N. K. Bhalla,[54] S. Bharthuar,[112] S. Bhatta,[151] P. Bhattarai,[149] Z. M. Bhatti,[120] K. D. Bhide,[54] V. S. Bhopatkar,[124]

R. M. Bianchi,[132] G. Bianco,[24b,24a] O. Biebel,[111] M. Biglietti,[77a] C. S. Billingsley,[45] Y. Bimgdi,[36f] M. Bindi,[55] A. Bingham,[177] A. Bingul,[22b] C. Bini,[75a,75b] G. A. Bird,[33] M. Birman,[175] M. Biros,[136] S. Biryukov,[152] T. Bisanz,[49] E. Bisceglie,[24b,24a] J. P. Biswal,[137] D. Biswas,[147] I. Bloch,[48] A. Blue,[59] U. Blumenschein,[96] J. Blumenthal,[102] V. S. Bobrovnikov,[39] M. Boehler,[54] B. Boehm,[172] D. Bogavac,[13] A. G. Bogdanchikov,[38] L. S. Boggia,[130] V. Boisvert,[97] P. Bokan,[37] T. Bold,[87a] M. Bomben,[5] M. Bona,[96] M. Boonekamp,[138] A. G. Borbély,[59] I. S. Bordulev,[38] G. Borissov,[93] D. Bortoletto,[129] D. Boscherini,[24b] M. Bosman,[13] K. Bouaouda,[36a] N. Bouchhar,[169] L. Boudet,[4] J. Boudreau,[132] E. V. Bouhova-Thacker,[93] D. Boumediene,[41] R. Bouquet,[57b,57a] A. Boveia,[122] J. Boyd,[37] D. Boye,[30] I. R. Boyko,[39] L. Bozianu,[56] J. Bracinik,[21] N. Brahimi,[4] G. Brandt,[177] O. Brandt,[33] B. Brau,[105] J. E. Brau,[126] R. Brener,[175] L. Brenner,[117] R. Brenner,[167] S. Bressler,[175] G. Brianti,[78a,78b] D. Britton,[59] D. Britzger,[112] I. Brock,[25] R. Brock,[109] G. Brooijmans,[42] A. J. Brooks,[68] E. M. Brooks,[162b] E. Brost,[30] L. M. Brown,[171,162a] L. E. Bruce,[61] T. L. Bruckler,[129] P. A. Bruckman de Renstrom,[88] B. Brüers,[48] A. Bruni,[24b] G. Bruni,[24b] D. Brunner,[47a,47b] M. Bruschi,[24b] N. Bruscino,[75a,75b] T. Buanes,[17] Q. Buat,[142] D. Buchin,[112] A. G. Buckley,[59] O. Bulekov,[82] B. A. Bullard,[149] S. Burdin,[94] C. D. Burgard,[49] A. M. Burger,[91] B. Burghgrave,[8] O. Burlayenko,[54] J. Burleson,[168] J. T. P. Burr,[33] J. C. Burzynski,[148] E. L. Busch,[42] V. Büscher,[102] P. J. Bussey,[59] J. M. Butler,[26] C. M. Buttar,[59] J. M. Butterworth,[98] W. Buttinger,[137] C. J. Buxo Vazquez,[109] A. R. Buzykaev,[39] S. Cabrera Urbán,[169] L. Cadamuro,[66] D. Caforio,[58] H. Cai,[132] Y. Cai,[24b,114c,24a] Y. Cai,[114a] V. M. M. Cairo,[37] O. Cakir,[3a] N. Calace,[37] P. Calafiura,[18a] G. Calderini,[130] P. Calfayan,[35] G. Callea,[59] L. P. Caloba,[83b] D. Calvet,[41] S. Calvet,[41] R. Camacho Toro,[130] S. Camarda,[37] D. Camarero Munoz,[27] P. Camarri,[76a,76b] C. Camincher,[171] M. Campanelli,[98] A. Camplani,[43] V. Canale,[72a,72b] A. C. Canbay,[3a] E. Canonero,[97] J. Cantero,[169] Y. Cao,[168] F. Capocasa,[27] M. Capua,[44b,44a] A. Carbone,[71a,71b] R. Cardarelli,[76a] J. C. J. Cardenas,[8] M. P. Cardiff,[27] G. Carducci,[44b,44a] T. Carli,[37] G. Carlino,[72a] J. I. Carlotto,[13] B. T. Carlson,[132,i] E. M. Carlson,[171] J. Carmignani,[94] L. Carminati,[71a,71b] A. Carnelli,[4] M. Carnesale,[37] S. Caron,[116] E. Carquin,[140f] I. B. Carr,[107] S. Carrá,[71a] G. Carratta,[24b,24a] A. M. Carroll,[126] M. P. Casado,[13,j] M. Caspar,[48] F. L. Castillo,[4] L. Castillo Garcia,[13] V. Castillo Gimenez,[169] N. F. Castro,[133a,133e] A. Catinaccio,[37] J. R. Catmore,[128] T. Cavaliere,[4] V. Cavaliere,[30] L. J. Caviedes Betancourt,[23b] Y. C. Cekmecelioglu,[48] E. Celebi,[82] S. Cella,[37] V. Cepaitis,[56] K. Cerny,[125] A. S. Cerqueira,[83a] A. Cerri,[74a,74b,k] L. Cerrito,[76a,76b] F. Cerutti,[18a] B. Cervato,[71a,71b] A. Cervelli,[24b] G. Cesarini,[53] S. A. Cetin,[82] P. M. Chabrillat,[130] S. Chakraborty,[173] J. Chan,[18a] W. Y. Chan,[159] J. D. Chapman,[33] E. Chapon,[138] B. Chargeishvili,[155b] D. G. Charlton,[21] C. Chauhan,[136] Y. Che,[114a] S. Chekanov,[6] S. V. Chekulaev,[162a] G. A. Chelkov,[39,l] B. Chen,[157] B. Chen,[171] H. Chen,[114a] H. Chen,[30] J. Chen,[144a] J. Chen,[148] M. Chen,[129] S. Chen,[89] S. J. Chen,[114a] X. Chen,[144a] X. Chen,[15,m] Z. Chen,[62] C. L. Cheng,[176] H. C. Cheng,[64a] S. Cheong,[149] A. Cheplakov,[39] E. Cheremushkina,[48] E. Cherepanova,[117] R. Cherkaoui El Moursli,[36e] E. Cheu,[7] K. Cheung,[65] L. Chevalier,[138] V. Chiarella,[53] G. Chiarelli,[74a] G. Chiodini,[70a] A. S. Chisholm,[21] A. Chitan,[28b] M. Chitishvili,[169] M. V. Chizhov,[39,n] K. Choi,[11] Y. Chou,[142] E. Y. S. Chow,[116] K. L. Chu,[175] M. C. Chu,[64a] X. Chu,[14,114c] Z. Chubinidze,[53] J. Chudoba,[134] J. J. Chwastowski,[88] D. Cieri,[112] K. M. Ciesla,[87a] V. Cindro,[95] A. Ciocio,[18a] F. Cirotto,[72a,72b] Z. H. Citron,[175] M. Citterio,[71a] D. A. Ciubotaru,[28b] A. Clark,[56] P. J. Clark,[52] N. Clarke Hall,[98] C. Clarry,[161] S. E. Clawson,[48] C. Clement,[47a,47b] Y. Coadou,[104] M. Cobal,[69a,69c] A. Coccaro,[57b] R. F. Coelho Barrue,[133a] R. Coelho Lopes De Sa,[105] S. Coelli,[71a] L. S. Colangeli,[161] B. Cole,[42] P. Collado Soto,[101] J. Collot,[60] R. Coluccia,[70a,70b] P. Conde Muiño,[133a,133g] M. P. Connell,[34c] S. H. Connell,[34c] E. I. Conroy,[129] M. Contreras Cossio,[11] F. Conventi,[72a,o] H. G. Cooke,[21] A. M. Cooper-Sarkar,[129] L. Corazzina,[75a,75b] F. A. Corchia,[24b,24a] A. Cordeiro Oudot Choi,[142] L. D. Corpe,[41] M. Corradi,[75a,75b] F. Corriveau,[106,p] A. Cortes-Gonzalez,[19] M. J. Costa,[169] F. Costanza,[4] D. Costanzo,[145] B. M. Cote,[122] J. Couthures,[4] G. Cowan,[97] K. Cranmer,[176] L. Cremer,[49] D. Cremonini,[24b,24a] S. Crépé-Renaudin,[60] F. Crescioli,[130] T. Cresta,[73a,73b] M. Cristinziani,[147] M. Cristoforetti,[78a,78b] V. Croft,[117] J. E. Crosby,[124] G. Crosetti,[44b,44a] A. Cueto,[101] H. Cui,[98] Z. Cui,[7] W. R. Cunningham,[59] F. Curcio,[169] J. R. Curran,[52] M. J. Da Cunha Sargedas De Sousa,[57b,57a] J. V. Da Fonseca Pinto,[83b] C. Da Via,[103] W. Dabrowski,[87a] T. Dado,[37] S. Dahbi,[154] T. Dai,[108] D. Dal Santo,[20] C. Dallapiccola,[105] M. Dam,[43] G. D'amen,[30] V. D'Amico,[111] J. Damp,[102] J. R. Dandoy,[35] D. Dannheim,[37] G. D'anniballe,[74a,74b] M. Danninger,[148] V. Dao,[151] G. Darbo,[57b] S. J. Das,[30] F. Dattola,[48] S. D'Auria,[71a,71b] A. D'Avanzo,[72a,72b] T. Davidek,[136] J. Davidson,[173] I. Dawson,[96] K. De,[8] C. De Almeida Rossi,[161]

R. De Asmundis,[72a] N. De Biase,[48] S. De Castro,[24b,24a] N. De Groot,[116] P. de Jong,[117] H. De la Torre,[118] A. De Maria,[114a] A. De Salvo,[75a] U. De Sanctis,[76a,76b] F. De Santis,[70a,70b] A. De Santo,[152] J. B. De Vivie De Regie,[60] J. Debevc,[95] D. V. Dedovich,[39] J. Degens,[94] A. M. Deiana,[45] J. Del Peso,[101] L. Delagrange,[130] F. Deliot,[138] C. M. Delitzsch,[49] M. Della Pietra,[72a,72b] D. Della Volpe,[56] A. Dell'Acqua,[37] L. Dell'Asta,[71a,71b] M. Delmastro,[4] C. C. Delogu,[102] P. A. Delsart,[60] S. Demers,[178] M. Demichev,[39] S. P. Denisov,[38] H. Denizli,[22a,q] L. D'Eramo,[41] D. Derendarz,[88] F. Derue,[130] P. Dervan,[94,a] K. Desch,[25] F. A. Di Bello,[57b,57a] A. Di Ciaccio,[76a,76b] L. Di Ciaccio,[4] A. Di Domenico,[75a,75b] C. Di Donato,[72a,72b] A. Di Girolamo,[37] G. Di Gregorio,[37] A. Di Luca,[78a,78b] B. Di Micco,[77a,77b] R. Di Nardo,[77a,77b] K. F. Di Petrillo,[40] M. Diamantopoulou,[35] F. A. Dias,[117] M. A. Diaz,[140a,140b] A. R. Didenko,[39] M. Didenko,[169] S. D. Diefenbacher,[18a] E. B. Diehl,[108] S. Díez Cornell,[48] C. Diez Pardos,[147] C. Dimitriadi,[150] A. Dimitrievska,[21] A. Dimri,[151] J. Dingfelder,[25] T. Dingley,[129] I-M. Dinu,[28b] S. J. Dittmeier,[63b] F. Dittus,[37] M. Divisek,[136] B. Dixit,[94] F. Djama,[104] T. Djobava,[155b] C. Doglioni,[103,100] A. Dohnalova,[29a] Z. Dolezal,[136] K. Domijan,[87a] K. M. Dona,[40] M. Donadelli,[83d] B. Dong,[109] J. Donini,[41] A. D'Onofrio,[72a,72b] M. D'Onofrio,[94] J. Dopke,[137] A. Doria,[72a] N. Dos Santos Fernandes,[133a] P. Dougan,[103] M. T. Dova,[92] A. T. Doyle,[59] M. A. Draguet,[129] M. P. Drescher,[55] E. Dreyer,[175] I. Drivas-koulouris,[10] M. Drnevich,[120] M. Drozdova,[56] D. Du,[62] T. A. du Pree,[117] Z. Duan,[114a] F. Dubinin,[39] M. Dubovsky,[29a] E. Duchovni,[175] G. Duckeck,[111] P. K. Duckett,[98] O. A. Ducu,[28b] D. Duda,[52] A. Dudarev,[37] E. R. Duden,[27] M. D'uffizi,[103] L. Duflot,[66] M. Dührssen,[37] I. Duminica,[28g] A. E. Dumitriu,[28b] M. Dunford,[63a] S. Dungs,[49] K. Dunne,[47a,47b] A. Duperrin,[104] H. Duran Yildiz,[3a] M. Düren,[58] A. Durglishvili,[155b] D. Duvnjak,[35] B. L. Dwyer,[118] G. I. Dyckes,[18a] M. Dyndal,[87a] B. S. Dziedzic,[37] Z. O. Earnshaw,[152] G. H. Eberwein,[129] B. Eckerova,[29a] S. Eggebrecht,[55] E. Egidio Purcino De Souza,[83e] G. Eigen,[17] K. Einsweiler,[18a] T. Ekelof,[167] P. A. Ekman,[100] S. El Farkh,[36b] Y. El Ghazali,[62] H. El Jarrari,[37] A. El Moussaouy,[36a] V. Ellajosyula,[167] M. Ellert,[167] F. Ellinghaus,[177] N. Ellis,[37] J. Elmsheuser,[30] M. Elsawy,[119a] M. Elsing,[37] D. Emeliyanov,[137] Y. Enari,[84] I. Ene,[18a] S. Epari,[110] D. Ernani Martins Neto,[88] F. Ernst,[37] M. Errenst,[177] M. Escalier,[66] C. Escobar,[169] E. Etzion,[157] G. Evans,[133a,133b] H. Evans,[68] L. S. Evans,[97] A. Ezhilov,[38] S. Ezzarqtouni,[36a] F. Fabbri,[24b,24a] L. Fabbri,[24b,24a] G. Facini,[98] V. Fadeyev,[139] R. M. Fakhrutdinov,[38] D. Fakoudis,[102] S. Falciano,[75a] L. F. Falda Ulhoa Coelho,[133a] F. Fallavollita,[112] G. Falsetti,[44b,44a] J. Faltova,[136] C. Fan,[168] K. Y. Fan,[64b] Y. Fan,[14] Y. Fang,[14,114c] M. Fanti,[71a,71b] M. Faraj,[69a,69b] Z. Farazpay,[99] A. Farbin,[8] A. Farilla,[77a] T. Farooque,[109] J. N. Farr,[178] S. M. Farrington,[137,52] F. Fassi,[36e] D. Fassouliotis,[9] L. Fayard,[66] P. Federic,[136] P. Federicova,[134] O. L. Fedin,[38,l] M. Feickert,[176] L. Feligioni,[104] D. E. Fellers,[18a] C. Feng,[143a] Z. Feng,[117] M. J. Fenton,[165] L. Ferencz,[48] B. Fernandez Barbadillo,[93] P. Fernandez Martinez,[67] M. J. V. Fernoux,[104] J. Ferrando,[93] A. Ferrari,[167] P. Ferrari,[117,116] R. Ferrari,[73a] D. Ferrere,[56] C. Ferretti,[108] M. P. Fewell,[1] D. Fiacco,[75a,75b] F. Fiedler,[102] P. Fiedler,[135] S. Filimonov,[39] M. S. Filip,[28b,r] A. Filipčič,[95] E. K. Filmer,[162a] F. Filthaut,[116] M. C. N. Fiolhais,[133a,133c,s] L. Fiorini,[169] W. C. Fisher,[109] T. Fitschen,[103] P. M. Fitzhugh,[138] I. Fleck,[147] P. Fleischmann,[108] T. Flick,[177] M. Flores,[34d,t] L. R. Flores Castillo,[64a] L. Flores Sanz De Acedo,[37] F. M. Follega,[78a,78b] N. Fomin,[33] J. H. Foo,[161] A. Formica,[138] A. C. Forti,[103] E. Fortin,[37] A. W. Fortman,[18a] L. Foster,[18a] L. Fountas,[9,u] D. Fournier,[66] H. Fox,[93] P. Francavilla,[74a,74b] S. Francescato,[61] S. Franchellucci,[56] M. Franchini,[24b,24a] S. Franchino,[63a] D. Francis,[37] L. Franco,[116] V. Franco Lima,[37] L. Franconi,[48] M. Franklin,[61] G. Frattari,[27] Y. Y. Frid,[157] J. Friend,[59] N. Fritzsche,[37] A. Froch,[56] D. Froidevaux,[37] J. A. Frost,[129] Y. Fu,[109] S. Fuenzalida Garrido,[140f] M. Fujimoto,[104] K. Y. Fung,[64a] E. Furtado De Simas Filho,[83e] M. Furukawa,[159] J. Fuster,[169] A. Gaa,[55] A. Gabrielli,[24b,24a] A. Gabrielli,[161] P. Gadow,[37] G. Gagliardi,[57b,57a] L. G. Gagnon,[18a] S. Gaid,[85b] S. Galantzan,[157] J. Gallagher,[1] E. J. Gallas,[129] A. L. Gallen,[167] B. J. Gallop,[137] K. K. Gan,[122] S. Ganguly,[159] Y. Gao,[52] A. Garabaglu,[142] F. M. Garay Walls,[140a,140b] C. García,[169] A. Garcia Alonso,[117] A. G. Garcia Caffaro,[178] J. E. García Navarro,[169] M. Garcia-Sciveres,[18a] G. L. Gardner,[131] R. W. Gardner,[40] N. Garelli,[164] R. B. Garg,[149] J. M. Gargan,[52] C. A. Garner,[161] C. M. Garvey,[34a] V. K. Gassmann,[164] G. Gaudio,[73a] V. Gautam,[13] P. Gauzzi,[75a,75b] J. Gavranovic,[95] I. L. Gavrilenko,[133a] A. Gavrilyuk,[38] C. Gay,[170] G. Gaycken,[126] E. N. Gazis,[10] A. Gekow,[122] C. Gemme,[57b] M. H. Genest,[60] A. D. Gentry,[115] S. George,[97] T. Geralis,[46] A. A. Gerwin,[123] P. Gessinger-Befurt,[37] M. E. Geyik,[177] M. Ghani,[173] K. Ghorbanian,[96] A. Ghosal,[147] A. Ghosh,[165] A. Ghosh,[7] B. Giacobbe,[24b] S. Giagu,[75a,75b] T. Giani,[117] A. Giannini,[62] S. M. Gibson,[97] M. Gignac,[139] D. T. Gil,[87b] A. K. Gilbert,[87a]

B. J. Gilbert,[42] D. Gillberg,[35] G. Gilles,[117] D. M. Gingrich,[2,e] M. P. Giordani,[69a,69c] P. F. Giraud,[138] G. Giugliarelli,[69a,69c] D. Giugni,[71a] F. Giuli,[76a,76b] I. Gkialas,[9,u] L. K. Gladilin,[38] C. Glasman,[101] M. Glazewska,[20] G. Glemža,[48] M. Glisic,[126] I. Gnesi,[44b] Y. Go,[30] M. Goblirsch-Kolb,[37] B. Gocke,[49] D. Godin,[110] B. Gokturk,[22a] S. Goldfarb,[107] T. Golling,[56] M. G. D. Gololo,[34c] D. Golubkov,[38] J. P. Gombas,[109] A. Gomes,[133a,133b] G. Gomes Da Silva,[147] A. J. Gomez Delegido,[169] R. Gonçalo,[133a] L. Gonella,[21] A. Gongadze,[155c] F. Gonnella,[21] J. L. Gonski,[149] R. Y. González Andana,[52] S. González de la Hoz,[169] M. V. Gonzalez Rodrigues,[48] R. Gonzalez Suarez,[167] S. Gonzalez-Sevilla,[56] L. Goossens,[37] B. Gorini,[37] E. Gorini,[70a,70b] A. Gorišek,[95] T. C. Gosart,[131] A. T. Goshaw,[51] M. I. Gostkin,[39] S. Goswami,[124] C. A. Gottardo,[37] S. A. Gotz,[111] M. Gouighri,[36b] A. G. Goussiou,[142] N. Govender,[34c] R. P. Grabarczyk,[129] I. Grabowska-Bold,[87a] K. Graham,[35] E. Gramstad,[128] S. Grancagnolo,[70a,70b] C. M. Grant,[1] P. M. Gravila,[28f] F. G. Gravili,[70a,70b] H. M. Gray,[18a] M. Greco,[112] M. J. Green,[1] C. Grefe,[25] A. S. Grefsrud,[17] I. M. Gregor,[48] K. T. Greif,[165] P. Grenier,[149] S. G. Grewe,[112] A. A. Grillo,[139] K. Grimm,[32] S. Grinstein,[13,v] J.-F. Grivaz,[66] E. Gross,[175] J. Grosse-Knetter,[55] L. Guan,[108] G. Guerrieri,[37] R. Guevara,[128] R. Gugel,[102] J. A. M. Guhit,[108] A. Guida,[19] E. Guilloton,[173] S. Guindon,[37] F. Guo,[14,114c] J. Guo,[144a] L. Guo,[48] L. Guo,[114b,w] Y. Guo,[108] A. Gupta,[49] R. Gupta,[132] S. Gupta,[27] S. Gurbuz,[25] S. S. Gurdasani,[48] G. Gustavino,[75a,75b] P. Gutierrez,[123] L. F. Gutierrez Zagazeta,[131] M. Gutsche,[50] C. Gutschow,[98] C. Gwenlan,[129] C. B. Gwilliam,[94] E. S. Haaland,[128] A. Haas,[120] M. Habedank,[59] C. Haber,[18a] H. K. Hadavand,[8] A. Haddad,[41] A. Hadef,[50] A. I. Hagan,[93] J. J. Hahn,[147] E. H. Haines,[98] M. Haleem,[172] J. Haley,[124] G. D. Hallewell,[104] L. Halser,[20] K. Hamano,[171] M. Hamer,[25] S. E. D. Hammoud,[66] E. J. Hampshire,[97] J. Han,[143a] L. Han,[114a] L. Han,[62] S. Han,[18a] K. Hanagaki,[84] M. Hance,[139] D. A. Hangal,[42] H. Hanif,[148] M. D. Hank,[131] J. B. Hansen,[43] P. H. Hansen,[43] D. Harada,[56] T. Harenberg,[177] S. Harkusha,[179] M. L. Harris,[105] Y. T. Harris,[25] J. Harrison,[13] N. M. Harrison,[122] P. F. Harrison,[173] M. L. E. Hart,[98] N. M. Hartman,[112] N. M. Hartmann,[111] R. Z. Hasan,[97,137] Y. Hasegawa,[146] F. Haslbeck,[129] S. Hassan,[17] R. Hauser,[109] M. Haviernik,[136] C. M. Hawkes,[21] R. J. Hawkings,[37] Y. Hayashi,[159] D. Hayden,[109] C. Hayes,[108] R. L. Hayes,[117] C. P. Hays,[129] J. M. Hays,[96] H. S. Hayward,[94] M. He,[14,114c] Y. He,[48] Y. He,[98] N. B. Heatley,[96] V. Hedberg,[100] C. Heidegger,[54] K. K. Heidegger,[54] J. Heilman,[35] S. Heim,[48] T. Heim,[18a] J. G. Heinlein,[131] J. J. Heinrich,[126] L. Heinrich,[112] J. Hejbal,[134] M. Helbig,[50] A. Held,[176] S. Hellesund,[17] C. M. Helling,[170] S. Hellman,[47a,47b] L. Henkelmann,[33] A. M. Henriques Correia,[37] H. Herde,[100] Y. Hernández Jiménez,[151] L. M. Herrmann,[25] T. Herrmann,[50] G. Herten,[54] R. Hertenberger,[111] L. Hervas,[37] M. E. Hesping,[102] N. P. Hessey,[162a] J. Hessler,[112] M. Hidaoui,[36b] N. Hidic,[136] E. Hill,[161] T. S. Hillersoy,[17] S. J. Hillier,[21] J. R. Hinds,[109] F. Hinterkeuser,[25] M. Hirose,[127] S. Hirose,[163] D. Hirschbuehl,[177] T. G. Hitchings,[103] B. Hiti,[95] J. Hobbs,[151] R. Hobincu,[28e] N. Hod,[175] A. M. Hodges,[168] M. C. Hodgkinson,[145] B. H. Hodkinson,[129] A. Hoecker,[37] D. D. Hofer,[108] J. Hofer,[169] M. Holzbock,[37] L. B. A. H. Hommels,[33] V. Homsak,[129] B. P. Honan,[103] J. J. Hong,[68] T. M. Hong,[132] B. H. Hooberman,[168] W. H. Hopkins,[6] M. C. Hoppesch,[168] Y. Horii,[113] M. E. Horstmann,[112] S. Hou,[154] M. R. Housenga,[168] A. S. Howard,[95] J. Howarth,[59] J. Hoya,[6] M. Hrabovsky,[125] T. Hryn'ova,[4] P. J. Hsu,[65] S.-C. Hsu,[142] T. Hsu,[66] M. Hu,[18a] Q. Hu,[62] S. Huang,[33] X. Huang,[14,114c] Y. Huang,[136] Y. Huang,[114b] Y. Huang,[102] Y. Huang,[14] Z. Huang,[66] Z. Hubacek,[135] M. Huebner,[25] F. Huegging,[25] T. B. Huffman,[129] M. Hufnagel Maranha De Faria,[83a] C. A. Hugli,[48] M. Huhtinen,[37] S. K. Huiberts,[17] R. Hulsken,[106] C. E. Hultquist,[18a] N. Huseynov,[12,x] J. Huston,[109] J. Huth,[61] R. Hyneman,[7] G. Iacobucci,[56] G. Iakovidis,[30] L. Iconomidou-Fayard,[66] J. P. Iddon,[37] P. Iengo,[72a,72b] R. Iguchi,[159] Y. Iiyama,[159] T. Iizawa,[159] Y. Ikegami,[84] D. Iliadis,[158] N. Ilic,[161] H. Imam,[36a] G. Inacio Goncalves,[83d] S. A. Infante Cabanas,[140c] T. Ingebretsen Carlson,[47a,47b] J. M. Inglis,[96] G. Introzzi,[73a,73b] M. Iodice,[77a] V. Ippolito,[75a,75b] R. K. Irwin,[94] M. Ishino,[159] W. Islam,[176] C. Issever,[19] S. Istin,[22a,y] K. Itabashi,[84] H. Ito,[174] R. Iuppa,[78a,78b] A. Ivina,[175] V. Izzo,[72a] P. Jacka,[134] P. Jackson,[1] P. Jain,[48] K. Jakobs,[54] T. Jakoubek,[175] J. Jamieson,[59] W. Jang,[159] S. Jankovych,[136] M. Javurkova,[105] P. Jawahar,[103] L. Jeanty,[126] J. Jejelava,[155a,z] P. Jenni,[54,aa] C. E. Jessiman,[35] C. Jia,[143a] H. Jia,[170] J. Jia,[151] X. Jia,[14,114c] Z. Jia,[114a] C. Jiang,[52] Q. Jiang,[64b] S. Jiggins,[48] M. Jimenez Ortega,[169] J. Jimenez Pena,[13] S. Jin,[114a] A. Jinaru,[28b] O. Jinnouchi,[141] P. Johansson,[145] K. A. Johns,[7] J. W. Johnson,[139] F. A. Jolly,[48] D. M. Jones,[152] E. Jones,[48] K. S. Jones,[8] P. Jones,[33] R. W. L. Jones,[93] T. J. Jones,[94] H. L. Joos,[55,37] R. Joshi,[122] J. Jovicevic,[16] X. Ju,[18a] J. J. Junggeburth,[37] T. Junkermann,[63a] A. Juste Rozas,[13,v] M. K. Juzek,[88] S. Kabana,[140e] A. Kaczmarska,[88]

M. Kado,[112] H. Kagan,[122] M. Kagan,[149] A. Kahn,[131] C. Kahra,[102] T. Kaji,[159] E. Kajomovitz,[156] N. Kakati,[175] N. Kakoty,[13] I. Kalaitzidou,[54] S. Kandel,[8] N. J. Kang,[139] D. Kar,[34g] K. Karava,[129] E. Karentzos,[25] O. Karkout,[117] S. N. Karpov,[39] Z. M. Karpova,[39] V. Kartvelishvili,[93] A. N. Karyukhin,[38] E. Kasimi,[158] J. Katzy,[48] S. Kaur,[35] K. Kawade,[146] M. P. Kawale,[123] C. Kawamoto,[89] T. Kawamoto,[62] E. F. Kay,[37] F. I. Kaya,[164] S. Kazakos,[109] V. F. Kazanin,[38] J. M. Keaveney,[34a] R. Keeler,[171] G. V. Kehris,[61] J. S. Keller,[35] J. J. Kempster,[152] O. Kepka,[134] J. Kerr,[162b] B. P. Kerridge,[137] B. P. Kerševan,[95] L. Keszeghova,[29a] R. A. Khan,[132] A. Khanov,[124] A. G. Kharlamov,[38] T. Kharlamova,[38] E. E. Khoda,[142] M. Kholodenko,[133a] T. J. Khoo,[19] G. Khoriauli,[172] Y. Khoulaki,[36a] J. Khubua,[155b,a] Y. A. R. Khwaira,[130] B. Kibirige,[34g] D. Kim,[6] D. W. Kim,[47a,47b] Y. K. Kim,[40] N. Kimura,[98] M. K. Kingston,[55] A. Kirchhoff,[55] C. Kirfel,[25] F. Kirfel,[25] J. Kirk,[137] A. E. Kiryunin,[112] S. Kita,[163] O. Kivernyk,[25] M. Klassen,[164] C. Klein,[35] L. Klein,[172] M. H. Klein,[45] S. B. Klein,[56] U. Klein,[94] A. Klimentov,[30] T. Klioutchnikova,[37] P. Kluit,[117] S. Kluth,[112] E. Kneringer,[79] T. M. Knight,[161] A. Knue,[49] M. Kobel,[50] D. Kobylianskii,[175] S. F. Koch,[129] M. Kocian,[149] P. Kodyš,[136] D. M. Koeck,[126] T. Koffas,[35] O. Kolay,[50] I. Koletsou,[4] T. Komarek,[88] K. Köneke,[55] A. X. Y. Kong,[1] T. Kono,[121] N. Konstantinidis,[98] P. Kontaxakis,[56] B. Konya,[100] R. Kopeliansky,[42] S. Koperny,[87a] K. Korcyl,[88] K. Kordas,[158,bb] A. Korn,[98] S. Korn,[55] I. Korolkov,[13] N. Korotkova,[38] B. Kortman,[117] O. Kortner,[112] S. Kortner,[112] W. H. Kostecka,[118] M. Kostov,[29a] V. V. Kostyukhin,[147] A. Kotsokechagia,[37] A. Kotwal,[51] A. Koulouris,[37] A. Kourkoumeli-Charalampidi,[73a,73b] C. Kourkoumelis,[9] E. Kourlitis,[112] O. Kovanda,[126] R. Kowalewski,[171] W. Kozanecki,[126] A. S. Kozhin,[38] V. A. Kramarenko,[38] G. Kramberger,[95] P. Kramer,[25] M. W. Krasny,[130] A. Krasznahorkay,[105] A. C. Kraus,[118] J. W. Kraus,[177] J. A. Kremer,[48] N. B. Krengel,[147] T. Kresse,[50] L. Kretschmann,[177] J. Kretzschmar,[94] K. Kreul,[19] P. Krieger,[161] K. Krizka,[21] K. Kroeninger,[49] H. Kroha,[112] J. Kroll,[134] J. Kroll,[131] K. S. Krowpman,[109] U. Kruchonak,[39] H. Krüger,[25] N. Krumnack,[81] M. C. Kruse,[51] O. Kuchinskaia,[39] S. Kuday,[3a] S. Kuehn,[37] R. Kuesters,[54] T. Kuhl,[48] V. Kukhtin,[39] Y. Kulchitsky,[39] S. Kuleshov,[140d,140b] J. Kull,[1] M. Kumar,[34g] N. Kumari,[48] P. Kumari,[162b] A. Kupco,[134] T. Kupfer,[49] A. Kupich,[38] O. Kuprash,[54] H. Kurashige,[86] L. L. Kurchaninov,[162a] O. Kurdysh,[4] Y. A. Kurochkin,[38] A. Kurova,[38] M. Kuze,[141] A. K. Kvam,[105] J. Kvita,[125] N. G. Kyriacou,[108] C. Lacasta,[169] F. Lacava,[75a,75b] H. Lacker,[19] D. Lacour,[130] N. N. Lad,[98] E. Ladygin,[39] A. Lafarge,[41] B. Laforge,[130] T. Lagouri,[178] F. Z. Lahbabi,[36a] S. Lai,[55] J. E. Lambert,[171] S. Lammers,[68] W. Lampl,[7] C. Lampoudis,[158,bb] G. Lamprinoudis,[102] A. N. Lancaster,[118] E. Lançon,[30] U. Landgraf,[54] M. P. J. Landon,[96] V. S. Lang,[54] O. K. B. Langrekken,[128] A. J. Lankford,[165] F. Lanni,[37] K. Lantzsch,[25] A. Lanza,[73a] M. Lanzac Berrocal,[169] J. F. Laporte,[138] T. Lari,[71a] D. Larsen,[17] L. Larson,[11] F. Lasagni Manghi,[24b] M. Lassnig,[37] S. D. Lawlor,[145] R. Lazaridou,[173] M. Lazzaroni,[71a,71b] H. D. M. Le,[109] E. M. Le Boulicaut,[178] L. T. Le Pottier,[18a] B. Leban,[24b,24a] F. Ledroit-Guillon,[60] T. F. Lee,[162b] L. L. Leeuw,[34c] M. Lefebvre,[171] C. Leggett,[18a] G. Lehmann Miotto,[37] M. Leigh,[56] W. A. Leight,[105] W. Leinonen,[116] A. Leisos,[158,cc] M. A. L. Leite,[83c] C. E. Leitgeb,[19] R. Leitner,[136] K. J. C. Leney,[45] T. Lenz,[25] S. Leone,[74a] C. Leonidopoulos,[52] A. Leopold,[150] J. H. Lepage Bourbonnais,[35] R. Les,[109] C. G. Lester,[33] M. Levchenko,[38] J. Levêque,[4] L. J. Levinson,[175] G. Levrini,[24b,24a] M. P. Lewicki,[88] C. Lewis,[142] D. J. Lewis,[4] L. Lewitt,[145] A. Li,[30] B. Li,[143a] C. Li,[108] C-Q. Li,[112] H. Li,[143a] H. Li,[103] H. Li,[15] H. Li,[62] H. Li,[143a] J. Li,[144a] K. Li,[14] L. Li,[144a] R. Li,[178] S. Li,[14,114c] S. Li,[144b,144a] T. Li,[5] X. Li,[106] Z. Li,[159] Z. Li,[14,114c] Z. Li,[62] S. Liang,[14,114c] Z. Liang,[14] M. Liberatore,[138] B. Liberti,[76a] K. Lie,[64c] J. Lieber Marin,[83e] H. Lien,[68] H. Lin,[108] S. F. Lin,[151] L. Linden,[111] R. E. Lindley,[7] J. H. Lindon,[37] J. Ling,[61] E. Lipeles,[131] A. Lipniacka,[17] A. Lister,[170] J. D. Little,[68] B. Liu,[14] B. X. Liu,[114b] D. Liu,[144b,144a] D. Liu,[139] E. H. L. Liu,[21] J. K. K. Liu,[120] K. Liu,[144b] K. Liu,[144b,144a] M. Liu,[62] M. Y. Liu,[62] P. Liu,[14] Q. Liu,[144b,142,144a] X. Liu,[62] X. Liu,[143a] Y. Liu,[114b,114c] Y. L. Liu,[143a] Y. W. Liu,[62] Z. Liu,[66,dd] S. L. Lloyd,[96] E. M. Lobodzinska,[48] P. Loch,[7] E. Lodhi,[161] T. Lohse,[19] K. Lohwasser,[145] E. Loiacono,[48] J. D. Lomas,[21] J. D. Long,[42] I. Longarini,[165] R. Longo,[168] A. Lopez Solis,[13] N. A. Lopez-canelas,[7] N. Lorenzo Martinez,[4] A. M. Lory,[111] M. Losada,[119a] G. Löschcke Centeno,[152] X. Lou,[47a,47b] X. Lou,[14,114c] A. Lounis,[66] P. A. Love,[93] M. Lu,[66] S. Lu,[131] Y. J. Lu,[154] H. J. Lubatti,[142] C. Luci,[75a,75b] F. L. Lucio Alves,[114a] F. Luehring,[68] B. S. Lunday,[131] O. Lundberg,[150] J. Lunde,[37] N. A. Luongo,[6] M. S. Lutz,[37] A. B. Lux,[26] D. Lynn,[30] R. Lysak,[134] V. Lysenko,[135] E. Lytken,[100] V. Lyubushkin,[39] T. Lyubushkina,[39] M. M. Lyukova,[151] M. Firdaus M. Soberi,[52] H. Ma,[30] K. Ma,[62] L. L. Ma,[143a] W. Ma,[62] Y. Ma,[124] J. C. MacDonald,[102] P. C. Machado De Abreu Farias,[83e] R. Madar,[41]

T. Madula,[98] J. Maeda,[86] T. Maeno,[30] P. T. Mafa,[34c,ee] H. Maguire,[145] V. Maiboroda,[66] A. Maio,[133a,133b,133d] K. Maj,[87a] O. Majersky,[48] S. Majewski,[126] R. Makhmanazarov,[38] N. Makovec,[66] V. Maksimovic,[16] B. Malaescu,[130] J. Malamant,[128] Pa. Malecki,[88] V. P. Maleev,[38] F. Malek,[60,ff] M. Mali,[95] D. Malito,[97] U. Mallik,[80,a] A. Maloizel,[5] S. Maltezos,[10] A. Malvezzi Lopes,[83d] S. Malyukov,[39] J. Mamuzic,[13] G. Mancini,[53] M. N. Mancini,[27] G. Manco,[73a,73b] J. P. Mandalia,[96] S. S. Mandarry,[152] I. Mandić,[95] L. Manhaes de Andrade Filho,[83a] I. M. Maniatis,[175] J. Manjarres Ramos,[91] D. C. Mankad,[175] A. Mann,[111] T. Manoussos,[37] M. N. Mantinan,[40] S. Manzoni,[37] L. Mao,[144a] X. Mapekula,[34c] A. Marantis,[158] R. R. Marcelo Gregorio,[96] G. Marchiori,[5] M. Marcisovsky,[134] C. Marcon,[71a] E. Maricic,[16] M. Marinescu,[48] S. Marium,[48] M. Marjanovic,[123] A. Markhoos,[54] M. Markovitch,[66] M. K. Maroun,[105] G. T. Marsden,[103] E. J. Marshall,[93] Z. Marshall,[18a] S. Marti-Garcia,[169] J. Martin,[98] T. A. Martin,[137] V. J. Martin,[52] B. Martin dit Latour,[17] L. Martinelli,[75a,75b] M. Martinez,[13,v] P. Martinez Agullo,[169] V. I. Martinez Outschoorn,[105] P. Martinez Suarez,[13] S. Martin-Haugh,[137] G. Martinovicova,[136] V. S. Martoiu,[28b] A. C. Martyniuk,[98] A. Marzin,[37] D. Mascione,[78a,78b] L. Masetti,[102] J. Masik,[103] A. L. Maslennikov,[39] S. L. Mason,[42] P. Massarotti,[72a,72b] P. Mastrandrea,[74a,74b] A. Mastroberardino,[44b,44a] T. Masubuchi,[127] T. T. Mathew,[126] J. Matousek,[136] D. M. Mattern,[49] J. Maurer,[28b] T. Maurin,[59] A. J. Maury,[66] B. Maček,[95] C. Mavungu Tsava,[104] D. A. Maximov,[38] A. E. May,[103] E. Mayer,[41] R. Mazini,[34g] I. Maznas,[118] S. M. Mazza,[139] E. Mazzeo,[71a,71b] J. P. Mc Gowan,[171] S. P. Mc Kee,[108] C. A. Mc Lean,[6] C. C. McCracken,[170] E. F. McDonald,[107] A. E. McDougall,[117] L. F. Mcelhinney,[93] J. A. Mcfayden,[152] R. P. McGovern,[131] R. P. Mckenzie,[34g] T. C. Mclachlan,[48] D. J. Mclaughlin,[98] S. J. McMahon,[137] C. M. Mcpartland,[94] R. A. McPherson,[171,p] S. Mehlhase,[111] A. Mehta,[94] D. Melini,[169] B. R. Mellado Garcia,[34g] A. H. Melo,[55] F. Meloni,[48] A. M. Mendes Jacques Da Costa,[103] L. Meng,[93] S. Menke,[112] M. Mentink,[37] E. Meoni,[44b,44a] G. Mercado,[118] S. Merianos,[158] C. Merlassino,[69a,69c] C. Meroni,[71a,71b] J. Metcalfe,[6] A. S. Mete,[6] E. Meuser,[102] C. Meyer,[68] J-P. Meyer,[138] Y. Miao,[114a] R. P. Middleton,[137] M. Mihovilovic,[66] L. Mijović,[52] G. Mikenberg,[175] M. Mikestikova,[134] M. Mikuž,[95] H. Mildner,[102] A. Milic,[37] D. W. Miller,[40] E. H. Miller,[149] L. S. Miller,[35] A. Milov,[175] D. A. Milstead,[47a,47b] T. Min,[114a] A. A. Minaenko,[38] I. A. Minashvili,[155b] A. I. Mincer,[120] B. Mindur,[87a] M. Mineev,[39] Y. Mino,[89] L. M. Mir,[13] M. Miralles Lopez,[59] M. Mironova,[18a] M. Missio,[116] A. Mitra,[173] V. A. Mitsou,[169] Y. Mitsumori,[113] O. Miu,[161] P. S. Miyagawa,[96] T. Mkrtchyan,[63a] M. Mlinarevic,[98] T. Mlinarevic,[98] M. Mlynarikova,[37] S. Mobius,[20] M. H. Mohamed Farook,[115] A. F. Mohammed,[14,114c] S. Mohapatra,[42] S. Mohiuddin,[124] G. Mokgatitswane,[34g] L. Moleri,[175] U. Molinatti,[129] L. G. Mollier,[20] B. Mondal,[134] S. Mondal,[135] K. Mönig,[48] E. Monnier,[104] L. Monsonis Romero,[169] J. Montejo Berlingen,[13] A. Montella,[47a,47b] M. Montella,[122] F. Montereali,[77a,77b] F. Monticelli,[92] S. Monzani,[69a,69c] A. Morancho Tarda,[43] N. Morange,[66] A. L. Moreira De Carvalho,[48] M. Moreno Llácer,[169] C. Moreno Martinez,[56] J. M. Moreno Perez,[23b] P. Morettini,[57b] S. Morgenstern,[37] M. Morii,[61] M. Morinaga,[159] M. Moritsu,[90] F. Morodei,[75a,75b] P. Moschovakos,[37] B. Moser,[54] M. Mosidze,[155b] T. Moskalets,[45] P. Moskvitina,[116] J. Moss,[32] P. Moszkowicz,[87a] A. Moussa,[36d] Y. Moyal,[175] H. Moyano Gomez,[13] E. J. W. Moyse,[105] O. Mtintsilana,[34g] S. Muanza,[104] M. Mucha,[25] J. Mueller,[132] R. Müller,[37] G. A. Mullier,[167] A. J. Mullin,[33] J. J. Mullin,[51] A. C. Mullins,[45] A. E. Mulski,[61] D. P. Mungo,[161] D. Munoz Perez,[169] F. J. Munoz Sanchez,[103] W. J. Murray,[173,137] M. Muškinja,[95] C. Mwewa,[48] A. G. Myagkov,[38,l] A. J. Myers,[8] G. Myers,[108] M. Myska,[135] B. P. Nachman,[18a] K. Nagai,[129] K. Nagano,[84] R. Nagasaka,[159] J. L. Nagle,[30,gg] E. Nagy,[104] A. M. Nairz,[37] Y. Nakahama,[84] K. Nakamura,[84] K. Nakkalil,[5] A. Nandi,[63b] H. Nanjo,[127] E. A. Narayanan,[45] Y. Narukawa,[159] I. Naryshkin,[38] L. Nasella,[71a,71b] S. Nasri,[119b] C. Nass,[25] G. Navarro,[23a] J. Navarro-Gonzalez,[169] A. Nayaz,[19] P. Y. Nechaeva,[38] S. Nechaeva,[24b,24a] F. Nechansky,[134] L. Nedic,[129] T. J. Neep,[21] A. Negri,[73a,73b] M. Negrini,[24b] C. Nellist,[117] C. Nelson,[106] K. Nelson,[108] S. Nemecek,[134] M. Nessi,[37,hh] M. S. Neubauer,[168] J. Newell,[94] P. R. Newman,[21] Y. W. Y. Ng,[168] B. Ngair,[119a] H. D. N. Nguyen,[110] J. D. Nichols,[123] R. B. Nickerson,[129] R. Nicolaidou,[138] J. Nielsen,[139] M. Niemeyer,[55] J. Niermann,[37] N. Nikiforou,[37] V. Nikolaenko,[38,l] I. Nikolic-Audit,[130] P. Nilsson,[30] I. Ninca,[48] G. Ninio,[157] A. Nisati,[75a] N. Nishu,[2] R. Nisius,[112] N. Nitika,[69a,69c] J-E. Nitschke,[50] E. K. Nkadimeng,[34b] T. Nobe,[159] T. Nommensen,[153] M. B. Norfolk,[145] B. J. Norman,[35] M. Noury,[36a] J. Novak,[95] T. Novak,[95] R. Novotny,[135] L. Nozka,[125] K. Ntekas,[165] N. M. J. Nunes De Moura Junior,[83b] J. Ocariz,[130] A. Ochi,[86] I. Ochoa,[133a] S. Oerdek,[48,ii] J. T. Offermann,[40] A. Ogrodnik,[136] A. Oh,[103]

C. C. Ohm,[150] H. Oide,[84] M. L. Ojeda,[37] Y. Okumura,[159] L. F. Oleiro Seabra,[133a] I. Oleksiyuk,[56] G. Oliveira Correa,[13] D. Oliveira Damazio,[30] J. L. Oliver,[165] Ö. O. Öncel,[54] A. P. O'Neill,[20] A. Onofre,[133a,133e,jj] P. U. E. Onyisi,[11] M. J. Oreglia,[40] D. Orestano,[77a,77b] R. Orlandini,[77a,77b] R. S. Orr,[161] L. M. Osojnak,[131] Y. Osumi,[113] G. Otero y Garzon,[31] H. Otono,[90] G. J. Ottino,[18a] M. Ouchrif,[36d] F. Ould-Saada,[128] T. Ovsiannikova,[142] M. Owen,[59] R. E. Owen,[137] V. E. Ozcan,[22a] F. Ozturk,[88] N. Ozturk,[8] S. Ozturk,[82] H. A. Pacey,[129] K. Pachal,[162a] A. Pacheco Pages,[13] C. Padilla Aranda,[13] G. Padovano,[75a,75b] S. Pagan Griso,[18a] G. Palacino,[68] A. Palazzo,[70a,70b] J. Pampel,[25] J. Pan,[178] T. Pan,[64a] D. K. Panchal,[11] C. E. Pandini,[117] J. G. Panduro Vazquez,[137] H. D. Pandya,[1] H. Pang,[138] P. Pani,[48] G. Panizzo,[69a,69c] L. Panwar,[130] L. Paolozzi,[56] S. Parajuli,[168] A. Paramonov,[6] C. Paraskevopoulos,[53] D. Paredes Hernandez,[64b] A. Pareti,[73a,73b] K. R. Park,[42] T. H. Park,[112] F. Parodi,[57b,57a] J. A. Parsons,[42] U. Parzefall,[54] B. Pascual Dias,[41] L. Pascual Dominguez,[101] E. Pasqualucci,[75a] S. Passaggio,[57b] F. Pastore,[97] P. Patel,[88] U. M. Patel,[51] J. R. Pater,[103] T. Pauly,[37] F. Pauwels,[136] C. I. Pazos,[164] M. Pedersen,[128] R. Pedro,[133a] S. V. Peleganchuk,[38] O. Penc,[37] E. A. Pender,[52] S. Peng,[15] G. D. Penn,[178] K. E. Penski,[111] M. Penzin,[38] B. S. Peralva,[83d] A. P. Pereira Peixoto,[142] L. Pereira Sanchez,[149] D. V. Perepelitsa,[30,gg] G. Perera,[105] E. Perez Codina,[162a] M. Perganti,[10] H. Pernegger,[37] S. Perrella,[75a,75b] O. Perrin,[41] K. Peters,[48] R. F. Y. Peters,[103] B. A. Petersen,[37] T. C. Petersen,[43] E. Petit,[104] V. Petousis,[135] A. R. Petri,[71a,71b] C. Petridou,[158,bb] T. Petru,[136] A. Petrukhin,[147] M. Pettee,[18a] A. Petukhov,[82] K. Petukhova,[37] R. Pezoa,[140f] L. Pezzotti,[24b,24a] G. Pezzullo,[178] L. Pfaffenbichler,[37] A. J. Pfleger,[37] T. M. Pham,[176] T. Pham,[107] P. W. Phillips,[137] G. Piacquadio,[151] E. Pianori,[18a] F. Piazza,[126] R. Piegaia,[31] D. Pietreanu,[28b] A. D. Pilkington,[103] M. Pinamonti,[69a,69c] J. L. Pinfold,[2] B. C. Pinheiro Pereira,[133a] J. Pinol Bel,[13] A. E. Pinto Pinoargote,[130] L. Pintucci,[69a,69c] K. M. Piper,[152] A. Pirttikoski,[56] D. A. Pizzi,[35] L. Pizzimento,[64b] A. Plebani,[33] M.-A. Pleier,[30] V. Pleskot,[136] E. Plotnikova,[39] G. Poddar,[96] R. Poettgen,[100] L. Poggioli,[130] S. Polacek,[136] G. Polesello,[73a] A. Poley,[148] A. Polini,[24b] C. S. Pollard,[173] Z. B. Pollock,[122] E. Pompa Pacchi,[123] N. I. Pond,[98] D. Ponomarenko,[68] L. Pontecorvo,[37] S. Popa,[28a] G. A. Popeneciu,[28d] A. Poreba,[37] D. M. Portillo Quintero,[162a] S. Pospisil,[135] M. A. Postill,[145] P. Postolache,[28c] K. Potamianos,[173] P. A. Potepa,[87a] I. N. Potrap,[39] C. J. Potter,[33] H. Potti,[153] J. Poveda,[169] M. E. Pozo Astigarraga,[37] R. Pozzi,[37] A. Prades Ibanez,[76a,76b] J. Pretel,[171] D. Price,[103] M. Primavera,[70a] L. Primomo,[69a,69c] M. A. Principe Martin,[101] R. Privara,[125] T. Procter,[87b] M. L. Proffitt,[142] N. Proklova,[131] K. Prokofiev,[64c] G. Proto,[112] J. Proudfoot,[6] M. Przybycien,[87a] W. W. Przygoda,[87b] A. Psallidas,[46] J. E. Puddefoot,[145] D. Pudzha,[53] D. Pyatiizbyantseva,[116] J. Qian,[108] R. Qian,[109] D. Qichen,[103] Y. Qin,[13] T. Qiu,[52] A. Quadt,[55] M. Queitsch-Maitland,[103] G. Quetant,[56] R. P. Quinn,[170] G. Rabanal Bolanos,[61] D. Rafanoharana,[54] F. Raffaeli,[76a,76b] F. Ragusa,[71a,71b] J. L. Rainbolt,[40] J. A. Raine,[56] S. Rajagopalan,[30] E. Ramakoti,[39] L. Rambelli,[57b,57a] I. A. Ramirez-Berend,[35] K. Ran,[48,114c] D. S. Rankin,[131] N. P. Rapheeha,[34g] H. Rasheed,[28b] D. F. Rassloff,[63a] A. Rastogi,[18a] S. Rave,[102] S. Ravera,[57b,57a] B. Ravina,[37] I. Ravinovich,[175] M. Raymond,[37] A. L. Read,[128] N. P. Readioff,[145] D. M. Rebuzzi,[73a,73b] A. S. Reed,[112] K. Reeves,[27] J. A. Reidelsturz,[177] D. Reikher,[126] A. Rej,[49] C. Rembser,[37] H. Ren,[62] M. Renda,[28b] F. Renner,[48] A. G. Rennie,[59] A. L. Rescia,[48] S. Resconi,[71a] M. Ressegotti,[57b,57a] S. Rettie,[37] W. F. Rettie,[35] E. Reynolds,[18a] O. L. Rezanova,[39] P. Reznicek,[136] H. Riani,[36d] N. Ribaric,[51] E. Ricci,[78a,78b] R. Richter,[112] S. Richter,[47a,47b] E. Richter-Was,[87b] M. Ridel,[130] S. Ridouani,[36d] P. Rieck,[120] P. Riedler,[37] E. M. Riefel,[47a,47b] J. O. Rieger,[117] M. Rijssenbeek,[151] M. Rimoldi,[37] L. Rinaldi,[24b,24a] P. Rincke,[167] G. Ripellino,[167] I. Riu,[13] J. C. Rivera Vergara,[171] F. Rizatdinova,[124] E. Rizvi,[96] B. R. Roberts,[18a] S. S. Roberts,[139] D. Robinson,[33] M. Robles Manzano,[102] A. Robson,[59] A. Rocchi,[76a,76b] C. Roda,[74a,74b] S. Rodriguez Bosca,[37] Y. Rodriguez Garcia,[23a] A. M. Rodríguez Vera,[118] S. Roe,[37] J. T. Roemer,[37] O. Røhne,[128] R. A. Rojas,[37] C. P. A. Roland,[130] A. Romaniouk,[79] E. Romano,[73a,73b] M. Romano,[24b] A. C. Romero Hernandez,[168] N. Rompotis,[94] L. Roos,[130] S. Rosati,[75a] B. J. Rosser,[40] E. Rossi,[129] E. Rossi,[72a,72b] L. P. Rossi,[61] L. Rossini,[54] R. Rosten,[122] M. Rotaru,[28b] B. Rottler,[54] D. Rousseau,[66] D. Rousso,[48] S. Roy-Garand,[161] A. Rozanov,[104] Z. M. A. Rozario,[59] Y. Rozen,[156] A. Rubio Jimenez,[169] V. H. Ruelas Rivera,[19] T. A. Ruggeri,[1] A. Ruggiero,[129] A. Ruiz-Martinez,[169] A. Rummler,[37] Z. Rurikova,[54] N. A. Rusakovich,[39] H. L. Russell,[171] G. Russo,[75a,75b] J. P. Rutherfoord,[7] S. Rutherford Colmenares,[33] M. Rybar,[136] P. Rybczynski,[87a] A. Ryzhov,[45] J. A. Sabater Iglesias,[56] H. F-W. Sadrozinski,[139] F. Safai Tehrani,[75a] S. Saha,[1] M. Sahinsoy,[82] B. Sahoo,[175] A. Saibel,[169] B. T. Saifuddin,[123] M. Saimpert,[138] G. T. Saito,[83c] M. Saito,[159] T. Saito,[159]

A. Sala,[71a,71b] A. Salnikov,[149] J. Salt,[169] A. Salvador Salas,[157] F. Salvatore,[152] A. Salzburger,[37] D. Sammel,[54] E. Sampson,[93] D. Sampsonidis,[158,bb] D. Sampsonidou,[126] J. Sánchez,[169] V. Sanchez Sebastian,[169] H. Sandaker,[128] C. O. Sander,[48] J. A. Sandesara,[176] M. Sandhoff,[177] C. Sandoval,[23b] L. Sanfilippo,[63a] D. P. C. Sankey,[137] T. Sano,[89] A. Sansoni,[53] L. Santi,[37] C. Santoni,[41] H. Santos,[133a,133b] A. Santra,[175] E. Sanzani,[24b,24a] K. A. Saoucha,[85b] J. G. Saraiva,[133a,133d] J. Sardain,[7] O. Sasaki,[84] K. Sato,[163] C. Sauer,[37] E. Sauvan,[4] P. Savard,[161,e] R. Sawada,[159] C. Sawyer,[137] L. Sawyer,[99] C. Sbarra,[24b] A. Sbrizzi,[24b,24a] T. Scanlon,[98] J. Schaarschmidt,[142] U. Schäfer,[102] A. C. Schaffer,[66,45] D. Schaile,[111] R. D. Schamberger,[151] C. Scharf,[19] M. M. Schefer,[20] V. A. Schegelsky,[38] D. Scheirich,[136] M. Schernau,[140e] C. Scheulen,[56] C. Schiavi,[57b,57a] M. Schioppa,[44b,44a] B. Schlag,[149] S. Schlenker,[37] J. Schmeing,[177] E. Schmidt,[112] M. A. Schmidt,[177] K. Schmieden,[102] C. Schmitt,[102] N. Schmitt,[102] S. Schmitt,[48] L. Schoeffel,[138] A. Schoening,[63b] P. G. Scholer,[35] E. Schopf,[147] M. Schott,[25] S. Schramm,[56] T. Schroer,[56] H-C. Schultz-Coulon,[63a] M. Schumacher,[54] B. A. Schumm,[139] Ph. Schune,[138] H. R. Schwartz,[139] A. Schwartzman,[149] T. A. Schwarz,[108] Ph. Schwemling,[138] R. Schwienhorst,[109] F. G. Sciacca,[20] A. Sciandra,[30] G. Sciolla,[27] F. Scuri,[74a] C. D. Sebastiani,[37] K. Sedlaczek,[118] S. C. Seidel,[115] A. Seiden,[139] B. D. Seidlitz,[42] C. Seitz,[48] J. M. Seixas,[83b] G. Sekhniaidze,[72a] L. Selem,[60] N. Semprini-Cesari,[24b,24a] A. Semushin,[179] D. Sengupta,[56] V. Senthilkumar,[169] L. Serin,[66] M. Sessa,[76a,76b] H. Severini,[123] F. Sforza,[57b,57a] A. Sfyrla,[56] Q. Sha,[14] E. Shabalina,[55] H. Shaddix,[118] A. H. Shah,[33] R. Shaheen,[150] J. D. Shahinian,[131] M. Shamim,[37] L. Y. Shan,[14] M. Shapiro,[18a] A. Sharma,[37] A. S. Sharma,[170] P. Sharma,[30] P. B. Shatalov,[38] K. Shaw,[152] S. M. Shaw,[103] Q. Shen,[14] D. J. Sheppard,[148] P. Sherwood,[98] L. Shi,[98] X. Shi,[14] S. Shimizu,[84] C. O. Shimmin,[178] I. P. J. Shipsey,[129,a] S. Shirabe,[90] M. Shiyakova,[39,kk] M. J. Shochet,[40] D. R. Shope,[128] B. Shrestha,[123] S. Shrestha,[122,ll] I. Shreyber,[39] M. J. Shroff,[171] P. Sicho,[134] A. M. Sickles,[168] E. Sideras Haddad,[34g,166] A. C. Sidley,[117] A. Sidoti,[24b] F. Siegert,[50] Dj. Sijacki,[16] F. Sili,[92] J. M. Silva,[52] I. Silva Ferreira,[83b] M. V. Silva Oliveira,[30] S. B. Silverstein,[47a] S. Simion,[66] R. Simoniello,[37] E. L. Simpson,[103] H. Simpson,[152] L. R. Simpson,[6] S. Simsek,[82] S. Sindhu,[55] P. Sinervo,[161] S. N. Singh,[27] S. Singh,[30] S. Sinha,[48] S. Sinha,[103] M. Sioli,[24b,24a] K. Sioulas,[9] I. Siral,[37] E. Sitnikova,[48] J. Sjölin,[47a,47b] A. Skaf,[55] E. Skorda,[21] P. Skubic,[123] M. Slawinska,[88] I. Slazyk,[17] V. Smakhtin,[175] B. H. Smart,[137] S. Yu. Smirnov,[140b] Y. Smirnov,[82] L. N. Smirnova,[38,l] O. Smirnova,[100] A. C. Smith,[42] D. R. Smith,[165] J. L. Smith,[103] M. B. Smith,[35] R. Smith,[149] H. Smitmanns,[102] M. Smizanska,[93] K. Smolek,[135] P. Smolyanskiy,[135] A. A. Snesarev,[39] H. L. Snoek,[117] S. Snyder,[30] R. Sobie,[171,p] A. Soffer,[157] C. A. Solans Sanchez,[37] E. Yu. Soldatov,[39] U. Soldevila,[169] A. A. Solodkov,[34g] S. Solomon,[27] A. Soloshenko,[39] K. Solovieva,[54] O. V. Solovyanov,[41] P. Sommer,[50] A. Sonay,[13] A. Sopczak,[135] A. L. Sopio,[52] F. Sopkova,[29b] J. D. Sorenson,[115] I. R. Sotarriva Alvarez,[141] V. Sothilingam,[63a] O. J. Soto Sandoval,[140c,140b] S. Sottocornola,[68] R. Soualah,[85a] Z. Soumaimi,[36e] D. South,[48] N. Soybelman,[175] S. Spagnolo,[70a,70b] M. Spalla,[112] D. Sperlich,[54] B. Spisso,[72a,72b] D. P. Spiteri,[59] L. Splendori,[104] M. Spousta,[136] E. J. Staats,[35] R. Stamen,[63a] E. Stanecka,[88] W. Stanek-Maslouska,[48] M. V. Stange,[50] B. Stanislaus,[18a] M. M. Stanitzki,[48] B. Stapf,[48] E. A. Starchenko,[38] G. H. Stark,[139] J. Stark,[91] P. Staroba,[134] P. Starovoitov,[85b] R. Staszewski,[88] G. Stavropoulos,[46] A. Stefl,[37] P. Steinberg,[30] B. Stelzer,[148,162a] H. J. Stelzer,[132] O. Stelzer,[162a] H. Stenzel,[58] T. J. Stevenson,[152] G. A. Stewart,[37] J. R. Stewart,[124] M. C. Stockton,[37] G. Stoicea,[28b] M. Stolarski,[133a] S. Stonjek,[112] A. Straessner,[50] J. Strandberg,[150] S. Strandberg,[47a,47b] M. Stratmann,[177] M. Strauss,[123] T. Strebler,[104] P. Strizenec,[29b] R. Ströhmer,[172] D. M. Strom,[126] R. Stroynowski,[45] A. Strubig,[47a,47b] S. A. Stucci,[30] B. Stugu,[17] J. Stupak,[123] N. A. Styles,[48] D. Su,[149] S. Su,[62] X. Su,[62] D. Suchy,[29a] K. Sugizaki,[131] V. V. Sulin,[38] M. J. Sullivan,[94] D. M. S. Sultan,[129] L. Sultanaliyeva,[38] S. Sultansoy,[3b] S. Sun,[176] W. Sun,[14] O. Sunneborn Gudnadottir,[167] N. Sur,[100] M. R. Sutton,[152] H. Suzuki,[163] M. Svatos,[134] P. N. Swallow,[33] M. Swiatlowski,[162a] T. Swirski,[172] I. Sykora,[29a] M. Sykora,[136] T. Sykora,[136] D. Ta,[102] K. Tackmann,[48,ii] A. Taffard,[165] R. Tafirout,[162a] Y. Takubo,[84] M. Talby,[104] A. A. Talyshev,[38] K. C. Tam,[64b] N. M. Tamir,[157] A. Tanaka,[159] J. Tanaka,[159] R. Tanaka,[66] M. Tanasini,[151] Z. Tao,[170] S. Tapia Araya,[140f] S. Tapprogge,[102] A. Tarek Abouelfadl Mohamed,[109] S. Tarem,[156] K. Tariq,[14] G. Tarna,[28b] G. F. Tartarelli,[71a] M. J. Tartarin,[91] P. Tas,[136] M. Tasevsky,[134] E. Tassi,[44b,44a] A. C. Tate,[168] G. Tateno,[159] Y. Tayalati,[36e,mm] G. N. Taylor,[107] W. Taylor,[162b] A. S. Tegetmeier,[91] P. Teixeira-Dias,[97] J. J. Teoh,[161] K. Terashi,[159] J. Terron,[101] S. Terzo,[13] M. Testa,[53] R. J. Teuscher,[161,p] A. Thaler,[79] O. Theiner,[56] T. Theveneaux-Pelzer,[104] D. W. Thomas,[97] J. P. Thomas,[21] E. A. Thompson,[18a]

P. D. Thompson,[21] E. Thomson,[131] R. E. Thornberry,[45] C. Tian,[62] Y. Tian,[56] V. Tikhomirov,[82] Yu. A. Tikhonov,[39] S. Timoshenko,[38] D. Timoshyn,[136] E. X. L. Ting,[1] P. Tipton,[178] A. Tishelman-Charny,[30] K. Todome,[141] S. Todorova-Nova,[136] S. Todt,[50] L. Toffolin,[69a,69c] M. Togawa,[84] J. Tojo,[90] S. Tokár,[29a] O. Toldaiev,[68] G. Tolkachev,[104] M. Tomoto,[84,113] L. Tompkins,[149,nn] E. Torrence,[126] H. Torres,[91] E. Torró Pastor,[169] M. Toscani,[31] C. Tosciri,[40] M. Tost,[11] D. R. Tovey,[145] T. Trefzger,[172] P. M. Tricarico,[13] A. Tricoli,[30] I. M. Trigger,[162a] S. Trincaz-Duvoid,[130] D. A. Trischuk,[27] A. Tropina,[39] L. Truong,[34c] M. Trzebinski,[88] A. Trzupek,[88] F. Tsai,[151] M. Tsai,[108] A. Tsiamis,[158] P. V. Tsiareshka,[39] S. Tsigaridas,[162a] A. Tsirigotis,[158,cc] V. Tsiskaridze,[161] E. G. Tskhadadze,[155a] M. Tsopoulou,[158] Y. Tsujikawa,[89] I. I. Tsukerman,[38] V. Tsulaia,[18a] S. Tsuno,[84] K. Tsuri,[121] D. Tsybychev,[151] Y. Tu,[64b] A. Tudorache,[28b] V. Tudorache,[28b] S. Turchikhin,[57b,57a] I. Turk Cakir,[3a] R. Turra,[71a] T. Turtuvshin,[39,oo] P. M. Tuts,[42] S. Tzamarias,[158,bb] E. Tzovara,[102] Y. Uematsu,[84] F. Ukegawa,[163] P. A. Ulloa Poblete,[140c,140b] E. N. Umaka,[30] G. Unal,[37] A. Undrus,[30] G. Unel,[165] J. Urban,[29b] P. Urrejola,[140a] G. Usai,[8] R. Ushioda,[160] M. Usman,[110] F. Ustuner,[52] Z. Uysal,[82] V. Vacek,[135] B. Vachon,[106] T. Vafeiadis,[37] A. Vaitkus,[98] C. Valderanis,[111] E. Valdes Santurio,[47a,47b] M. Valente,[37] S. Valentinetti,[24b,24a] A. Valero,[169] E. Valiente Moreno,[169] A. Vallier,[91] J. A. Valls Ferrer,[169] D. R. Van Arneman,[117] T. R. Van Daalen,[142] A. Van Der Graaf,[49] H. Z. Van Der Schyf,[34g] P. Van Gemmeren,[6] M. Van Rijnbach,[37] S. Van Stroud,[98] I. Van Vulpen,[117] P. Vana,[136] M. Vanadia,[76a,76b] U. M. Vande Voorde,[150] W. Vandelli,[37] E. R. Vandewall,[124] D. Vannicola,[157] L. Vannoli,[53] R. Vari,[75a] M. Varma,[178] E. W. Varnes,[7] C. Varni,[18b] D. Varouchas,[66] L. Varriale,[169] K. E. Varvell,[153] M. E. Vasile,[28b] L. Vaslin,[84] M. D. Vassilev,[149] A. Vasyukov,[39] L. M. Vaughan,[124] R. Vavricka,[136] T. Vazquez Schroeder,[13] J. Veatch,[32] V. Vecchio,[103] M. J. Veen,[105] I. Veliscek,[30] I. Velkovska,[95] L. M. Veloce,[161] F. Veloso,[133a,133c] S. Veneziano,[75a] A. Ventura,[70a,70b] S. Ventura Gonzalez,[138] A. Verbytskyi,[112] M. Verducci,[74a,74b] C. Vergis,[96] M. Verissimo De Araujo,[83b] W. Verkerke,[117] J. C. Vermeulen,[117] C. Vernieri,[149] M. Vessella,[165] M. C. Vetterli,[148,e] A. Vgenopoulos,[102] N. Viaux Maira,[140f] T. Vickey,[145] O. E. Vickey Boeriu,[145] G. H. A. Viehhauser,[129] L. Vigani,[63b] M. Vigl,[112] M. Villa,[24b,24a] M. Villaplana Perez,[169] E. M. Villhauer,[40] E. Vilucchi,[53] M. G. Vincter,[35] A. Visibile,[117] C. Vittori,[37] I. Vivarelli,[24b,24a] E. Voevodina,[112] F. Vogel,[111] J. C. Voigt,[50] P. Vokac,[135] Yu. Volkotrub,[87b] E. Von Toerne,[25] B. Vormwald,[37] K. Vorobev,[51] M. Vos,[169] K. Voss,[147] M. Vozak,[37] L. Vozdecky,[123] N. Vranjes,[16] M. Vranjes Milosavljevic,[16] M. Vreeswijk,[117] N. K. Vu,[144b,144a] R. Vuillermet,[37] O. Vujinovic,[102] I. Vukotic,[40] I. K. Vyas,[35] J. F. Wack,[33] S. Wada,[163] C. Wagner,[149] J. M. Wagner,[18a] W. Wagner,[177] S. Wahdan,[177] H. Wahlberg,[92] C. H. Waits,[123] J. Walder,[137] R. Walker,[111] W. Walkowiak,[147] A. Wall,[131] E. J. Wallin,[100] T. Wamorkar,[18a] A. Z. Wang,[139] C. Wang,[102] C. Wang,[11] H. Wang,[18a] J. Wang,[64c] P. Wang,[103] P. Wang,[98] R. Wang,[61] R. Wang,[6] S. M. Wang,[154] S. Wang,[14] T. Wang,[62] T. Wang,[62] W. T. Wang,[80] W. Wang,[14] X. Wang,[168] X. Wang,[144a] X. Wang,[48] Y. Wang,[114a] Y. Wang,[62] Z. Wang,[108] Z. Wang,[144b] Z. Wang,[108] C. Wanotayaroj,[84] A. Warburton,[106] A. L. Warnerbring,[147] N. Warrack,[59] S. Waterhouse,[97] A. T. Watson,[21] H. Watson,[52] M. F. Watson,[21] E. Watton,[59] G. Watts,[142] B. M. Waugh,[98] J. M. Webb,[54] C. Weber,[30] H. A. Weber,[19] M. S. Weber,[20] S. M. Weber,[63a] C. Wei,[62] Y. Wei,[54] A. R. Weidberg,[129] E. J. Weik,[120] J. Weingarten,[49] C. Weiser,[54] C. J. Wells,[48] T. Wenaus,[30] B. Wendland,[49] T. Wengler,[37] N. S. Wenke,[112] N. Wermes,[25] M. Wessels,[63a] A. M. Wharton,[93] A. S. White,[61] A. White,[8] M. J. White,[1] D. Whiteson,[165] L. Wickremasinghe,[127] W. Wiedenmann,[176] M. Wielers,[137] R. Wierda,[150] C. Wiglesworth,[43] H. G. Wilkens,[37] J. J. H. Wilkinson,[33] D. M. Williams,[42] H. H. Williams,[131] S. Williams,[33] S. Willocq,[105] B. J. Wilson,[103] D. J. Wilson,[103] P. J. Windischhofer,[40] F. I. Winkel,[31] F. Winklmeier,[126] B. T. Winter,[54] M. Wittgen,[149] M. Wobisch,[99] T. Wojtkowski,[60] Z. Wolffs,[117] J. Wollrath,[37] M. W. Wolter,[88] H. Wolters,[133a,133c] M. C. Wong,[139] E. L. Woodward,[42] S. D. Worm,[48] B. K. Wosiek,[88] K. W. Woźniak,[88] S. Wozniewski,[55] K. Wraight,[59] C. Wu,[161] C. Wu,[21] J. Wu,[159] M. Wu,[114b] M. Wu,[116] S. L. Wu,[176] S. Wu,[14] X. Wu,[62] Y. Wu,[62] Z. Wu,[4] J. Wuerzinger,[112] T. R. Wyatt,[103] B. M. Wynne,[52] S. Xella,[43] L. Xia,[114a] M. Xia,[15] M. Xie,[62] A. Xiong,[126] J. Xiong,[18a] D. Xu,[14] H. Xu,[62] L. Xu,[62] R. Xu,[131] T. Xu,[108] Y. Xu,[142] Z. Xu,[52] Z. Xu,[114a] B. Yabsley,[153] S. Yacoob,[34a] Y. Yamaguchi,[84] E. Yamashita,[159] H. Yamauchi,[163] T. Yamazaki,[18a] Y. Yamazaki,[86] S. Yan,[59] Z. Yan,[105] H. J. Yang,[144a,144b] H. T. Yang,[62] S. Yang,[62] T. Yang,[64c] X. Yang,[37] X. Yang,[14] Y. Yang,[159] Y. Yang,[62] W-M. Yao,[18a] C. L. Yardley,[152] J. Ye,[14] S. Ye,[30] X. Ye,[62] Y. Yeh,[98] I. Yeletskikh,[39] B. Yeo,[18b] M. R. Yexley,[98] T. P. Yildirim,[129] P. Yin,[42] K. Yorita,[174] C. J. S. Young,[37]

C. Young,[149] N. D. Young,[126] Y. Yu,[62] J. Yuan,[14,114c] M. Yuan,[108] R. Yuan,[144b,144a] L. Yue,[98] M. Zaazoua,[62] B. Zabinski,[88] I. Zahir,[36a] A. Zaio,[57b,57a] Z. K. Zak,[88] T. Zakareishvili,[169] S. Zambito,[56] J. A. Zamora Saa,[140d] J. Zang,[159] D. Zanzi,[54] R. Zanzottera,[71a,71b] O. Zaplatilek,[135] C. Zeitnitz,[177] H. Zeng,[14] J. C. Zeng,[168] D. T. Zenger Jr.,[27] O. Zenin,[38] T. Ženiš,[29a] S. Zenz,[96] D. Zerwas,[66] M. Zhai,[14,114c] D. F. Zhang,[145] G. Zhang,[14] J. Zhang,[143a] J. Zhang,[6] K. Zhang,[14,114c] L. Zhang,[62] L. Zhang,[114a] P. Zhang,[14,114c] R. Zhang,[176] S. Zhang,[91] T. Zhang,[159] X. Zhang,[144a] Y. Zhang,[142] Y. Zhang,[98] Y. Zhang,[62] Y. Zhang,[114a] Z. Zhang,[18a] Z. Zhang,[143a] Z. Zhang,[66] H. Zhao,[142] T. Zhao,[143a] Y. Zhao,[35] Z. Zhao,[62] Z. Zhao,[62] A. Zhemchugov,[39] J. Zheng,[114a] K. Zheng,[168] X. Zheng,[62] Z. Zheng,[149] D. Zhong,[168] B. Zhou,[108] H. Zhou,[7] N. Zhou,[144a] Y. Zhou,[15] Y. Zhou,[114a] Y. Zhou,[7] C. G. Zhu,[143a] J. Zhu,[108] X. Zhu,[144b] Y. Zhu,[144a] Y. Zhu,[62] X. Zhuang,[14] K. Zhukov,[68] N. I. Zimine,[39] J. Zinsser,[63b] M. Ziolkowski,[147] L. Živković,[16] A. Zoccoli,[24b,24a] K. Zoch,[61] T. G. Zorbas,[145] O. Zormpa,[46] and L. Zwalinski[37]

(ATLAS Collaboration)

[1]*Department of Physics, University of Adelaide, Adelaide, Australia*
[2]*Department of Physics, University of Alberta, Edmonton AB, Canada*
[3a]*Department of Physics, Ankara University, Ankara, Türkiye*
[3b]*Division of Physics, TOBB University of Economics and Technology, Ankara, Türkiye*
[4]*LAPP, Université Savoie Mont Blanc, CNRS/IN2P3, Annecy, France*
[5]*APC, Université Paris Cité, CNRS/IN2P3, Paris, France*
[6]*High Energy Physics Division, Argonne National Laboratory, Argonne Illinois, USA*
[7]*Department of Physics, University of Arizona, Tucson Arizona, USA*
[8]*Department of Physics, University of Texas at Arlington, Arlington Texas, USA*
[9]*Physics Department, National and Kapodistrian University of Athens, Athens, Greece*
[10]*Physics Department, National Technical University of Athens, Zografou, Greece*
[11]*Department of Physics, University of Texas at Austin, Austin Texas, USA*
[12]*Institute of Physics, Azerbaijan Academy of Sciences, Baku, Azerbaijan*
[13]*Institut de Física d'Altes Energies (IFAE), Barcelona Institute of Science and Technology, Barcelona, Spain*
[14]*Institute of High Energy Physics, Chinese Academy of Sciences, Beijing, China*
[15]*Physics Department, Tsinghua University, Beijing, China*
[16]*Institute of Physics, University of Belgrade, Belgrade, Serbia*
[17]*Department for Physics and Technology, University of Bergen, Bergen, Norway*
[18a]*Physics Division, Lawrence Berkeley National Laboratory, Berkeley California, USA*
[18b]*University of California, Berkeley California, USA*
[19]*Institut für Physik, Humboldt Universität zu Berlin, Berlin, Germany*
[20]*Albert Einstein Center for Fundamental Physics and Laboratory for High Energy Physics, University of Bern, Bern, Switzerland*
[21]*School of Physics and Astronomy, University of Birmingham, Birmingham, United Kingdom*
[22a]*Department of Physics, Bogazici University, Istanbul, Türkiye*
[22b]*Department of Physics Engineering, Gaziantep University, Gaziantep, Türkiye*
[22c]*Department of Physics, Istanbul University, Istanbul, Türkiye*
[23a]*Facultad de Ciencias y Centro de Investigaciónes, Universidad Antonio Nariño, Bogotá, Colombia*
[23b]*Departamento de Física, Universidad Nacional de Colombia, Bogotá, Colombia*
[24a]*Dipartimento di Fisica e Astronomia A. Righi, Università di Bologna, Bologna, Italy*
[24b]*INFN Sezione di Bologna, Italy*
[25]*Physikalisches Institut, Universität Bonn, Bonn, Germany*
[26]*Department of Physics, Boston University, Boston Massachusetts, USA*
[27]*Department of Physics, Brandeis University, Waltham Massachusetts, USA*
[28a]*Transilvania University of Brasov, Brasov, Romania*
[28b]*Horia Hulubei National Institute of Physics and Nuclear Engineering, Bucharest, Romania*
[28c]*Department of Physics, Alexandru Ioan Cuza University of Iasi, Iasi, Romania*
[28d]*National Institute for Research and Development of Isotopic and Molecular Technologies, Physics Department, Cluj-Napoca, Romania*
[28e]*National University of Science and Technology Politechnica, Bucharest, Romania*
[28f]*West University in Timisoara, Timisoara, Romania*
[28g]*Faculty of Physics, University of Bucharest, Bucharest, Romania*

[29a]*Faculty of Mathematics, Physics and Informatics, Comenius University, Bratislava, Slovak Republic*
[29b]*Department of Subnuclear Physics, Institute of Experimental Physics of the Slovak Academy of Sciences, Kosice, Slovak Republic*
[30]*Physics Department, Brookhaven National Laboratory, Upton New York, USA*
[31]*Universidad de Buenos Aires, Facultad de Ciencias Exactas y Naturales, Departamento de Física, y CONICET, Instituto de Física de Buenos Aires (IFIBA), Buenos Aires, Argentina*
[32]*California State University, California, USA*
[33]*Cavendish Laboratory, University of Cambridge, Cambridge, United Kingdom*
[34a]*Department of Physics, University of Cape Town, Cape Town, South Africa*
[34b]*iThemba Labs, Western Cape, South Africa*
[34c]*Department of Mechanical Engineering Science, University of Johannesburg, Johannesburg, South Africa*
[34d]*National Institute of Physics, University of the Philippines Diliman (Philippines), Philippines*
[34e]*University of South Africa, Department of Physics, Pretoria, South Africa*
[34f]*University of Zululand, KwaDlangezwa, South Africa*
[34g]*School of Physics, University of the Witwatersrand, Johannesburg, South Africa*
[35]*Department of Physics, Carleton University, Ottawa ON, Canada*
[36a]*Faculté des Sciences Ain Chock, Université Hassan II de Casablanca, Morocco*
[36b]*Faculté des Sciences, Université Ibn-Tofail, Kénitra, Morocco*
[36c]*Faculté des Sciences Semlalia, Université Cadi Ayyad, LPHEA-Marrakech, Morocco*
[36d]*LPMR, Faculté des Sciences, Université Mohamed Premier, Oujda, Morocco*
[36e]*Faculté des sciences, Université Mohammed V, Rabat, Morocco*
[36f]*Institute of Applied Physics, Mohammed VI Polytechnic University, Ben Guerir, Morocco*
[37]*CERN, Geneva, Switzerland*
[38]*Affiliated with an institute formerly covered by a cooperation agreement with CERN*
[39]*Affiliated with an international laboratory covered by a cooperation agreement with CERN*
[40]*Enrico Fermi Institute, University of Chicago, Chicago Illinois, USA*
[41]*LPC, Université Clermont Auvergne, CNRS/IN2P3, Clermont-Ferrand, France*
[42]*Nevis Laboratory, Columbia University, Irvington New York, USA*
[43]*Niels Bohr Institute, University of Copenhagen, Copenhagen, Denmark*
[44a]*Dipartimento di Fisica, Università della Calabria, Rende, Italy*
[44b]*INFN Gruppo Collegato di Cosenza, Laboratori Nazionali di Frascati, Italy*
[45]*Physics Department, Southern Methodist University, Dallas Texas, USA*
[46]*National Centre for Scientific Research "Demokritos", Agia Paraskevi, Greece*
[47a]*Department of Physics, Stockholm University, Sweden*
[47b]*Oskar Klein Centre, Stockholm, Sweden*
[48]*Deutsches Elektronen-Synchrotron DESY, Hamburg and Zeuthen, Germany*
[49]*Fakultät Physik, Technische Universität Dortmund, Dortmund, Germany*
[50]*Institut für Kern- und Teilchenphysik, Technische Universität Dresden, Dresden, Germany*
[51]*Department of Physics, Duke University, Durham NC, USA*
[52]*SUPA—School of Physics and Astronomy, University of Edinburgh, Edinburgh, United Kingdom*
[53]*INFN e Laboratori Nazionali di Frascati, Frascati, Italy*
[54]*Physikalisches Institut, Albert-Ludwigs-Universität Freiburg, Freiburg, Germany*
[55]*II. Physikalisches Institut, Georg-August-Universität Göttingen, Göttingen, Germany*
[56]*Département de Physique Nucléaire et Corpusculaire, Université de Genève, Genève, Switzerland*
[57a]*Dipartimento di Fisica, Università di Genova, Genova, Italy*
[57b]*INFN Sezione di Genova, Italy*
[58]*II. Physikalisches Institut, Justus-Liebig-Universität Giessen, Giessen, Germany*
[59]*SUPA—School of Physics and Astronomy, University of Glasgow, Glasgow, United Kingdom*
[60]*LPSC, Université Grenoble Alpes, CNRS/IN2P3, Grenoble INP, Grenoble, France*
[61]*Laboratory for Particle Physics and Cosmology, Harvard University, Cambridge Massachusetts, USA*
[62]*Department of Modern Physics and State Key Laboratory of Particle Detection and Electronics, University of Science and Technology of China, Hefei, China*
[63a]*Kirchhoff-Institut für Physik, Ruprecht-Karls-Universität Heidelberg, Heidelberg, Germany*
[63b]*Physikalisches Institut, Ruprecht-Karls-Universität Heidelberg, Heidelberg, Germany*
[64a]*Department of Physics, Chinese University of Hong Kong, Shatin, New Territories, Hong Kong, China*
[64b]*Department of Physics, University of Hong Kong, Hong Kong, China*
[64c]*Department of Physics and Institute for Advanced Study, Hong Kong University of Science and Technology, Clear Water Bay, Kowloon, Hong Kong, China*
[65]*Department of Physics, National Tsing Hua University, Hsinchu, Taiwan*

[66]IJCLab, Université Paris-Saclay, CNRS/IN2P3, 91405, Orsay, France
[67]Centro Nacional de Microelectrónica (IMB-CNM-CSIC), Barcelona, Spain
[68]Department of Physics, Indiana University, Bloomington Indiana, USA
[69a]INFN Gruppo Collegato di Udine, Sezione di Trieste, Udine, Italy
[69b]ICTP, Trieste, Italy
[69c]Dipartimento Politecnico di Ingegneria e Architettura, Università di Udine, Udine, Italy
[70a]INFN Sezione di Lecce, Italy
[70b]Dipartimento di Matematica e Fisica, Università del Salento, Lecce, Italy
[71a]INFN Sezione di Milano, Italy
[71b]Dipartimento di Fisica, Università di Milano, Milano, Italy
[72a]INFN Sezione di Napoli, Italy
[72b]Dipartimento di Fisica, Università di Napoli, Napoli, Italy
[73a]INFN Sezione di Pavia, Italy
[73b]Dipartimento di Fisica, Università di Pavia, Pavia, Italy
[74a]INFN Sezione di Pisa, Italy
[74b]Dipartimento di Fisica E. Fermi, Università di Pisa, Pisa, Italy
[75a]INFN Sezione di Roma, Italy
[75b]Dipartimento di Fisica, Sapienza Università di Roma, Roma, Italy
[76a]INFN Sezione di Roma Tor Vergata, Italy
[76b]Dipartimento di Fisica, Università di Roma Tor Vergata, Roma, Italy
[77a]INFN Sezione di Roma Tre, Italy
[77b]Dipartimento di Matematica e Fisica, Università Roma Tre, Roma, Italy
[78a]INFN-TIFPA, Italy
[78b]Università degli Studi di Trento, Trento, Italy
[79]Universität Innsbruck, Department of Astro and Particle Physics, Innsbruck, Austria
[80]University of Iowa, Iowa City Iowa, USA
[81]Department of Physics and Astronomy, Iowa State University, Ames Iowa, USA
[82]Istinye University, Sariyer, Istanbul, Türkiye
[83a]Departamento de Engenharia Elétrica, Universidade Federal de Juiz de Fora (UFJF), Juiz de Fora, Brazil
[83b]Universidade Federal do Rio De Janeiro COPPE/EE/IF, Rio de Janeiro, Brazil
[83c]Instituto de Física, Universidade de São Paulo, São Paulo, Brazil
[83d]Rio de Janeiro State University, Rio de Janeiro, Brazil
[83e]Federal University of Bahia, Bahia, Brazil
[84]KEK, High Energy Accelerator Research Organization, Tsukuba, Japan
[85a]Khalifa University of Science and Technology, Abu Dhabi, United Arab Emirates
[85b]University of Sharjah, Sharjah, United Arab Emirates
[86]Graduate School of Science, Kobe University, Kobe, Japan
[87a]AGH University of Krakow, Faculty of Physics and Applied Computer Science, Krakow, Poland
[87b]Marian Smoluchowski Institute of Physics, Jagiellonian University, Krakow, Poland
[88]Institute of Nuclear Physics Polish Academy of Sciences, Krakow, Poland
[89]Faculty of Science, Kyoto University, Kyoto, Japan
[90]Research Center for Advanced Particle Physics and Department of Physics, Kyushu University, Fukuoka, Japan
[91]L2IT, Université de Toulouse, CNRS/IN2P3, UPS, Toulouse, France
[92]Instituto de Física La Plata, Universidad Nacional de La Plata and CONICET, La Plata, Argentina
[93]Physics Department, Lancaster University, Lancaster, United Kingdom
[94]Oliver Lodge Laboratory, University of Liverpool, Liverpool, United Kingdom
[95]Department of Experimental Particle Physics, Jožef Stefan Institute and Department of Physics, University of Ljubljana, Ljubljana, Slovenia
[96]Department of Physics and Astronomy, Queen Mary University of London, London, United Kingdom
[97]Department of Physics, Royal Holloway University of London, Egham, United Kingdom
[98]Department of Physics and Astronomy, University College London, London, United Kingdom
[99]Louisiana Tech University, Ruston Louisiana, USA
[100]Fysiska institutionen, Lunds universitet, Lund, Sweden
[101]Departamento de Física Teorica C-15 and CIAFF, Universidad Autónoma de Madrid, Madrid, Spain
[102]Institut für Physik, Universität Mainz, Mainz, Germany
[103]School of Physics and Astronomy, University of Manchester, Manchester, United Kingdom
[104]CPPM, Aix-Marseille Université, CNRS/IN2P3, Marseille, France
[105]Department of Physics, University of Massachusetts, Amherst Massachusetts, USA

[106]*Department of Physics, McGill University, Montreal QC, Canada*
[107]*School of Physics, University of Melbourne, Victoria, Australia*
[108]*Department of Physics, University of Michigan, Ann Arbor Michigan, USA*
[109]*Department of Physics and Astronomy, Michigan State University, East Lansing Michigan, USA*
[110]*Group of Particle Physics, University of Montreal, Montreal QC, Canada*
[111]*Fakultät für Physik, Ludwig-Maximilians-Universität München, München, Germany*
[112]*Max-Planck-Institut für Physik (Werner-Heisenberg-Institut), München, Germany*
[113]*Graduate School of Science and Kobayashi-Maskawa Institute, Nagoya University, Nagoya, Japan*
[114a]*Department of Physics, Nanjing University, Nanjing, China*
[114b]*School of Science, Shenzhen Campus of Sun Yat-sen University, China*
[114c]*University of Chinese Academy of Science (UCAS), Beijing, China*
[115]*Department of Physics and Astronomy, University of New Mexico, Albuquerque New Mexico, USA*
[116]*Institute for Mathematics, Astrophysics and Particle Physics, Radboud University/Nikhef, Nijmegen, Netherlands*
[117]*Nikhef National Institute for Subatomic Physics and University of Amsterdam, Amsterdam, Netherlands*
[118]*Department of Physics, Northern Illinois University, DeKalb Illinois, USA*
[119a]*New York University Abu Dhabi, Abu Dhabi, United Arab Emirates*
[119b]*United Arab Emirates University, Al Ain, United Arab Emirates*
[120]*Department of Physics, New York University, New York New York, USA*
[121]*Ochanomizu University, Otsuka, Bunkyo-ku, Tokyo, Japan*
[122]*Ohio State University, Columbus Ohio, USA*
[123]*Homer L. Dodge Department of Physics and Astronomy, University of Oklahoma, Norman Oklahoma, USA*
[124]*Department of Physics, Oklahoma State University, Stillwater Oklahoma, USA*
[125]*Palacký University, Joint Laboratory of Optics, Olomouc, Czech Republic*
[126]*Institute for Fundamental Science, University of Oregon, Eugene, Oregon, USA*
[127]*Graduate School of Science, University of Osaka, Osaka, Japan*
[128]*Department of Physics, University of Oslo, Oslo, Norway*
[129]*Department of Physics, Oxford University, Oxford, United Kingdom*
[130]*LPNHE, Sorbonne Université, Université Paris Cité, CNRS/IN2P3, Paris, France*
[131]*Department of Physics, University of Pennsylvania, Philadelphia Pennsylvania, USA*
[132]*Department of Physics and Astronomy, University of Pittsburgh, Pittsburgh Pennsylvania, USA*
[133a]*Laboratório de Instrumentação e Física Experimental de Partículas—LIP, Lisboa, Portugal*
[133b]*Departamento de Física, Faculdade de Ciências, Universidade de Lisboa, Lisboa, Portugal*
[133c]*Departamento de Física, Universidade de Coimbra, Coimbra, Portugal*
[133d]*Centro de Física Nuclear da Universidade de Lisboa, Lisboa, Portugal*
[133e]*Departamento de Física, Escola de Ciências, Universidade do Minho, Braga, Portugal*
[133f]*Departamento de Física Teórica y del Cosmos, Universidad de Granada, Granada (Spain), Spain*
[133g]*Departamento de Física, Instituto Superior Técnico, Universidade de Lisboa, Lisboa, Portugal*
[134]*Institute of Physics of the Czech Academy of Sciences, Prague, Czech Republic*
[135]*Czech Technical University in Prague, Prague, Czech Republic*
[136]*Charles University, Faculty of Mathematics and Physics, Prague, Czech Republic*
[137]*Particle Physics Department, Rutherford Appleton Laboratory, Didcot, United Kingdom*
[138]*IRFU, CEA, Université Paris-Saclay, Gif-sur-Yvette, France*
[139]*Santa Cruz Institute for Particle Physics, University of California Santa Cruz, Santa Cruz California, USA*
[140a]*Departamento de Física, Pontificia Universidad Católica de Chile, Santiago, Chile*
[140b]*Millennium Institute for Subatomic physics at high energy frontier (SAPHIR), Santiago, Chile*
[140c]*Instituto de Investigación Multidisciplinario en Ciencia y Tecnología, y Departamento de Física, Universidad de La Serena, Chile*
[140d]*Universidad Andres Bello, Department of Physics, Santiago, Chile*
[140e]*Instituto de Alta Investigación, Universidad de Tarapacá, Arica, Chile*
[140f]*Departamento de Física, Universidad Técnica Federico Santa María, Valparaíso, Chile*
[141]*Department of Physics, Institute of Science, Tokyo, Japan*
[142]*Department of Physics, University of Washington, Seattle Washington, USA*
[143a]*Institute of Frontier and Interdisciplinary Science and Key Laboratory of Particle Physics and Particle Irradiation (MOE), Shandong University, Qingdao, China*
[143b]*School of Physics, Zhengzhou University, China*
[144a]*State Key Laboratory of Dark Matter Physics, School of Physics and Astronomy, Shanghai Jiao Tong University, Key Laboratory for Particle Astrophysics and Cosmology (MOE), SKLPPC, Shanghai, China*

[144b]State Key Laboratory of Dark Matter Physics, Tsung-Dao Lee Institute, Shanghai Jiao Tong University, Shanghai, China
[145]Department of Physics and Astronomy, University of Sheffield, Sheffield, United Kingdom
[146]Department of Physics, Shinshu University, Nagano, Japan
[147]Department Physik, Universität Siegen, Siegen, Germany
[148]Department of Physics, Simon Fraser University, Burnaby BC, Canada
[149]SLAC National Accelerator Laboratory, Stanford California, USA
[150]Department of Physics, Royal Institute of Technology, Stockholm, Sweden
[151]Departments of Physics and Astronomy, Stony Brook University, Stony Brook New York, USA
[152]Department of Physics and Astronomy, University of Sussex, Brighton, United Kingdom
[153]School of Physics, University of Sydney, Sydney, Australia
[154]Institute of Physics, Academia Sinica, Taipei, Taiwan
[155a]E. Andronikashvili Institute of Physics, Iv. Javakhishvili Tbilisi State University, Tbilisi, Georgia
[155b]High Energy Physics Institute, Tbilisi State University, Tbilisi, Georgia
[155c]University of Georgia, Tbilisi, Georgia
[156]Department of Physics, Technion, Israel Institute of Technology, Haifa, Israel
[157]Raymond and Beverly Sackler School of Physics and Astronomy, Tel Aviv University, Tel Aviv, Israel
[158]Department of Physics, Aristotle University of Thessaloniki, Thessaloniki, Greece
[159]International Center for Elementary Particle Physics and Department of Physics, University of Tokyo, Tokyo, Japan
[160]Graduate School of Science and Technology, Tokyo Metropolitan University, Tokyo, Japan
[161]Department of Physics, University of Toronto, Toronto ON, Canada
[162a]TRIUMF, Vancouver BC, Canada
[162b]Department of Physics and Astronomy, York University, Toronto ON, Canada
[163]Division of Physics and Tomonaga Center for the History of the Universe, Faculty of Pure and Applied Sciences, University of Tsukuba, Tsukuba, Japan
[164]Department of Physics and Astronomy, Tufts University, Medford Massachusetts, USA
[165]Department of Physics and Astronomy, University of California Irvine, Irvine California, USA
[166]University of West Attica, Athens, Greece
[167]Department of Physics and Astronomy, University of Uppsala, Uppsala, Sweden
[168]Department of Physics, University of Illinois, Urbana Illinois, USA
[169]Instituto de Física Corpuscular (IFIC), Centro Mixto Universidad de Valencia—CSIC, Valencia, Spain
[170]Department of Physics, University of British Columbia, Vancouver BC, Canada
[171]Department of Physics and Astronomy, University of Victoria, Victoria BC, Canada
[172]Fakultät für Physik und Astronomie, Julius-Maximilians-Universität Würzburg, Würzburg, Germany
[173]Department of Physics, University of Warwick, Coventry, United Kingdom
[174]Waseda University, Tokyo, Japan
[175]Department of Particle Physics and Astrophysics, Weizmann Institute of Science, Rehovot, Israel
[176]Department of Physics, University of Wisconsin, Madison Wisconsin, USA
[177]Fakultät für Mathematik und Naturwissenschaften, Fachgruppe Physik, Bergische Universität Wuppertal, Wuppertal, Germany
[178]Department of Physics, Yale University, New Haven Connecticut, USA
[179]Yerevan Physics Institute, Yerevan, Armenia

[a]Deceased.
[b]Also at Department of Physics, King's College London, London, United Kingdom
[c]Also at Institute of Physics, Azerbaijan Academy of Sciences, Baku, Azerbaijan
[d]Also at Imam Mohammad Ibn Saud Islamic University, Saudi Arabia
[e]Also at TRIUMF, Vancouver BC, Canada
[f]Also at Department of Physics, University of Thessaly, Greece
[g]Also at An-Najah National University, Nablus, Palestine
[h]Also at Department of Physics, University of Fribourg, Fribourg, Switzerland
[i]Also at Department of Physics, Westmont College, Santa Barbara, USA
[j]Also at Departament de Fisica de la Universitat Autonoma de Barcelona, Barcelona, Spain
[k]Also at University of Sienna, Italy
[l]Also at Affiliated with an institute formerly covered by a cooperation agreement with CERN
[m]Also at The Collaborative Innovation Center of Quantum Matter (CICQM), Beijing, China
[n]Also at Faculty of Physics, Sofia University, 'St. Kliment Ohridski', Sofia, Bulgaria
[o]Also at Università di Napoli Parthenope, Napoli, Italy
[p]Also at Institute of Particle Physics (IPP), Canada

[q]Also at Department of Physics, Bolu Abant Izzet Baysal University, Bolu, Türkiye
[r]Also at Faculty of Physics, University of Bucharest, Romania
[s]Also at Borough of Manhattan Community College, City University of New York, New York NY, USA
[t]Also at National Institute of Physics, University of the Philippines Diliman (Philippines), Philippines
[u]Also at Department of Financial and Management Engineering, University of the Aegean, Chios, Greece
[v]Also at Institucio Catalana de Recerca i Estudis Avancats, ICREA, Barcelona, Spain
[w]Also at Henan University, China
[x]Also at CMD-AC UNEC Research Center, Azerbaijan State University of Economics (UNEC), Azerbaijan
[y]Also at Yeditepe University, Physics Department, Istanbul, Türkiye
[z]Also at Institute of Theoretical Physics, Ilia State University, Tbilisi, Georgia
[aa]Also at CERN, Geneva, Switzerland
[bb]Also at Center for Interdisciplinary Research and Innovation (CIRI-AUTH), Thessaloniki, Greece
[cc]Also at Hellenic Open University, Patras, Greece
[dd]Also at Department of Modern Physics and State Key Laboratory of Particle Detection and Electronics, University of Science and Technology of China, Hefei, China
[ee]Also at Department of Mathematical Sciences, University of South Africa, Johannesburg, South Africa
[ff]Also at Department of Physics, Stellenbosch University, South Africa
[gg]Also at University of Colorado Boulder, Department of Physics, Colorado, USA
[hh]Also at Département de Physique Nucléaire et Corpusculaire, Université de Genève, Genève, Switzerland
[ii]Also at Institut für Experimentalphysik, Universität Hamburg, Hamburg, Germany
[jj]Also at Centre of Physics of the Universities of Minho and Porto (CF-UM-UP), Portugal
[kk]Also at Institute for Nuclear Research and Nuclear Energy (INRNE) of the Bulgarian Academy of Sciences, Sofia, Bulgaria
[ll]Also at Washington College, Chestertown, Maryland, USA
[mm]Also at Institute of Applied Physics, Mohammed VI Polytechnic University, Ben Guerir, Morocco
[nn]Also at Department of Physics, Stanford University, Stanford California, USA
[oo]Also at Institute of Physics and Technology, Mongolian Academy of Sciences, Ulaanbaatar, Mongolia